# An investigation of visual field asymmetry indices for detecting early Primary Open Angle Glaucoma

A thesis submitted to The University of Manchester for the degree of Doctor of Philosophy in the Faculty of Biology, Medicine and Health

2016

Naqibah Ghazali

School of Health Sciences

# LIST OF CONTENTS

Final word count: 42075

# LIST OF FIGURES

5

# LIST OF TABLES

# LIST OF ABBREVIATION

**ACG:** Angle Closure Glaucoma

**AGIS:** Advanced Glaucoma Intervention Study

**AUROC**: Areas Under Receiver Operating Characteristic

**BEAP**: Bridlington Eye Assessment Project

**BMES:** Blue Mountains Eye Study

**BMOMRW**: Bruch's Membrane Opening Minimum Rim Width

**CDR**: Cup-to-Disc Ratio

**CI**: Confidence Interval

**CIGTS:** Collaborative Initial Glaucoma Treatment Study

**CL:** Confidence Limit

**CNTG**: Collaborative Normal Tension Glaucoma Study

**CSLO:** Confocal Scanning Laser Tomography

**DDLS**: Disc Damage Likelihood Scale

**EMGT:** Early Manifest Glaucoma Trial

**FDT**: Frequency Doubling Technology

**FN:** False Negative

**FP**: False Positive

**FT**: Full Threshold

**FVFA**: Friedmann Visual Field Analyser

**GCP**: Glaucoma Change Probability

**GHT**: Glaucoma Hemifield Hest

**GPA**: Glaucoma Progression Analysis

**GPS**: Glaucoma Probability Score

**GSS 2**: Glaucoma Staging System II

**HFA:** Humphrey Field Analyser

**HMD**: Hemifield Mean Difference

**HRT:** Heidelberg Retina Tomography

**HSD**: Hemifield Standard Deviation

**IOD**: Inter-Ocular Difference

**IOP**: Intraocular Pressure

**IQR**: Interquartile Range

**LR**: Likelihood Ratio

**MD**: Mean Deviation

**mfVEP**: Multifocal Visual Evoked Potential

**MLR**: Multivariate Logistic Regression

**MRA**: Moorfields Regression Analysis

**MREH**: Manchester Royal Eye Hospital

**NHS:** National Health Service

**NICE**: National Institute for Health and Clinical Excelle

**NP**: Number of test Pairs

**NRR**: Neuroretinal Rim

**NTG**: Normal Tension Glaucoma

**OCT**: Ocular Coherent Tomography

**OHTS:** Ocular Hypertension Treatment Study

**ONH :** Optic Nerve Head

**PD:** Pattern deviation

**POAG**: Primary Open Angle Glaucoma

**PSD**: Pattern standard deviation

**R/L MD**: Right/left mean deviation

**R/L NP**: Right/left Number of test Pairs

**R/L SD**: Right/left Standard Deviation

**RAC:** Relative Asymmetry Coefficient

**RAD:** Retinal Asymmetry Difference

**RADAAR:** Rim Area to Disc Area Asymmetry

**RAI**: Retinal Asymmetry Index

**RGC**: Retinal Ganglion Cell

**RNFL**: Retinal Nerve Fibre Layer

**ROC**: Receiver Operating Characteristic

**RPE**: Retinal Pigment Epithelium

**SAP**: Standard automated perimetry

**SITA**: Swedish Interactive Threshold Algorithm

**SLP:** Scanning Laser Polarimetry

**SWAP**: Short-wavelength automated perimetry

**TD**: Total deviation

**TOP**: Tendency Oriented Perimetry

**VEP**: Visual evoked Potential

**VFI**: Visual Field Index

**WNL**: Within Normal Limits

**ZATA**: Zippy Adaptive Threshold Algorithm

**ZEST**: Zippy Estimation by Sequential Testing

# ABSTRACT

Glaucoma can be defined as group of optic neuropathies associated with structural changes to the optic nerve head and the presence of irreversible visual field loss that may derive from various pathological mechanisms. One of the commonest types of glaucoma is primary open angle glaucoma (POAG). Evaluation of the visual field is an essential component in the diagnosis and management of glaucoma. Visual field loss in POAG is often asymmetric both within and between eyes.

This thesis extracts samples from a large database of visual field records collected at Manchester Royal Eye Hospital to measure the discriminatory power of various asymmetry indices in the detection of POAG.

The first investigation describes and evaluates 3 new Sup/Inf hemifield asymmetry indices; hemifield mean difference, hemifield standard deviation and the number of asymmetric test pairs, for detecting POAG and compares the performance of these new indices with the well-established Glaucoma Hemifield Test (GHT). A good performance was observed for the new indices. GHT can fail to detect significant asymmetry, detected by hemifield standard deviation and number of asymmetric test pairs, when an early defect crosses the GHT sector boundaries.

The second investigation looked at the performance of R/L asymmetry indices and whether these indices are superior to the previously investigated Sup/Inf hemifield indices. This study found that, the new R/L asymmetry indices did not perform better than worse eye uniocular hemifield asymmetry indices in differentiating between normal and POAG eyes. Their performance was similar to that of combined uniocular indices.

The third investigation describes and measures the discriminatory power of 2 indices that quantify the clustering of Sup/Inf hemifield asymmetric test locations.

The final experimental chapter determines the discriminatory power of a multi-factorial model that combines a range of asymmetry indices. In a sample selected to critically evaluate early functional loss the model correctly classified 89% of controls and 80% of POAG cases and performed better than GHT and single asymmetry analyses.

# DECLARATION

No portion of the work referred to in the thesis has been submitted in support of an application for another degree or qualification at this or any other university or other institute of learning.

# COPYRIGHT STATEMENT

The author of this thesis (including any appendices and/or schedules to this thesis) owns certain copyright or related rights in it (the "Copyright") and she has given The University of Manchester certain rights to use such Copyright, including administrative purposes.

Copies of this thesis, either in full or in extracts and whether in hard or electronic copy, may be made only in accordance with the Copyright, Designs and Patents Act 1988 (as amended) and regulations issued under it or, where appropriate, in accordance with licencing agreements which the University has from time to time. This page must form part of any such copies made.

The ownership of certain Copyright, patents, designs, trademarks and other intellectual property (the "Intellectual Property") and any reproductions of copyright works in the thesis, for example graphs and tables ("Reproductions"), which may be described in this thesis, may not be owned by the author and may be owned by third parties. Such Intellectual Property and Reproductions cannot and must not be made available for use without the prior written permission of the owner(s) of the relevant Intellectual Property and/or Reproductions.

Further information on the conditions under which disclosure, publication and commercialisation of this thesis, the Copyright and any Intellectual Property University IP Policy (see http://documents.manchester.ac.uk/display.aspx?DocID=24420), in any relevant Thesis restriction declarations deposited in the University Library, The University Library's regulations (see http://www.library.manchester.ac.uk/about/regulations/) and in The University's policy on Presentation of Theses

*Dedicate to my father*

# ACKNOWLEDGEMENT

First and foremost, I would like to thank God, whose many blessings have made me who I am today. I knew from the beginning that pursuing PhD is a demanding and challenging task. Throughout this long journey, I have gained a lot by learning to persevere despite hardship. I am grateful for all of the support and contribution along this journey. I would never have successfully completed this thesis without the assistance of numerous people who I am indebted to.

I would like to express my special appreciation and thanks to my supervisor Professor David B. Henson, you have been a tremendous mentor for me. My PhD has been an amazing experience and I thank David wholeheartedly, not only for his tremendous academic support, but also for giving me so many wonderful opportunities. I would also like to thank my co-supervisor, professor Tariq Aslam, for your brilliant comments and suggestions. I would especially like to thank Ministry of Health Malaysia for  their sponsorship through the program 'Hadiah Latihan Persekutuan (HLP)' for its financial support throughout my PhD Program. Also, I would also like to thank Mrs Che Ruhani Che Jaafar and Mrs Noor Zahirah, Head of Optometrist, Ministry of Health Malaysia, Kate Barugh from Research Office and Joy Stewart from postgraduate office, School of Health Sciences, University of Manchester. All of you have been there to support me at the beginning of the study, during data collection and throughout my whole Ph.D. journey.

I must thank my unbelievably supportive husband, Khairul Nizam Siron and my kids; Salahuddin, Aisyah and Fatimah. Their love and support without any complaint has enabled me to complete this Ph.D. Also, a special thank you to all my

# Thesis layout

The overall structure of this thesis takes the form of 7 chapters, including 2 introductory chapters, followed by 4 chapters describing the experimental work that has been undertaken. Each experimental chapter starts with a section describing my contribution to the work followed by an abstract, short introduction, methods, results and discussion. The first introductory chapter (chapter 1) begins by laying out the theoretical dimensions of the basic understanding of glaucoma including definition, epidemiology, pathophysiology, risk factors and assessment, which form the fundamental elements of glaucoma diagnosis and management. Included in this chapter are topics concerned with the structural and functional evaluation of the glaucomatous eye.

The second introductory chapter focuses on studies investigating the structural and functional asymmetry in early glaucoma; both Sup/Inf hemifield and R/L. Included in this review are studies investigating the normal symmetry in the optic nerve head (ONH), retinal nerve fibre layer (RNFL) thickness and visual field. The understanding of the normal symmetry is essential when devising new methods to analyze asymmetric characteristics in primary open angle glaucoma (POAG).

The experimental work in Chapter 3 describes the discriminatory performance of three new Sup/Inf hemifield asymmetry indices for detecting POAG and compares these with the Glaucoma Hemifield Test (GHT) (Ghazali et al., 2015). In this

chapter, the disagreement between proposed Sup/Inf asymmetry indices with GHT is also discussed in selected cases.

In chapter 4 the performance of several new R/L asymmetry indices are investigated and compared to that of Sup/Inf hemifield indices.

In chapter 5 the value of a clustering of Sup/Inf hemifield asymmetric test locations is investigated with the generation of 2 new indices, N clusters and N clustered.

The performance of a multi-regression model, that incorporated most of the above indices, is investigated in chapter 6.

A summary of the main findings and suggestions for further work, which have arisen in the discussions, are provided in the final chapter (chapter 7) followed by references as the last section in this thesis.

# 1. General Introduction

## 1.1 Definition of glaucoma

Glaucoma can be defined as group of ocular disorders with multifactorial aetiology derived from various pathological mechanisms united by clinically visible changes to the ONH and corresponding functional changes to the visual field. Structural changes include focal or generalized thinning of the neuroretinal rim (NRR) with excavation and enlargement of the optic cup. Functional changes include diffuse and localized visual field loss. Visual acuity is normally maintained until the disease reaches an advanced stage when total loss of vision can occur.

There are many types of glaucoma, which can be classified according to aetiology, ocular structure and age of onset. POAG, the commonest type of glaucoma (Kroese and Burton, 2003), is age related in nature and often but not always associated with high intraocular pressure (IOP). Detection of POAG relies upon the structural assessment of ONH and retinal nerve fibre layer combined with functional examination of the visual field. Raised IOP (>21mmHg) is a risk factor for POAG, however, up to 40% people with POAG have IOPs consistently within the normal range (Kroese and Burton, 2003).

POAG is known as 'the silent thief of sight' as it is often asymptomatic until it reaches an advanced stage. It is a chronic, progressive and generally bilateral but often asymmetric disease. Unlike Angle Closure Glaucoma (ACG), sufferers of POAG

are often unaware of their gradually progressive loss of peripheral visual field until it reaches an advanced stage when the central field of vision is affected. Treatment is currently focused on lowering the IOP, which has been shown to slow down its progression (Garway-Heath et al., 2013). Considering the importance of early detection, improved diagnostic criteria in identifying early glaucomatous changes would seem beneficial in reducing the burden of this disease. For the rest of this introduction, I will concentrate on POAG, as this is the main theme of the research described within this thesis.

## 1.2 Epidemiology

Glaucoma is the leading cause of irreversible and preventable blindness worldwide. By the year of 2020, it has been estimated that 5.8 million glaucoma patients worldwide will be bilaterally blind from this disease (Quigley and Broman, 2006).

*1.21 Prevalence*

Prevalence is the proportion of a population affected by a specific condition at a point in time. In recent years, there has been an increasing amount of literature investigating the prevalence of POAG according to racial group and age from many parts of the world. For the purpose of this review, I will include the prevalence surveys of races that are present in United Kingdom, which include; Whites, Blacks and Asian. The large body of evidence for POAG in 'blacks' comes from studies in Baltimore and more recently in Barbados.

There are two meta-analyses on the prevalence of glaucoma in the different races (Friedman et al, 2004; Rudnicka et al, 2006). The first study was conducted to estimate the prevalence and distribution of POAG in United States according to ethnicity age and gender. The estimated rates were based on recent population-based studies in United States, Australia and Europe. These rates were applied to the 2000 US census data to estimate the prevalence of POAG in 2020. This study concentrated on data from; the Baltimore Eye Survey, the Barbados Eye Study, the Beaver Dam Eye Study, the Blue Mountains Eye Study, the Kongwa Eye Project, Proyecto Vision Evaluation Research, the Rotterdam study and the Melbourne Visual Impairment Project. This report estimated that, the prevalence of POAG in US population above 40 years is 1.86%. Blacks were estimated to have 3 times the age-adjusted prevalence of white subjects.

Rudnicka and associates conducted a meta-analyses to determine the variation in POAG prevalence with age, gender, race, year of publication, and survey methodology (Rudnicka et al., 2006). It looked at the results from 46 studies involving 103,567 participants including 2509 subjects with POAG. It highlighted that the prevalence of POAG in black population was the highest in all age groups. The estimated prevalence according to age and race is shown in Table1.1.

**Table 1.1: Estimated prevalence according to age and race (Rudnicka et al., 2006)**

| Age Range (Years) | Predicted Prevalence According to Age and Race (95% Crude Interval) | | |
|---|---|---|---|
| | White | Black | Asian |
| 30-39 | - | 1.8 (1.2-2.7) | 0.4 (0.3-0.6) |
| 40-49 | 0.4 (0.3-0.6) | 2.9 (1.9-4.4) | 0.6 (0.4-1.0) |
| 50-59 | 0.8 (0.5-1.2) | 4.6 (3.1-6.8) | 1.0 (0.6-1.6) |
| 60-69 | 1.6 (1.1-2.5) | 7.2 (4.9-10.6) | 1.6 (1.0-2.4) |
| 70-79 | 3.3 (2.2-4.9) | 11.2 (7.6-16.1) | 2.5 (1.6-3.8) |
| 80-89 | 6.6 (4.4-9.7) | 16.9 (11.7-23.8) | 3.8 (2.3-5.9) |
| 90-95 | 10.8 (7.2-15.8) | 22.5 (15.7-31.2) | - |

1.2.2 Incidence

Incidence of a disease can be described as the rate of occurrence of new cases. The cumulative incidence is calculated as the number of new cases in a time period, divided by a total population at risk. In POAG incidence studies are important to identify new risk factors that may help to direct future research into the pathophysiologic mechanism and define disease patterns. Unlike prevalence studies, there are a limited number of papers reporting the incidence of POAG.

The incidence of POAG in a white population was reported by Mukesh et. al, in 2002 involving 3271 participants aged >40 years in Melbourne, Australia (Mukesh et al., 2002). This study was conducted to determine the 5-year incidence of POAG from 1994 to 1999. Data from this study has indicated that the overall incidence of definite POAG was 0.5% per year. In participants aged 40-49 years there was no increase with age (0% per year) but the incidence was found to reached 4.1% per year in participants aged ≥80 years. Another study, in a predominantly white population in the Netherlands, reported an incidence of POAG of 0.6% per year (De Voogd et al., 2005). In a largely black population in Barbados, a study of the 9-year incidence of open angle glaucoma was found to be 4.4% or 0.5% per year. All these studies reach a similar conclusion that, the incidence rate rose with increasing age (Leske et al., 2007).

## 1.3 Pathophysiology of POAG

Early detection of POAG requires an in depth understanding of glaucoma pathophysiology. However, the exact pathogenesis of POAG is still not fully understood. There are two well documented theories related to the pathophysiology of POAG, the mechanical theory and vascular theory (Fechtner and Weinreb, 1994b)

1.3.1 Mechanical Theory (IOP-related)

The mechanical theory proposes that damage of ONH is induced by mechanical pressure upon the ganglion cell axons as they pass through the ONH. In primate studies, when IOP is elevated for a period of time, optic neuropathy develops

(Gaasterland et al., 1978, Harwerth et al., 1997). Supporting this proposal, are the findings of Cartwright and Anderson, 1988 who reported that in cases of POAG where the IOPs are within the normal range (normal tension glaucoma; NTG) the eye with higher IOP tends to have greater visual field loss. However, their findings were not supported by a later study of 60 NTG patients where only 13 were found to have significantly higher IOP in the eye with the more severe visual field defect (Haefliger and Hitchings, 1990a). This data suggests that there might be other factors contributing to the pathogenesis of glaucoma in NTG and POAG.

Evidence from previous experimental studies has revealed that in POAG, damaged of the ONH occurs at the lamina cribrosa (see figure 1.1)
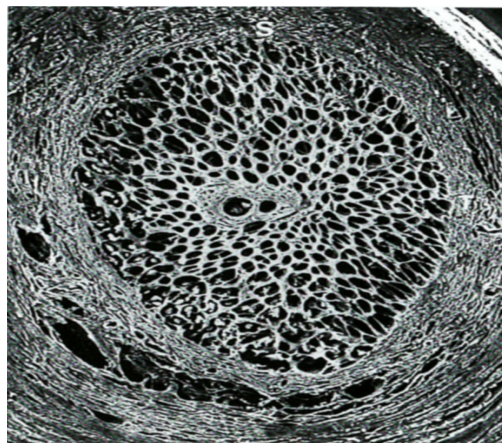


Figure 1.1: Collagenous beam of lamina cribrosa (Fechtner and Weinreb, 1994b)

The lamina cribrosa contains 400 to 500 channels through which the axons of the retinal ganglion cell (RGC) pass. There are approximately ten lamellar sheets with pores, which are aligned to allow nerve fibre bundles to pass through. Within the collagenous beams of the lamina cribrosa, there are blood vessels and extracellular matrix components, which are vital for axonal transport and nourishment of the axons. Apart from offering a conduit for optic nerve fibres and vascular supply, the lamina cribrosa is important in providing structural support for optic nerve fibers. Jonas suggested that the lamina cribrosa is the site where the elevated IOP could produce the damaging forces which lead to glaucomatous optic neuropathy (Jonas et al., 1991).

The largest pores of lamina cribrosa are located in superior and inferior section of the ONH giving it an hourglass configuration (Figure 1.2). The superior and inferior sections, with larger pores, have thinner connective tissue septae and offer less structural support to maintain pore integrity. In contrast the horizontal region consists of thicker connective tissue septae with smaller pores and is theoretically more resistant to mechanical distortion and damage from a raised IOP (Fechtner and Weinreb, 1994a). These sectional differences may account for some of the specific functional patterns of damage seen in glaucoma and the vertical elongation of the optic cup and thinning of the superior and inferior rim that are common early signs of glaucomatous damage (Quigley and Addicks, 1981, Radius and Gonzales, 1981). In addition, there are larger numbers of fibres passing through the superior and inferior part of the lamina cribrosa.
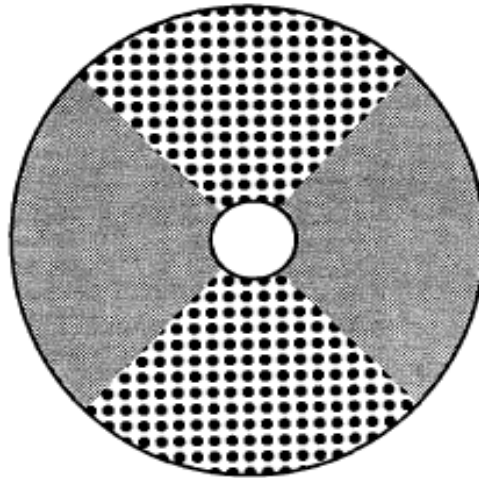
Figure 1.2: Sectional differences in lamina cribosa pores. The larger pores located in superior and inferior poles (Fechtner and Weinreb, 1994a)

1.3.2 Vascular theory

Many glaucoma patients do not have an elevated IOP when POAG is detected (Kroese and Burton, 2003). Furthermore, there are a group of patients with NTG who, even when carefully monitored, have never been found to have an elevated IOP. This is why elevated IOP alone is unable to explain the mechanism of damage in POAG. An alternative theory is that vascular mechanisms may play a role in the pathogenesis of glaucoma.

Vascular supply of the optic nerve head

A large and growing body of literature has investigated the vascular supply of the ONH (Fechtner and Weinreb, 1994a, Hayreh, 1995, Hayreh, 2001, Hayreh, 2009). There are three major sources of blood supply to ONH; from retinal arterioles, from

peripapillary choroid and from centripetal branches of the short posterior ciliary arteries, figure 1.3. With regard to a pathogenesis of glaucomatous damage, there are several mechanisms involved in the failure of microvasculature of the optic nerve to nourishing the axons (Hayreh, 2009). These include:

1. Loss of capillaries or alteration of blood flow in capillaries

2. Interference of nutrient delivery or removal of metabolic products from axons

3. Alterations in choroidal blood flow

4. Failure in blood flow regulation

5. Delivery of injurious vasoactive substance to the blood vessels of the optic nerve

6. Any combination of the above factors.
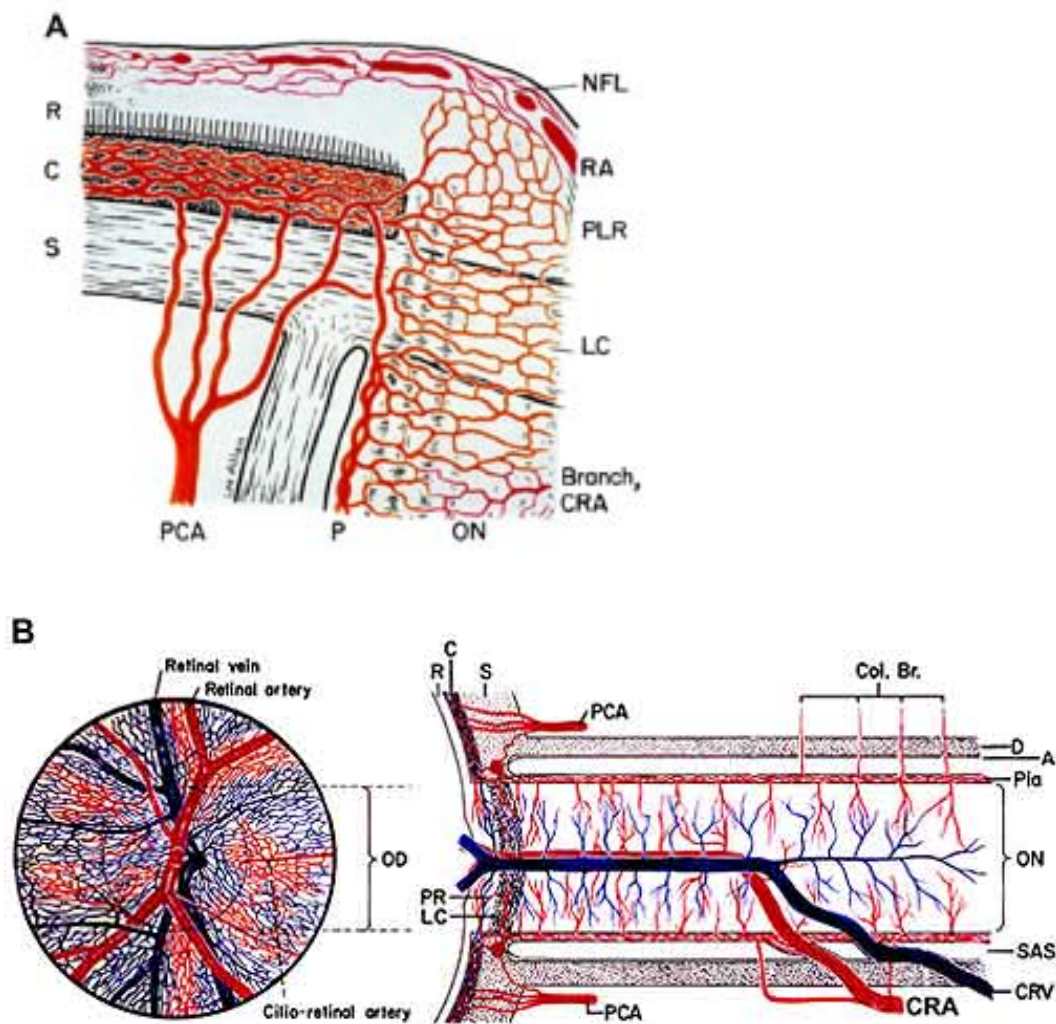
Figure 1.3: Schematic representation of blood supply at the optic nerve head (Hayreh, 2009)

## 1.4 POAG risk factors

Risk factors are features that may be causal in the disease. Risk factors are statistically correlated with the disease and may be present before the disease occurrence and play a significant role with other factor in the incidence of the disease. In POAG, although the exact mechanisms of glaucomatous damage are not

fully understood, there are a few risk factors have been identified from epidemiological studies.

## 1.4.1 Age

There is positive correlation between age and POAG (Boland and Quigley, 2007). People over 70 years of age are at 3-4 times higher risk of developing POAG than those who are 40-50 years old (Rudnicka et al., 2007). The death of ganglion cells and the length of time that the person is exposed to other risk factors before developing disease are factors which have a positive correlation with age (Boland and Quigley, 2007)

## 1.4.2 Individual Characteristic

Risk factors that explain the individual characteristic include gender, ethnicity and family history. There are inconsistencies in epidemiological and clinical studies, which express the strength of gender as a risk factor for POAG (Friedman et al., 2005, Lee et al., 2003a, Weih et al., 2001).

Numerous studies have indicated that those of an African derived race are more likely to have POAG than other ethnicities (Leske et al., 1994, Tielsch JM, 1991). The onset of POAG was found to be earlier in Africans and they are more frequently blind from POAG. There are two factors correlated with the increased risk in African decedents in developing POAG (Racette et al., 2003). Most African descendants are found to have larger optic discs with a smaller NRR area. This combines with lower number of nerve fibres. Second, the cornea thickness was found to be thinner than in other races.

Another well-known risk factor for POAG is having a first-degree relative with glaucoma. The Rotterdam Glaucoma Study reported that the relative risk for POAG was more than 10 times higher where there was a first degree relative (Wolfs et al., 1998). In the Barbados Population Family Study, 10% of living relatives examined had POAG (Nemesure et al., 2001).

1.4.3 Ocular Anatomy and Physiology

a. IOP

Almost every study has agreed that IOP is a well-established risk factor for POAG (Buhrmann et al., 2000, Quigley and Broman, 2006, Weih et al., 2001). Both clinical studies and population-based studies are consistent in showing that the level of IOP is an important factor in the mechanism of glaucomatous damage even when the level is within the normal range. This is in line with a study that demonstrated 25% to 75% of people with POAG have an IOP in the normal range (Quigley et al., 1992). Diurnal variation in IOP (Asrani et al., 2000), has also been implicated (Liu et al., 2003).

b. Myopia

Myopia as a risk factor for POAG has been identified in one population based study (Ramakrishnan et al., 2003). A possible explanation for this might be that myopic patients in developed countries access eye care more frequently than emmetropes. As POAG is asymptomatic in nature, the detection rate will inevitably be higher in those seeking regular eye care. However, there is also possibility that abnormal

collagen and connective tissue found in myopes may predispose to pathology at the lamina cribrosa and the ONH (Mitchell et al 1999; Jonas et al 2004).

### c. Central Corneal Thickness

The risk of developing POAG is higher in people who have a thinner central cornea. The positive correlation between central corneal thickness and POAG could be explained by two factors (Gordon et al., 2002). First, a thinner cornea gives lower applanation IOP values. Therefore, those with thinner corneas will present with lower IOPs and may have a delayed diagnosis. Second, it may be that central corneal thickness is a confounding factor for other undetermined parameters that have an impact in POAG.  It is postulated that, as the coats of the eye form a continuous structure, central cornea thickness is a surrogate measure of posterior scleral thickness. This may also explain the higher prevalence of glaucoma among myopic patients as they often have regional thinning of the sclera (Mitchell et al 1999; Jonas et al 2004).

### d. Optic Disc Diameter

Two population studies among European derived and African derived populations have demonstrated that a larger disc diameter is associated with increased risk of POAG (Healey and Mitchell, 2000, Quigley et al., 1999). Larger disc are found to have more nerve fibres and would have more initial structural reserve to delay glaucomatous damage. However, African derived people are found to have larger discs with relatively less NRR area. In contrast, European derived people and other ethnicity have equivalent disc diameter with a larger NRR area.

1.4.3 Systemic Diseases

a. Hypertension

Previous published data and case control studies have demonstrated that hypertension is a POAG risk factor. However, data from population-based surveys indicate that the correlation between hypertension and POAG is not straightforward and confounded by other risk factors that interact with blood pressure. Results from the Baltimore Eye Survey show that hypertension did not increase the risk of developing POAG in a population (Tielsch et al., 1995b). The finding that older hypertensives are more likely to have POAG than young hypertensives might be explained by the fact that age was a surrogate for duration of hypertension. The duration of hypertension might affect blood vessel function and the development of POAG. Interestingly, one study has found a modest association of uncontrolled hypertension with OAG. The result indicated that young hypertensive could benefit from higher perfusion pressure to preserve ganglion cell function (Bonomi et al., 2000).

b. Diabetes

Diabetes mellitus has been reported to be protective risk factor for the incidence of glaucoma (Gordon et al., 2002). Data from The Baltimore Eye Survey has reported that diabetic patients with high IOPs were not at risk of POAG (Tielsch et al., 1995a).

c. Migraine

A few studies have reported an association between migraine and POAG (Klein et al., 1993, Phelps and Corbett, 1985, Wang et al., 1997) and a clinical trial has

shown a relationship with rate of progression in POAG. The findings might be explained by a vasospastic phenomenon affecting neuronal nutrition at the ONH.

d. Sleep Apnoea

Several clinic-based studies have demonstrated that sleep apnoea is a risk factor for POAG, measured by different modalities including polysomnography, oximetry or questionnaire (Marcus et al., 2001, Mojon et al., Onen et al., 2000).

## 1.5 Detecting early structural changes

In considering the triad of glaucoma (raised IOP, visual field defect and ONH changes), structural assessment of ONH is one of the most important evaluations. Detailed and thorough examination of ONH is paramount in the management of glaucoma.  Although several imaging techniques are available in the clinical setting, these technologies do not replace ophthalmoscopic examination. Imaging devices can be used as adjuncts to facilitate the documentation or help quantify change. Clinicians rarely rely on photographs or ONH analysers in isolation. This is because the imaging technologies tend to report on a limited number of structures. For instance, Scanning Laser Polarimetry (SLP) measures the RNFL thickness and provides a probabilistic measure of glaucoma. Another example is Heidelberg Retina Tomography (HRT), which obtains high-resolution topographic images of the ONH. In contrast, ophthalmoscopic examination looks at many different parameters; the existence of a haemorrhage, changes to the vessels, peripapillary atrophy, optic disc shape and size, optic cup depth and others. By looking at the

wide range of parameters, the sensitivity to detect the early signs of POAG is improved.

### 1.5.1 Normal anatomy

The ONH includes the optic disc, peripapillary retina and the pre/post trabecular areas of the optic nerve. The normal optic disc is round or oval and pink in colour. Its diameter varies in size from 0.95 to 2.9mm, with the average dimensions being 1.9mm vertically and 1.7mm horizontally. Typically, it is flat or mildly elevated at the periphery with a central depression called the cup. RGC axons make up almost all the NRR tissue of the optic disc. These axons sweep in from all parts of the retina travelling in the RNFL. At the optic disc, they make a 90-degree turn to enter the optic nerve. A fine complex of capillaries surround and infiltrate the optic disc to supply oxygen and nutrition to the RGC fibres as they traverse this area. The blood supply and the axoplasm within the axons give the NRR and orange-red appearance. Within the central cup, there are no such axons and the lamina cribrosa can often be visualized. The lamina cribrosa is the sieve-like area of the scleral shell, which allows the exit of the nerve fibres. It is white in colour and thus the cup usually appears paler than surrounding NRR, see figure 1.4.

Figure 1.4: Anatomy of normal retina showing normal optic disc in and fovea

## 1.5.2 Sign of Damage in Optic Nerve Head

A thorough evaluation of optic nerve requires a stereoscopic view through a dilated pupil to obtain a detailed impression of topographic contour of the optic disc with accurate assessment of optic cup and NRR tissue. The most widely used technique of evaluation is with a slit lamp biomicroscope with a non-contact condensing lens;  90D, 78D and 60D lens. ONH parameters include:

*1.5.2.a. Optic disc size*

Optic disc size varies from one individual to another. The optic disc size is correlated with the size of the optic cup and NRR area. Normally, large optic disc have large optic cup with a large NRR area. However, small optic disc with small optic cup could suggest glaucomatous optic nerve damage (Jonas et al 1990a). Several studies, investigating biologic and demographic correlates in normal eyes, have shown that the optic disk area varies from about 0.80 to almost 6.00 mm$^2$, or about 1:7 (Bengtsson, 1976, Britton et al., 1987, Jonas et al., 1988). In normal eyes, the disc area is independent of age beyond an age of about 3 to 10 years (Bengtsson, 1976, Britton et al., 1987, Jonas et al., 1988)


*1.5.2.b. Optic disc shape*

The shape of the normal optic disc is slightly oval vertically; with the vertical diameter  7-10% larger than horizontal diameter. An abnormal optic disc shape is significantly correlated with corneal astigmatism and amblyopia (Jonas et al., 1997). Eyes with a tilted optic disc can present with a visual field defect similar to that seen in POAG. Eyes with tilted disc are very difficult to evaluate and any diagnosis of POAG will be largely focused on functional loss.


*1.5.2.c. Neuroretinal rim size and shape*

The NRR area is positively correlated with optic disc size and optic nerve fibre count (Quigley et al, 1999; Jonas et al., 1992c). It is also correlated with the number and area of lamina cribrosa pores (Jonas et al., 1991d). The NRR is usually broadest in the Inferior disc region, followed by the Superior disc region, the Nasal disc region

and finally the Temporal disc region. This relationship is known as the ISN'T rule, as termed by Elliot Werner/Philadelphia (Jonas, 1988). Breakdown of the ISNT rule is common in early glaucoma due to the selective loss of superior and inferior fibres, see figure 1.5.

Notching is seen most frequently in the inferior NRR (Airaksinen PJ et al., 1985, Spaeth G et al., 1976) and refers to localized thinning, which outpaces generalized rim loss. Inferior notching is usually associated with a superior well-localized scotoma. Thinning at the inferior and superior NRR is associated with a loss of supportive connective tissue resulting in reduced mechanical support for the nerve fibres in those regions (Quigley et al., 1981; Dondana L et al., 1996).
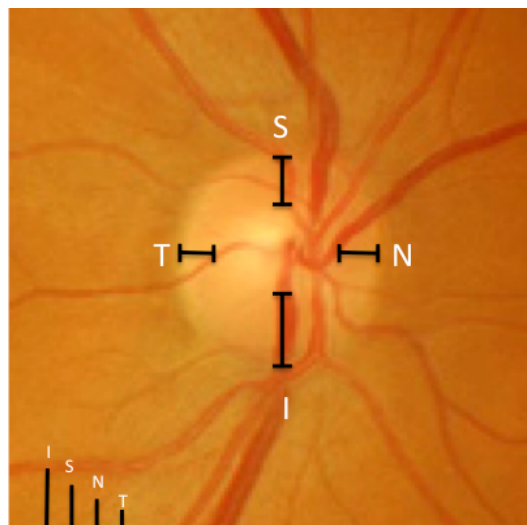


Figure 1.5: Neuroretinal rim width evaluation using ISNT rule. Normally the NRR is thickest Inferiorly and thinnest Temporally.

*1.5.2.d. Cup-to-disc ratio (CDR)*

The CDR compares the vertical and horizontal size of the cup to the overall size of the disc. As a rule of thumb, the greater the CDR, the higher the likelihood of glaucoma. However, the CDR is highly variable and dependent upon the size of the optic disc and the number of nerve fibres (see figure 1.6). Spaeth et al., 2002, introduced the Disc Damage Likelihood Scale (DDLS). DDLS is based on the ratio of appearance of the NRR to optic disc size and focal thinning of the rim area (see figure 1.7). Several studies have evaluated the performance of this method and found it to have good reproducibility (Spaeth et al., 2002) and better performance than the cup/disc ratio (Danesh-Meyer et al., 2006).
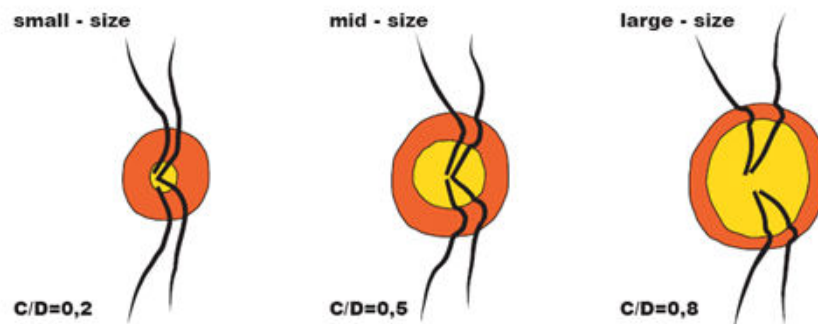


Figure 1.6: Illustration of variability in physiological cup size with disc size (European Glaucoma Society, 2003)

| | Narrowest width of rim (rim/disk ratio) | | | | Examples | | |
|---|---|---|---|---|---|---|---|
| DDLS stage | For small disk < 1.50 mm | For average size disk 1.50-2.00 mm | For large disk > 2.00 mm | DDLS stage | 1.25 mm optic nerve | 1.75 mm optic nerve | 2.25 mm optic nerve |
| 1 | 0.5 or more | 0.4 or more | 0.3 or more | 0a | | | |
| 2 | 0.4 to 0.49 | 0.3 to 0.39 | 0.2 to 0.39 | 0b | | | |
| 3 | 0.3 to 0.39 | 0.2 to 0.29 | 0.1 to 0.19 | 1 | | | |
| 4 | 0.2 to 0.29 | 0.1 to 0.19 | Less than 0.1 | 2 | | | |
| 5 | 0.1 to 0.19 | Less than 0.1 | 0 for less than 45° | 3 | | | |
| 6 | Less than 0.1 | 0 for less than 45° | 0 for 46° to 90° | 4 | | | |
| 7 | 0 for less than 45° | 0 for 46° to 90° | 0 for 91° to 180° | 5 | | | |
| 8 | 0 for 46° to 90° | 0 fo 91° to 180° | 0 for 181° to 270° | 6 | | | |
| 9 | 0 fo 91° to 180° | 0 for 181° to 270° | 0 for more than 270° | 7a | | | |
| 10 | 0 for more than 180° | 0 for more than 270° | | 7b | | | |

Figure 1.7: The disc damage likelihood scale (reproduced from Spaeth et al., 2002)

## 1.5.2.e. Configuration and depth of the optic cup

Normal optic cup shape is horizontally oval; with horizontal diameter ~8% longer than vertical diameter (Jonas et al, 1088c). The combination of a horizontally oval cup with a vertically oval disc explains the configuration of the normal NRR, which has the broadest area in the inferior and superior regions. There is also a

relationship between the depth of the cup and degree of peripapillary atrophy (Jonas et al., 1992 a). The deeper the optic cup, the smaller the peripapillary atrophy

*1.5.2.f Optic disc haemorrhages*

Splinter-shaped or flame-shaped haemorrhages at the border of the optic disc are A Hallmark of glaucomatous optic nerve atrophy (Drance and Begg, 1970; Drance et al., 1977), see figure 1.8. The exact pathophysiology of optic disc haemorrhages is not known. Disc haemorrhages are normally found at the infero-temporal or supero-temporal disc regions. They are associated with localized RNFL defects, NRR notches and significant glaucomatous field loss (Airaksinen et al 1981b). Since the optic disc haemorrhages are rarely found in normal eyes, their presence is an important diagnostic sign of POAG (Susanna et al., 1979; (Airaksinen et al., 1981).

a. Notching in inferior NRR     b. Optic disc hemorrhages     c. Normal optic disc
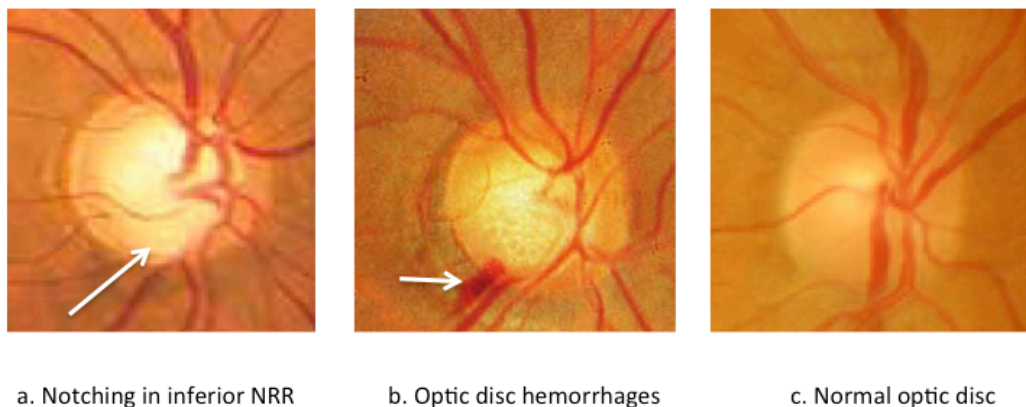
Figure 1.8: Sign of glaucomatous ONH including; a) Clinical feature of inferior NRR notching and b) Optic disc haemorrhages at 7o'clock position. c) Normal optic disc

*1.5.2.g. Peripapillary Atrophy*

Peripapillary arophy (PPA) has so far been differentiated into a central beta zone and a peripheral alpha zone (Jonas et al., 1989b). Recent studies have demonstrated now that in some medium myopic eyes, the end of Bruch's membrane did not touch the optic disc border (Lee et al., 2010, Manjunath et al., 2011, Hayashi et al., 2012, Park et al., 2012, Reis et al., 2012). Since this region without Bruch's membrane did not fulfill the definition of the alpha zone nor of the beta zone, it may be called the gamma zone, see figure 1.9. The alpha zone is characterized by an irregular hypopigmentation and thinning of the chorioretinal tissue layer. The outer border is adjacent to the retina, whereas the inner border is in touch with beta zone or with the peripapillary scleral ring. Alpha zone PPA has less clinical significance in the setting of glaucoma. Beta zone is usually a crescent of depigmentation caused by retraction of the retinal pigment epithelium (RPE) layer next to the disc allowing relative baring of sclera. Beta zone PPA is common

finding in glaucomatous eyes. If both zones are present, beta zone is always closer to the optic disc than alpha zone. The location of PPA is spatially correlated with the NRR loss in the intra papillary region (Jonas and Naumann, 1989a; Jonas 1992a). It is larger at the sector with more marked loss of NRR. The region without Bruch's membrane was termed gamma zone and it was correlated stronger with axial myopia than with glaucomatous optic nerve damage (Jonas et al., 2016).
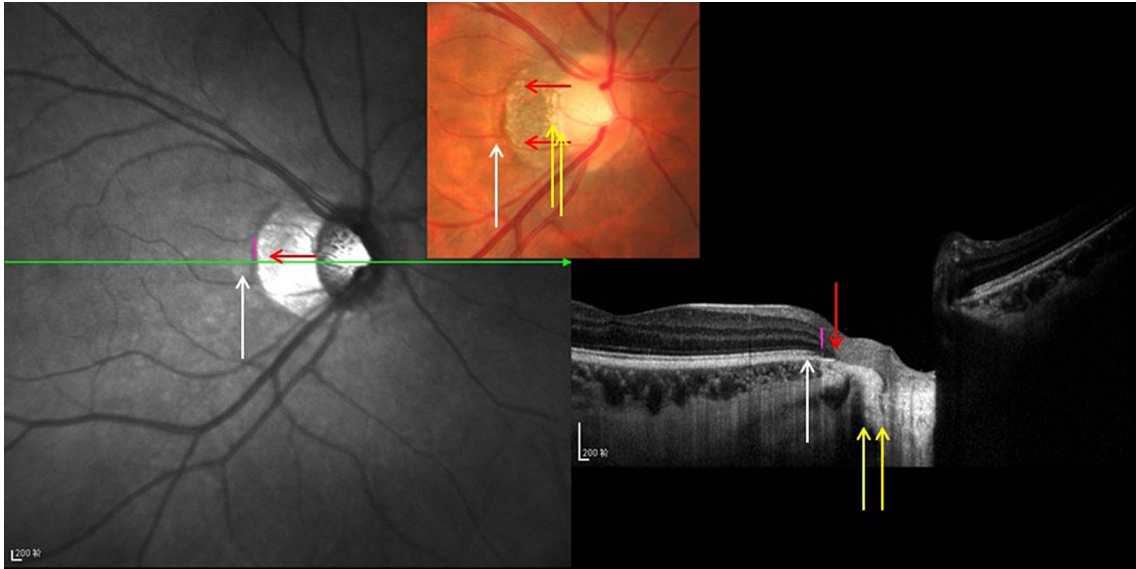
Figure 1.9: Optical coherence tomogram showing the parapapillary gamma zone between the end of Bruch's membrane (red arrows) and the peripapillary ring (between the yellow double arrows), parapapillary beta zone between the end of Bruch's membrane (red arrows) and the beginning of irregular retinal pigment epithelium (short vertical purple stroke), and the parapapillary alpha zone between the beginning of irregular retinal pigment epithelium (short vertical purple stroke) and the beginning of the regular retinal pigment epithelium (vertical white arrow). Length of macular Bruch's membrane was defined as the distance between the foveola (shown by the foveal depression) and the end of Bruch's membrane (red arrows) (reproduced from Jonas et al., 2016).

### 1.5.2.h. Retinal nerve fibre layer

The evaluation of RNFL is important in discriminating between early glaucoma and normal eyes. POAG can be associated with a diffuse or localised loss of the RNFL. In early POAG, localised RNFL defects are seen more often than in advanced POAG (Sugiyama et al., 1999). Localised loss can be seen as dark stripes or wedge shaped defects in the usual reflective sheen of the RNFL. These defects follow the

normal retinal striation and are best seen at the transition point between normal and abnormal areas. They are highly correlated with visual field loss (Quigley et al., 1980; Sommer et.al., 1977). Results from experimental studies suggested that localized RNFL defects can only be detected ophthalmoscopically if more than 50% of the thickness of the RNFL is lost (Quigley and Addicks, 1982)

**1.5.3 Detecting structural changes using imaging devices**

There is wide variety of optic disc appearance in the normal population and many parameters show a great deal of overlap between glaucomatous and normal eyes. A single abnormal feature is rarely sufficient to make a diagnosis. Despite the fact that in some cases functional changes may be recognized before structural changes, for many patients, the earliest detectable manifestation of glaucoma is a structural change of the ONH or RNFL (Kass et al., 2002, Miglior et al., 2005). Glaucomatous structural changes are usually detected by slit lamp fundoscopic examination or from assessment of stereo photographs; however, due to inter-observer variability, diagnosing early changes in this manner can be challenging (Jampel et al., 2009, Reus et al., 2010). Imaging devices can provide objective repeatable structural measure of the ONH and RNFL (Leung et al., 2009, Mwanza et al., 2012, Zangwill et al., 2001).

1.5.3.a Fundus photography

Subjective assessment of ONH and RNFL photographs, using a fundus camera, is valuable for the detection and diagnosis of glaucoma. The photographs can be used

to document the status of the ONH and RNFL and aid the recognition of change. Imaging may also focus on particular structure or aspect of the retina. In colour fundus photography, contrast filters can be used to modify the spectral range of the illumination source and enhance the visibility of certain structures. For example, the visibility of choroid and choroidal pattern of vessels can be enhanced using red light due to the poor absorption of red light by retinal pigment epithelium (RPE). Green light is absorbed by blood and reflected by RPE, increasing the contrast of the retinal vascular network and haemorrhages. Evaluation of optic disc damage through photographs has been used in 3 randomized control trials; European glaucoma prevention study, Early Manifest glaucoma Trial (EMGT) and Ocular Hypertension Treatment Study (OHTS). These studies have shown that structural evaluation of ONH is reproducible (Parrish et al., 2005, Zeyen et al., 2003).

### 1.5.3.b Confocal Scanning Laser Tomography

Confocal Scanning Laser Tomography (CSLO) is an imaging device that allows quantitative three-dimensional imaging of the ONH and posterior segment. The HRT is a commercially available CSLO instrument. The HRT uses a 670nm diode laser beam to obtain 32 scans of the retina. The stack of 32 coronal planes, each with 384x384 pixels are assembled to give height measurements of the retinal nerve fibre layer and ONH topography (Weinreb et al., 1989).

The scans are done three times and three maps are generated. Each pixel will thus have three height values attributed to it and the software presents the mean of these as well as the standard deviation. The closer the three scans are to each

other, the more reliable the analysis will be. Once the scan is obtained, the operator will draw a line (disc contour) manually around the disc and the software calculates stereo-metric parameters within the ring. Values are presented for the whole disc and for the six predefined sectors.

Some of the parameters obtained from this technology are rim area, rim volume, cup shape measure, linear CDR, retinal height variation along the contour line and RNFL thickness. The Moorfields Regression Analysis is used to analyse the data generated by the HRT II and HRT III. It is based upon a sample size of 112 normal white subjects and 77 patients with early glaucoma. Eyes included had a refractive error less than 6D and a disc size between 1.2 and 2.8 mm$^2$. In HRT III, a Glaucoma Probability Score is also included. This is a new automated algorithm that evaluates both optic disc and parapappillary RNFL topography to provide probabilistic score of glaucoma. The results from several studies investigating the diagnostic accuracy between Moorfields Regression Analysis and Glaucoma Probability Score have been conflicting; especially regarding sensitivity where it seems that Moorfields Regression Analysis offers slightly higher specificity than Glaucoma Probability Score (Bozkurt et al., 2010, Coops et al., 2006, De Leon-Ortega et al., 2007, Harizman et al., 2006)

The usefulness of CSLO in measuring longitudinal changes can be seen from previous studies (Harasymowycz et al., 2005, Miglior et al., 2003, Wollstein et al., 2000, Wollstein et al., 1998). A recent study evaluating NRR area changes in in eyes with suspected glaucoma found the average rate of rim area loss, measured using CSLO, to be almost 4 times faster in eyes that developed visual field loss over an average follow-up period of more than 6 years (Medeiros et al., 2014). In the

glaucoma sample, change in NRR area, as measured using CSLO morphologic loss analysis, is associated with subsequent visual field progression (Chauhan et al., 2009).

### 1.5.3.d  Scanning Laser Polarimetry

Scanning Laser Polarimetry  (SLP) is a non-invasive method for evaluating RNFL thickness. The first available commercial SLP was the GDx Nerve Fiber Analyzer (Laser Diagnostic Technologies, Inc., San Diego, CA). The instrument consists of a confocal scanning laser ophthalmoscope with a polarized laser beam. When polarized light passes through a thin grating, the plane of polarisation is rotated. If the grating is thick, then the degree of rotation will be large (Sehi et al., 2007). The rotation of the plane of polarisation is a manifestation of birefringence. SLP measures changes in polarization occurring when a light beam encounters tissues with birefringent properties (Anton et al., 1997, Bowd et al., 2003, Weinreb et al., 1990). The main sources of birefringence in the eye are the cornea and the RNFL due to the linear orientation of the corneal fibres and RGC axons. Fortune and colleagues recently demonstrated that loss of RNFL polarization could occur earlier than RNFL thinning (Fortune et al., 2013). In this study, 41 rhesus macaques with experimental glaucoma had been examined using spectra domain Ocular Coherent Tomography (OCT) and SLP to obtain measurements of RNFL thickness and RNFL retardance. During follow-up, 33 of 41 eyes reached a structural endpoint and of these 79% had evidence of reduced RNFL retardance before a reduction in RNFL thickness. They hypothesized that axonal cytoskeletal disruption precedes axonal loss, and measurement of RNFL birefringence and might allow earlier detection of glaucomatous damage than measurements of the RNFL thickness.

The updated version of GDx, known as GDxVCC (device with variable cornea compensation) has been developed to allow individualized eye-specific compensation of anterior segment birefringence.

### 1.5.3.e Optical Coherence Tomography

OCT uses low-coherence interferometry to perform high-resolution cross-sectional imaging of retina and optic nerve head. It is like an ultrasound device, except it uses light instead of sound.

Since its first application for ocular imaging in 1991, OCT has undergone tremendous technological improvements. The early time-domain OCT has been superseded by spectral domain OCT. Spectral domain OCT offers a better temporal and spatial resolution and allows 3D imaging of the retina and optic disc with high resolution and high speed. In addition, improved segmentation of the retinal layers has aided detection of subtle changes in optic disc and RNFL morphology. Spectral domain OCT has lower measurement variability than time domain OCT with improved performance in detecting glaucoma progression (Leung et al., 2009, Leung et al., 2011).

Early work on POAG with OCT focused on the optic nerve head and circumpapillary RNFL. More recently the value of macular imaging has been recognized (Mwanza et al., 2012).

Several studies have reported on the discriminatory power of OCT to differentiate between POAG and normal healthy eyes. Time domain OCT achieved specificities of ~90%, with sensitivities of 70–80% (Mwanza et al., 2012). Although the

performance of spectral domain OCT was found to be similar, the reproducibility was found to be better (Leung et al., 2009, Park et al., 2009, Vizzeri et al., 2009). The work of Leung et al looked at the RNFL in 97 POAG eyes and 83 health eyes using spectral domain OCT and reported a sensitivity of 91.6%, for a specificity of 87.6%, and an area under the ROC curve of 0.962 (Leung et al., 2009).

As mentioned in the earlier part of this chapter, recognizing the localized RNFL loss, particularly in the most frequently affected regions; inferotemporal and superotemporal sectors (Lisboa et al., 2012, Moreno-Montanes et al., 2010, Park et al., 2009) is important when detecting early stage disease. Recent findings suggested that RNFL thinning in the supero-temporal and infero-temporal sectors tends to have the best diagnostic performance in early disease (Lisboa et al., 2012).

Recent histological study and clinical observations utilizing spectral domain OCT in nonhuman primates has proposed new structural measure in glaucoma diagnosis, known as Bruch's membrane opening-minimum rim width (BMOMRW) (Chauhan et al., 2013). This study provides new insights in glaucoma diagnosis using novel techniques and challenges the traditional way of determining the landmark of the NRR width, normally measured from disc margin to inner rim. BMOMRW measures minimum rim width from the true outer border of the rim in contrast to old method that suffers from an error affected by tissue orientation and the possibility that NRR may extend inside the disc margin. Comparing the performance of RNFL thickness and BMOMRW in 107 patients with early glaucoma (average MD of -3.92dB) and 48 healthy controls, Chauhan reported 81% sensitivity at 95% specificity compared to only 70% for RNFL thickness (Chauhan et al., 2013), see figure 1.10.

Danthurebandara and colleagues carried out similar study of 151 glaucoma patients and report that the structure–function relationship with BMOMRW was not significantly different from that of RNFL (Danthurebandara et al., 2015). Further work is required to determine the usefulness of BMOMRW as a better index than RNFL for detecting early glaucoma.
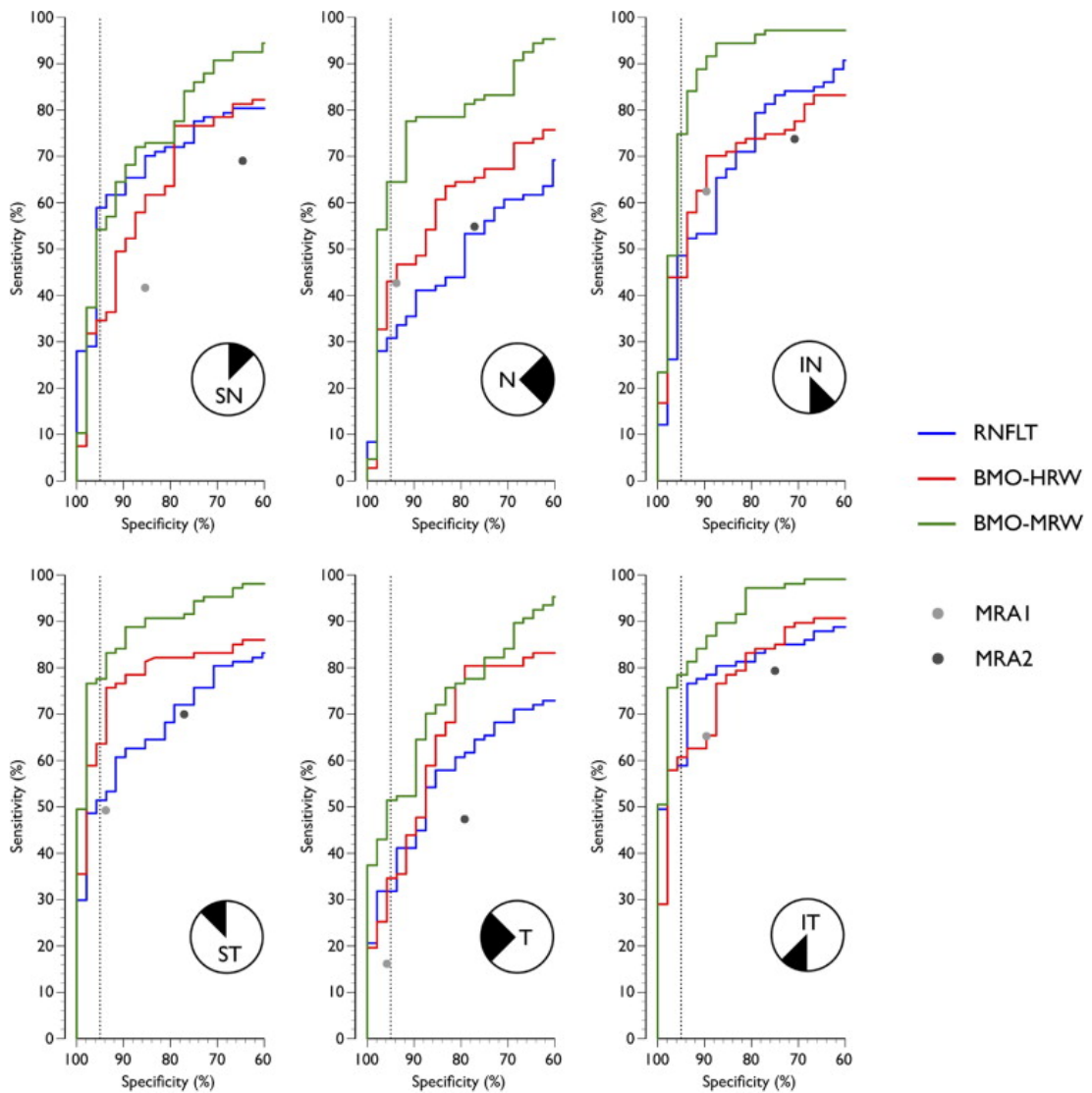
Figure 1.10: The confocal scanning laser tomography ROC curves illustrating the diagnostic performance of retinal nerve fiber layer thickness, Bruch's membrane opening-horizontal rim width, and Bruch's membrane opening-minimum rim width computed for the 6 sectors. Also shown are the 2 discrete points of the sectoral Moorfields Regression Analysis from confocal scanning laser tomography, conservative Moorfields Regression Analysis (MRA1) where "borderline" cases were classified as normal, and liberal Moorfields Regression Analysis (MRA2) where "borderline" cases were classified as abnormal. *Dashed vertical line* indicates specificity of 95%. IN = inferonasal; IT=inferotemporal; N=nasal; SN=superonasal; ST=superotemporal; T=temporal (Chauhan et al., 2013).

Images of the lamina cribosa could become routinely available in the near future (Burgoyne et al., 2005, Lee et al., 2014a, Park et al., 2012, Seo et al., 2014, Sigal et al., 2014). Evidence from histological and spectral domain OCT studies reveal IOP-related changes in the lamina cribosa including posterior lamina displacement, lamina thinning, pore deformities, and lamina defects (Kim et al., 2013, Park et al., 2012, Sigal et al., 2014, Tatham et al., 2014).

## 1.5.4 Agreement between the imaging devices

Medeiros et al undertook ONH and RNFL assessments using 3 optical imaging techniques; SLP with variable corneal compensation (GDx VCC), CSLO (HRT II), and OCT (Stratus OCT) in 75 patients with glaucomatous visual field loss and 66 healthy age matched subjects to compare the discrimination abilities of these devices. Results found that there were no significant difference between the areas under the receiver operating characteristic curves (AUROC) for the best parameters from the GDx VCC (nerve fiber indicator, AUROC=0.91), Stratus OCT (retinal nerve fiber layer inferior thickness, AUROC=0.92), and HRT II (linear discriminant function, AUROC=0.86) (Figure 1.11). The agreement between these devices, which is poor, is illustrated in Figure 1.12. The author concluded that performance of best parameters from each device in detecting glaucomatous defect were similar (Medeiros et al., 2004).
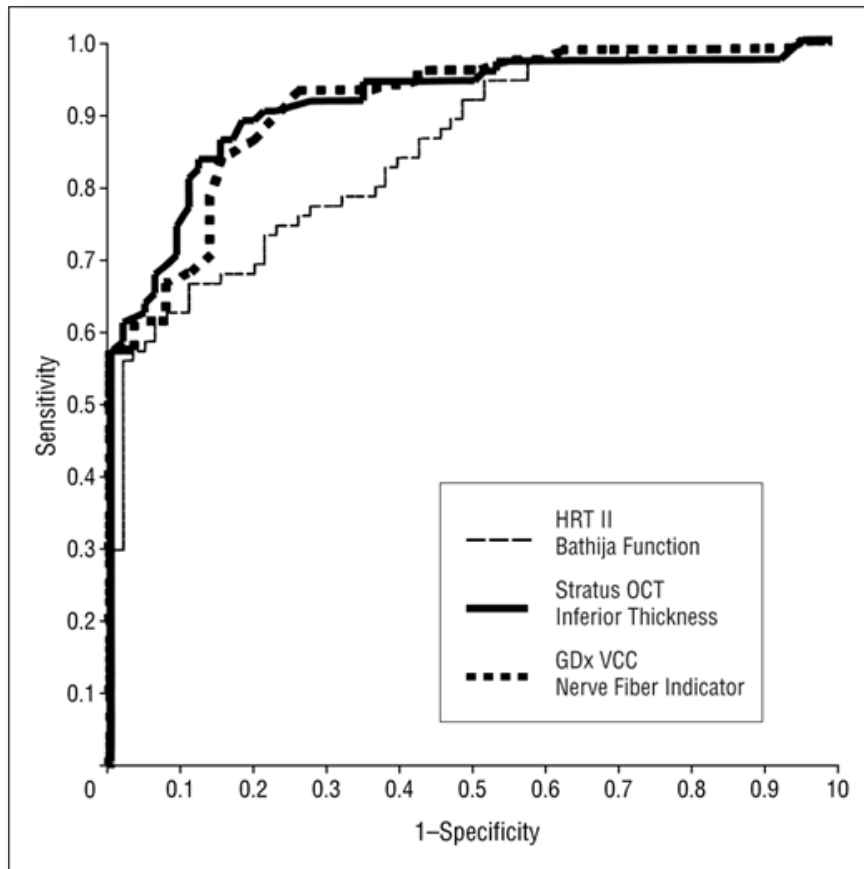
Figure 1.11: Receiver operating characteristic curves of the best parameters from the GDx VCC scanning laser polarimeter, HRT II confocal scanning laser ophthalmoscope and Stratus OCT optical coherence tomograph (Medeiros Fa, 2004, Medeiros et al., 2004)
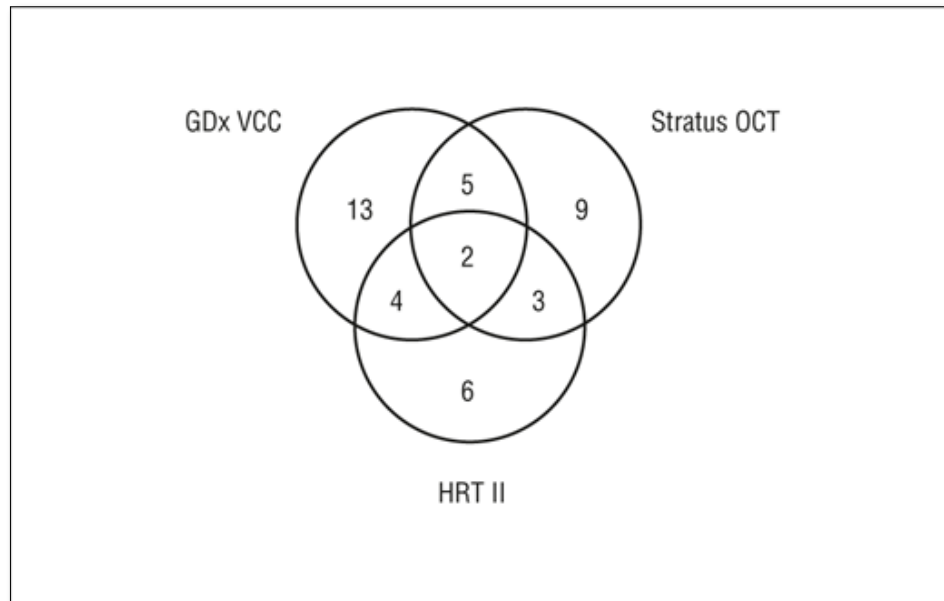
Figure 1.12: Venn diagram showing the agreement between the GDx (Laser Diagnostic Technologies, Inc, San Diego, Calif), HRT II (Heidelberg Retina Tomograph; Heidelberg Engineering, Dossenheim, Germany), and Stratus OCT (Carl ZeissMeditec, Inc, Dublin, Calif) (Medeiros et al., 2004) in identification of images classified as unacceptable from each devices. Image reproduced from (Medeiros et al., 2004)

## 1.6 Detecting early functional change

### 1.6.1 Glaucomatous visual field defect

The visual field has been defined as "all the space that one eye can see at any given instant" (Tate and Lynn, 1977). In this definition, the term 'space' is used to highlight the three-dimensional volume of the visual field. The extent of the normal visual field, measured from the point of fixation for a bright stimulus are approximately 60 degrees up, 75 degrees down, 100 degrees temporal and 60 degrees nasal. With both eyes open, the visual field extends 200 degrees horizontally (100 degrees temporal for each eye), while the vertical extent remains the same

A number of different methods have been proposed in the past for classifying both the severity and characteristics of visual field defects. In 2002, Foster and associates proposed a standardize definition of glaucomatous damage which included the following:

1. *The glaucoma hemifield test (GHT) graded "outside normal limits"*

2. *Cluster of three contiguous points at the 5% level on the pattern deviation plot, using the threshold test strategy with the 24-2 test pattern of the Zeiss-Humphrey Field Analyzer 2*

(Foster et al., 2002)

In this standardize definition, 2 important aspects of visual field response are evaluated in order to discriminate between normal and glaucomatous eyes; vertical asymmetry between the defects in the superior and inferior hemifields and the occurrence of group of depressed points within a certain radius. Sup/Inf hemifield

asymmetry in the eye will be discussed in Chapter 3. The following will briefly discuss the clustering of defective test locations.

### 1.6.1.a Clustering of defective test locations in POAG
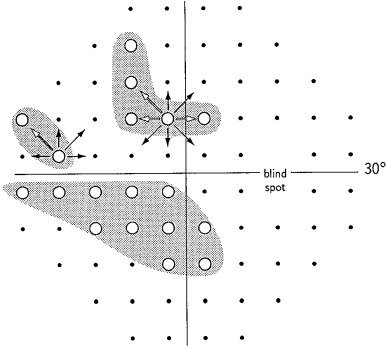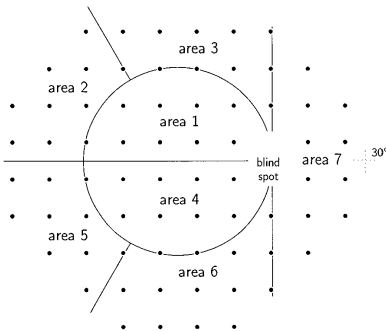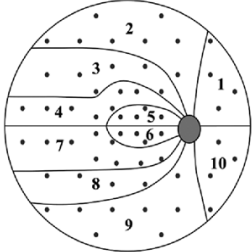
A cluster is defined as a group of test points within a certain radius of area with abnormally depressed sensitivity – e.g. points with differential light sensitivity $p<0.05$ in the Statpac Pattern Deviation Probability (PDP) map (Heijl et al., 1987b).

Previous studies have validated the importance of cluster analysis in the early detection of glaucomatous visual field loss (Asman and Heijl, 1993, Chauhan et al., 1988, Henson and Dix, 1984). Using a supra-threshold algorithm with the Friedmann Visual Field Analyser (FVFA) in 146 normal eyes, Henson et al (1984) found that 13% had a cluster of two or more 4dB defects and that 0.7% had a cluster of three 4dB defects. However, none of their sample had a cluster of two or more defects at ≥6dB. In this study the included radius was 7.5° (Henson and Dix, 1984).

Asman and Heijl evaluated cluster analysis in 87 eyes of 87 normal subjects and 101 eyes of 101 patients with glaucoma. In this analysis, test locations were assigned into 7 different sectors which corresponded to the anatomy of the normal retinal nerve fibre layer. Their findings suggested that an analysis using sectors was superior to traditional cluster analysis for discriminating early glaucomatous visual field loss (Asman and Heijl, 1993).

Different methods of clusters evaluation have been proposed in previous studies, see Table 1.2.

**Table 1.2: Different methods in evaluating cluster defect in glaucomatous field loss.**

| Study | Type of cluster | Perimeter |
|---|---|---|
| **Cluster analysis in visual field quantification**<br>**(Chauhan et al., 1988)** |  | Friedman Visual Field Analyser (FVFA) |
| **Arcuate cluster Analysis in glaucoma perimetry.**<br>**(Asman and Heijl, 1993)** |  | Humphrey Field Analyser (HFA) |
| **Detection of early glaucomatous progression with octopus cluster trend analysis**<br>**(Naghizadeh and Hollo, 2014)** | In Octopus perimetry the test points follow the nerve fiber bundle distribution and their density is higher around the macula | Octopus perimetry |

## 1.6.2 Visual Field Tests

Visual field tests can be divided into two main types; kinetic and static. Kinetic refers to a test in which a stimulus of constant size and intensity is moved around the visual field. In static tests the stimuli remain stationary and the intensity varies. Some static tests use a supra-threshold algorithm, where the stimuli are present at an intensity that is calculated to be slightly above the patient's threshold. Other types of static test use a threshold algorithm and derive an estimate of the eye's threshold at a whole series of different test locations. Several threshold algorithms have been developed including; Full threshold (FT), Fast-Threshold, Dynamic Strategy, Tendency Oriented Perimetry (TOP) and the Swedish Interactive Threshold Algorithm (SITA). SITA is currently the most widely used algorithm for the detection and follow-up of glaucomatous functional loss (Alencar and Medeiros, 2011).

Static threshold testing with a white stimulus on a white background is commonly termed Standard Automated Perimetry (SAP).

In an effort to facilitate the interpretation of functional loss, the results of a SAP test are often subjected to a series of mathematical and graphical procedures. These include the grey scale plot, the computation of sensitivity deviations from normal age-corrected values and the calculation of probability values. Many of these indices can be seen in the standard print out from a SAP test, see figure 1.13.

CENTRAL 24-2 THRESHOLD TEST

FIXATION MONITOR: GAZE/BLIND SPOT          STIMULUS: III. WHITE          PUPIL DIAMETER:          DATE:
FIXATION TARGET: CENTRAL                   BACKGROUND: 31.5 ASB          VISUAL ACUITY:           TIME:
FIXATION LOSSES: 0/11                       STRATEGY: SITA-FAST          RX: −0.75 DS  −0.25 DC X 65    AGE: 74
FALSE POS ERRORS:  1 %
FALSE NEG ERRORS:  0 %
TEST DURATION: 03:46

FOVEA: OFF

```
                    25  25   20  21
                28  28  26  24  25  22
            27  29  32  29  28  26  26  25
        28  26  29  32  33  31  29   8  27
    30  24  25  30  32  33  33  30  13  30  ─── 30
        29  30  30  32  31  32  30  29
            28  30  30  29  30  28
                26  28   26  29
```

```
        -1 -1 |-6 -4                           -2 -2 |-7 -5
      0 -1 -3 |-4 -3 -5                       -1 -2 -3 |-5 -3 -6
   -1 -1  1 -1 |-2 -3 -2 -3                   -2 -2  1 -2 |-3 -4 -3 -4
   2 -3 -1  1  1 | 0 -1    -1                  1 -4 -2  0  0 |-1 -2    -2
  -2 -4  0  1  1 | 1 -1     1                 -3 -5 -1  0  0 | 0 -2     0
     0  0 -1  0 |-1  1  0  0                  -1 -1 -2 -1 |-1  0 -1 -1
      -1 -1  0 |-2  0 -1                        -2 -1 -1 |-2 -1 -2
        -3 -3 |-3  0                              -4 -4 |-4 -1
```
Total deviation                              Pattern deviation

GHT

Within normal limits

VFI      98%

MD      −1.02 dB

PSD      1.72 dB  P < 10%

```
       ·  · | ::  ·                              ·  · |◪  ·
     ·  ·  · |::  ·  ::                         ·  ·  · |◪  ·  ::
   ·  ·  ·  · | ·  :: ·                       ·  ·  ·  · | ·  :: · ::
  · :: |::  ·  ·  ·                          · :: |  ·  ·  · ·
   · ◪  ·  ·  · |  ·  ·                       · ◪  ·  ·  · |  ·  ·
     ·  ·  ·  · |  ·  ·                         ·  ·  ·  · |  ·  ·
       · :: ::  ·                                :: :: :: ·
```

:: < 5%
◪ < 2%
▨ < 1%
■ < 0.5%
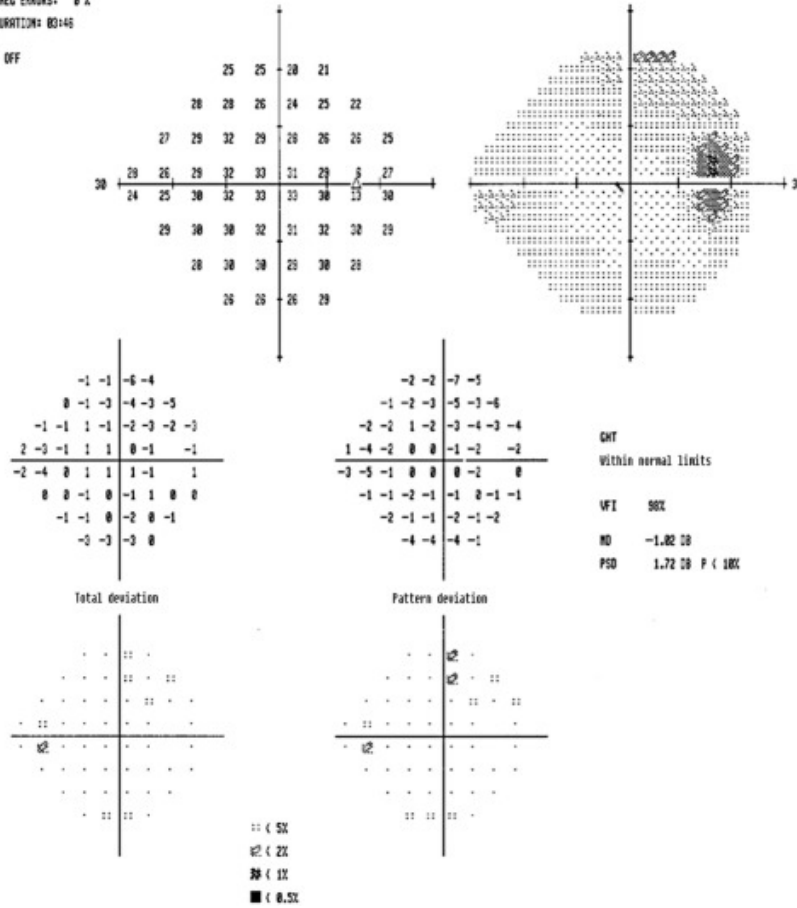
### 1.6.2.1 Statistical Indices found in SAP

#### 1.6.2.1 a. Fixation losses

The fixation losses rate provides an estimate of how steadily an eye fixates during the test. The rate is determined using Heijil-Krakau technique, which periodically presents a supra-threshold target in the predetermined location of the blind spot. If the patient responds positively to the stimulus, it is assumed that they were not fixating appropriately. Katz and Sommer suggested that fixation losses of more than 30% are not acceptable (Katz and Sommer, 1988). High fixation losses together with high false positive rates indicate a 'trigger-happy' patient with low reliability. The Humphrey Field Analyzer (HFA) II also incorporates a gaze tracking method that displays a bar chart on the printout. A full-scale spike indicates a 10° or greater eye movement.

#### 1.6.2.1 b. False positive catch trials

False positive (FP) errors indicate a trigger-happy patient who is responding when no stimulus is presented. The cut off point for the result to be acceptable is below 33%.

#### 1.6.2.1 c. False negative catch trials

False negative (FN) errors occur when the patient fails to respond to a supra-threshold target (9dB brighter than threshold) at a given location and are

associated with fatigue and/or inattention. The FN value should be less than 20%. In an abnormal field, particularly glaucoma, FN rates are higher.

### 1.6.2.2. Global Indices

Global indices reduce all the threshold data to a single number that is designed to describe specific characteristics of loss seen in glaucomatous eyes (Heijil et al, 1987). The value of the index and the probability of it being within normal limits are given on the standard printout, see figure 1.13.

#### 1.6.2.2 *a. Mean Deviation*

Mean Deviation (MD) is a measure of the average difference between the measured sensitivity and that of an age matched normal patient (defect values) weighted for the test location. It is used to monitor the overall change in the visual field.

#### 1.6.2.2 b. *Pattern standard deviation*

Pattern Standard Deviation (PSD) is a measure of non-uniformity in the shape of hill of visions i.e. it sensitive to early scotoma. It is a measure of variance in the defect values that have been weighted according to the normally occurring scatter that occurs at each retinal location.

### 1.6.2.3. Total Deviation Map

The total deviation map (TD) compares the result with an age matched normal population and gives the difference on a point-by-point basis. The numerical display illustrates the deviation (in Decibels) from the age-matched sensitivity. Positive values represent the increase from the normal range, while the negative value represent the reduction from normal. The accompanying Total Deviation Probability map takes into account normal variability at each location to give a probability score (Heijl et al., 1987a).

### 1.6.2.4. Pattern Deviation Map

The Pattern Deviation map (PD) compares the result with an age-matched normal population corrected for the overall level of sensitivity. This is obtained by adjusting the TD values according to the seventh most sensitive non-edge value, adding this decibel offset to each location. The accompanying PDP map takes into account normal variability at each location. A cluster of two or more non-edge points on the PDP map ($p<0.05$) should be considered suspicious. An isolated point within the central 10° ($p<0.05$) should also be considered suspicious (Heijl et al., 1987a).

### 1.6.2.5. Glaucoma Hemifield Test

The GHT analyses the relative symmetry of five predefined sectors in the superior and inferior field, as well as judging the overall level of sensitivity (Asman and Heijl, 1992b). The visual fields are then classified in a short statement as being:

- 'Outside normal limits' when one or more zone in the superior field is significantly different from its corresponding zone in the inferior field (p<0.01)

- 'Borderline', when one or more zones in the superior field is classified as different from its corresponding zone in the inferior field, but does not reach the significance level required to be 'outside normal limits' (0.01-<0.03)

- 'Within normal limits', when all corresponding zones are considered to be similar (p≥0.03)

- 'Abnormally high sensitivity', when the highest sensitivities are greater than the average for normal eyes and the probability of being within normal limits is 0.05% or less (p<0.05).

- 'General reduction of sensitivity', when the highest sensitivities are lower than average and the probability of being within normal limits is 0.05% or less (p<0.05%), provided that the hemifield asymmetry is not great enough to classify the field as being 'outside normal limits'.

### 1.6.2.6. Guided Progression Analysis

Guided progression analysis (GPA) is an updated version of the original glaucoma change probability (GCP) analysis, which is used to aid detection of progression. This method of analysis compares a patient's current result with a baseline set of data to report on locations that have changed. It also does a regression analysis of the global Visual Field Index

### 1.6.2.7. Visual Field Index

The Visual Field Index (VFI) estimates the extent of loss in percentage terms. A completely normal visual field would have 100% while a patient with total blindness would have 0%. Similar to MD, VFI is effective for estimating the rate of any global change, but these indices are less ideal for detecting early visual field loss (Chauhan et al., 1990, Smith et al., 1996, Vesti et al., 2003). Artes and associates reported that the change of visual field progression estimated by VFI and MD was closely related. However, VFI might underestimate the true change in glaucoma progression in eyes with early damage due to the fact that this index is less sensitivity to diffuse loss often caused by factors such as media opacities (Artes et al., 2011). Furthermore, in advanced stages of glaucoma, VFI was found to be highly variable and to often show a sudden step change when MD reaches $-20$dB and the VFI computation method switch from pattern deviation to total deviation values (Lee et al., 2014b, Rao et al., 2013).

### 1.6.3 Diagnostic performance of SAP

Several studies have evaluated the diagnostic performance of SAP. Sample and coworkers compared the MD and PSD results using AUROCs (MD=0.731; PSD=0.762) (Sample et al., 2006). At a specificity of 90% and 80%, SAP PSD had sensitivities of 48% and 52% whereas MD had of sensitivities of 55% and 65%. This study suggests that if SAP MD were used alone to detect glaucoma, only 65% of glaucomatous subjects would be correctly identified and that there would be a relatively large number of false positives (20%).

Further studies investigating the capabilities of PSD as an early predictor of

functional loss have shown mixed results. In the Ocular Hypertension Treatment Trial (OHTS) PSD was found to be a better predictor of early glaucoma than MD (Gordon et al., 2002). In contrast, Henson and coworkers have demonstrated that PSD alone, which is a summary index of localized visual field loss, was not an early indicator of glaucoma and would not detect generalized reductions in sensitivity (Henson et al., 1999). This inconsistency may be due to the chosen reference standard for defining glaucoma and its severity. In more advanced glaucoma, better sensitivity and specificity for SAP would be expected. Medeiros and colleagues evaluated the effect of disease severity on detection using SAP and found PSD to achieve a sensitivity of 85% for 80% specificity in eyes with marked glaucomatous structural changes (70% loss of NRR area), compared to a sensitivity of only 40% for 80% specificity in eyes with early disease (10% loss of NRR area) (Medeiros et al., 2006b).

An issue that has dominated the 'structural-function' relationship debate is the presence of structural loss before functional SAP loss (Kass et al., 2002, Medeiros et al., 2012a, Medeiros et al., 2012b). Histological studies in humans and primates have suggested that large numbers of RGC may be lost before statistically significant visual field abnormalities occur (Harwerth et al., 1999, Harwerth et al., 2004, Kerrigan-Baumrind et al., 2000, Quigley et al., 1989). Early evidence came from a study of cadaver eyes, which suggested that at least 23–35% of RGC would need to be lost for an abnormality on conventional perimetry could be detected (Kerrigan-Baumrind et al., 2000). However, this theory has been vigorously challenged in recent years by a number of researchers. Questions have been raised about the small sample size and the variability in the relationship between SAP sensitivity and RGC counts. SAP uses a logarithmic (Decibel) scale, which

compresses data in the early stages of disease; in the early stage of the disease one would expect SAP to be relatively insensitive to RGC loss (Garway-Heath et al., 2000, Hood and Kardon, 2007, Swanson et al., 2004). Another theory is that there is substantial overlap in the receptive fields of retinal ganglion cells and redundancy for measure of differential sensitivity (Medeiros et al., 2006a).

### 1.6.4 Alternate Perimetric Tests

To address some of the drawbacks of SAP in detecting early glaucoma, other psychophysical tests of visual function have been introduced including short-wavelength automated perimetry (SWAP) (Swanson et al., 2011), and frequency-doubling technology (FDT) perimetry; (Johnson et al., 1993, Landers et al., 2003, Liu et al., 2011a, Sample et al., 2006). These tests are designed to target specific sub-populations of RGC that are thought to be sensitive to glaucoma (Sample and Weinreb, 1990).

### 1.6.4 .1 Short Wavelength Automated Perimetry

SWAP is a modification of SAP, which is available in both the HFA and Octupus Perimeter (Interzeag AG, Geneva, Swirtzerland). It is designed to evaluate the short wavelength sensitive colour system by isolating the blue-yellow pathway (Swanson et al., 2011). SWAP uses a 440nm, narrow band, 1.8-degree target (V stimulus) presented for 200ms on a bright $100cd/m^2$ yellow background to selectively test the short-wavelength sensitive pathway. The theory behind SWAP is

that early functional loss can be identified earlier by selectively testing RGC that show sparse neural representation (Johnson, 1994).

In the HFA, SWAP tests are performed and analyzed in the same way as SAP. The Full Threshold algorithm is used in SWAP, resulting in longer testing times than SITA. SWAP has higher intra test variability than SAP (Hutching et al, 2001). Furthermore, SWAP was found to be limited by the influence of cataracts and other media opacities. These limitations have reduced the clinical value of SWAP as it enlarges the confidence intervals for normality. To overcome the longer testing time, SITA SWAP has been introduced in the latest version of HFA II.

### 1.6.4.2 Frequency Doubling Perimetry

FDT applies the principle of the frequency-doubling illusion. When a low spatial frequency grating is viewed at high temporal rates the spatial frequency appears doubled. The test is targeting the magnocellular RGC pathway (about 10% of the population). The original FDT instrument tested 19 locations (10x10°) in either a threshold mode or rapid (<1 minute) supra-threshold mode. During testing the stimulus flicker and the spatial frequency is held constant while the contrast is modified in a stepwise process, similar to the bracketing method used in conventional perimetry. As the large targets limited the spatial resolution of the test a second-generation machine was introduced, FDT Matrix, which employs smaller 5° targets and measures with a standard 24-2 pattern of stimulus locations. Similar to SAP, FDT Matrix also provides raw sensitivity values, total and pattern deviation probability plots, and the summary indices MD and PSD.

Several studies comparing the ability of SAP, SWAP, and/or FDT to detect functional

loss in glaucoma have been undertaken (Liu et al., 2011b, Medeiros et al., 2006a, Sample et al., 2006, Tafreshi et al., 2009). Results have often been inconsistent and contradictory. Sample and colleagues found first-generation FDT to have higher sensitivity than both SAP (SITA) and full-threshold SWAP (Sample et al., 2006). Racette and colleagues reported that Matrix FDT performs better than SAP (Racette et al., 2008) while an earlier studies by Spry et al and Liu et al reported no difference between Matrix FDT and SAP. SWAP (SITA) was reported as being no better than SAP (Bengtsson and Heijl, 2006). Liu et al used the latest versions of each test (Matrix FDT, SWAP SITA, and SAP) and the RNFL thickness deviation map generated from OCT as the reference standard. SAP and Matrix FDT were found to be superior to SWAP SITA, with sensitivities of 82%, 84%, and 57% at 90% specificity (Liu et al., 2011a), see figure 1.14. However, this finding was inconsistent with a study done by Tafreshi and colleagues who found tests to be equally sensitive (Tafreshi et al., 2009). Many of these differences can be attributed to sampling and reference standard differences. It is, however, clear that no single test is consistently better than the others.
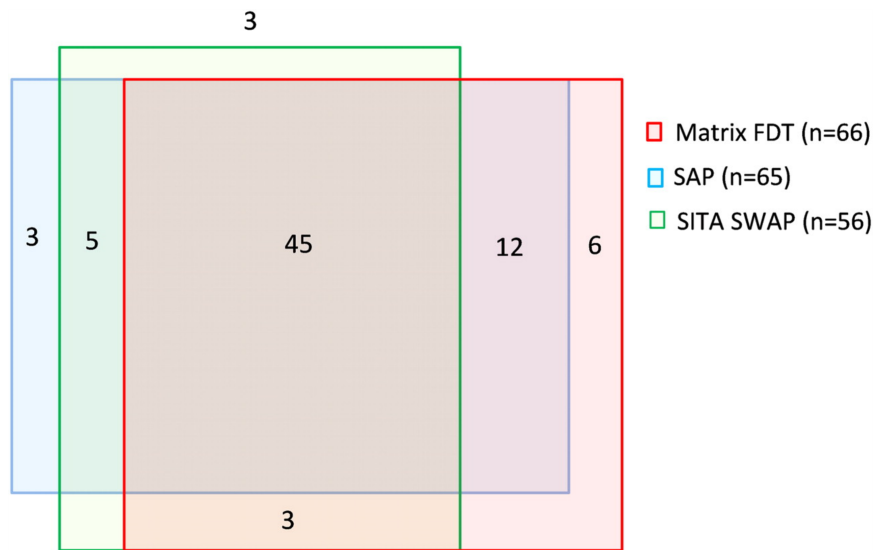
Figure 1.14: Proportional agreement of visual field defects detected by SAP, Matrix FDT perimetry, and SITA SWAP. The number of subjects (eyes) with visual field defects detected by each of the perimetric tests is shown in parentheses (Liu et al., 2011b).

Medeiros and colleagues evaluated the effect of disease severity on the diagnostic performance of Matrix FDT and SAP in 196 healthy eyes and 174 eyes with glaucoma (Medeiros et al., 2006a). Severity was determined from CSLO measurements of the NRR. This study found that Matrix FDT and SAP had similar performances to detect glaucoma in eyes with advanced structural losses but Matrix FDT performed better in eyes with early loss.

# 2. Introduction to experiments

## 2.1 Structural and Functional Asymmetries in POAG

The purpose of this chapter is to review the literature on structural and functional asymmetries in POAG. It begins by discussing current literature on Sup/Inf hemifield asymmetry followed by R/L asymmetry, or inter-eye asymmetry. When available it gives the discriminating power of asymmetry analyses.

Asymmetry is a hallmark of POAG. In 1970s, Fishman recognized the inter-eye structural asymmetry of optic disc as a sign of ocular hypertension (Fishman, 1970). Since then, a considerable amount of literature has been published highlighting the asymmetric nature of structure and function loss in POAG.

## 2.2 Sup/Inf Hemifield Asymmetry in Glaucomatous Eye

The RGC axons form the retinal NFL on their way to the ONH (see figure 2.1). Temporal to the fovea, the horizontal raphe divides the retina into superior and inferior halves. In the superior half of the retina, axons radiate over the fovea and enter the ONH at the superior pole, whereas in the inferior half of the retina, axons radiate below the fovea and enter the ONH at inferior pole. Fibres from nasal and central retina run directly from their cell bodies to the ONH. Because glaucoma damage to the ONH is often vertically asymmetric, field loss is often asymmetric between the superior and inferior fields. Therefore, methods which compare the superior and inferior hemiretinas/hemifields are often used to look for glaucomatous change in individual eyes both structurally and functionally.
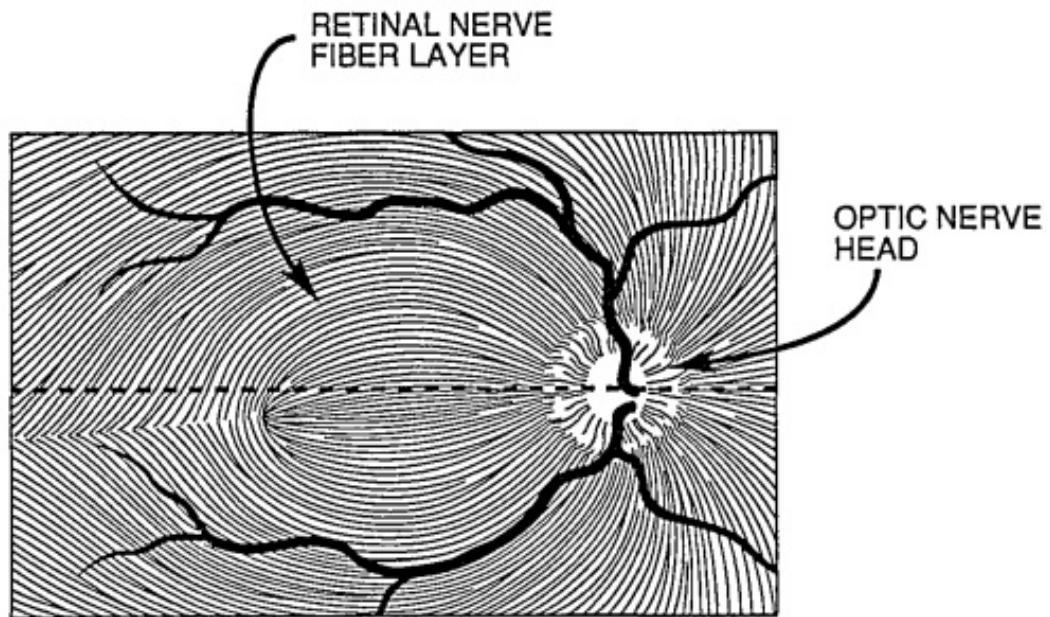
Figure 2.1: Nerve fiber pattern of retina in its relationship to optic nerve head. (Image reproduced from (Dreher et al., 1992).

### 2.2.1. Sup/Inf asymmetry in RNFL

One of the major challenges for discriminating between glaucomatous structural changes and healthy eyes is the large degree of overlap and inter-individual variability in the structural characteristics.

While Airaksinen (1981) has demonstrated that careful observation and in-depth assessment of RNFL may facilitate the early detection of glaucomatous structural damage most research groups have approached the problem through the development of asymmetry indices. Gramer et al introduced the retinal asymmetry index (RAI) and retinal asymmetry difference (RAD) to aid early discrimination.

RAI, which measures differences in the height profile of the upper and lower peripapillary NFL using the HRT, was found to be independent of the patient's age and disc diameter in contrast to the absolute value of the RNFL thickness. Furthermore, RAD measurements were also shown to be independent of the selected reference plane (Gramer and Tausch, 1998).

In 2011 the Spectralis spectral domain OCT (Heidelberg, Germany) introduced a new retinal thickness analysis. The analysis uses a color-coded map that gives mean retinal thickness values on an 8x8 grid centered on the fovea (see figure 2.2). The analysis used the fovea-disc axis as a standard reference line and a cell grid of 3x3°. Furthermore, the posterior pole asymmetry analysis protocol compares corresponding cells of the two Sup/Inf hemispheres and between R/L eyes. The asymmetry map is displayed as a grayscale depiction of difference in thickness from 0-30µm (Asrani et al., 2011).
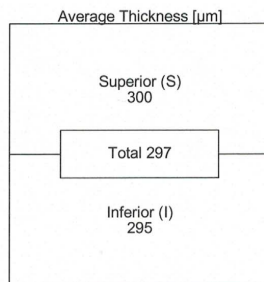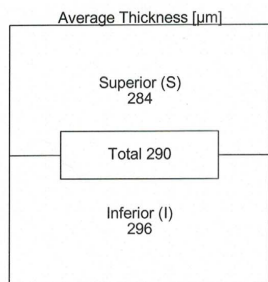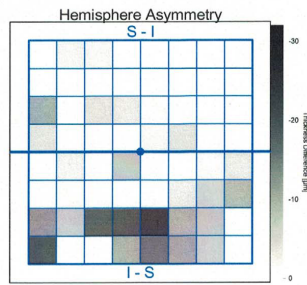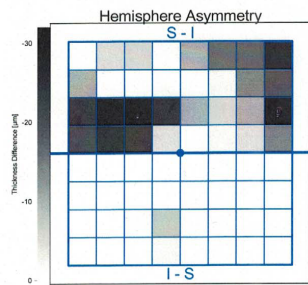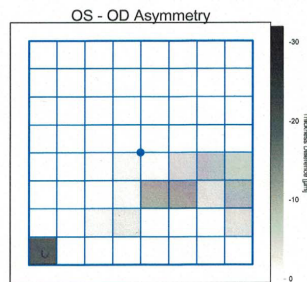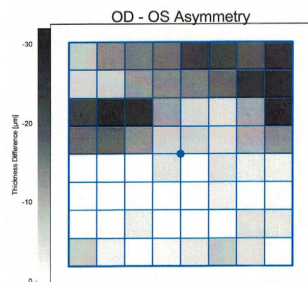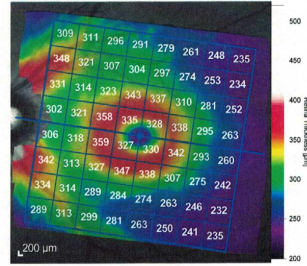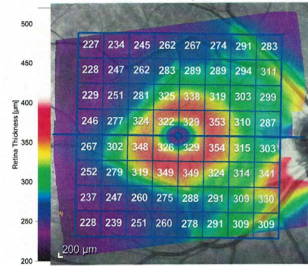
Figure 2.2: Posterior pole asymmetry analysis of spectral domains OCT. The color-coded images show the posterior pole thickness map. The middle images show the interocular asymmetry analysis (right eye–left eye/left eye–right eye) and the intraocular asymmetry analysis (S-I/I-S), respectively. The intraocular hemisphere asymmetry analysis displays the asymmetry between the superior and inferior hemisphere. The fovea-disc axis is the horizontal symmetry line. Asymmetry is presented in a grayscale where darker gray indicates thinner retina and white indicates equal retinal thickness. The bottom images show the mean superior, total, and inferior retinal thickness. S, superior hemisphere; I, inferior hemisphere

(Image reproduced Jacobsen et al (Jacobsen et al., 2015)).

Utilizing version 2 of the Spectralis spectral domain OCT and time domain OCT Reis et al (2012) compared RNFL thicknesses in healthy and glaucomatous patients with asymmetric field loss. Unaffected hemifields of glaucoma patients were found to have a thinner retinal nerve fiber layer than healthy eyes. Furthermore, RNFL measurements were thicker with time domain than spectral domain OCT. This study suggested that time domain OCT detected abnormal retinal nerve fiber layer thickness less often than spectral domain OCT.

In a study investigating the properties of circumpapillary RNFL measured by Cirrus OCT (Badlani et al., 2006) a positive correlation was found with functional defects detected by SAP. Choi et al., (2014) found that bi-hemispheric RNFL defects in early stage glaucoma were associated with optic disc tilt and could also reflects the greater overall optic nerve susceptibility to glaucoma resulting in the accelerated rate of glaucoma progression (De Moraes et al., 2009).

### 2.2.2. Sup/Inf asymmetry in macular thickness

In the human macula, the peak density of RGC is located 750-100um from the centre of the fovea (see figures 2.3 and 2.4) with thicknesses of up to 6 layers of cell bodies. Recently, there have been several studies describing changes to the thickness of the macular in glaucoma (Arvanitaki et al., 2012, Dickmann et al., 2012, Greenfield et al., 2003b, Gurses-Ozden et al., 2004, Huang et al., 2011). The

recent developments and widespread availability of OCT has promoted the study of such changes.
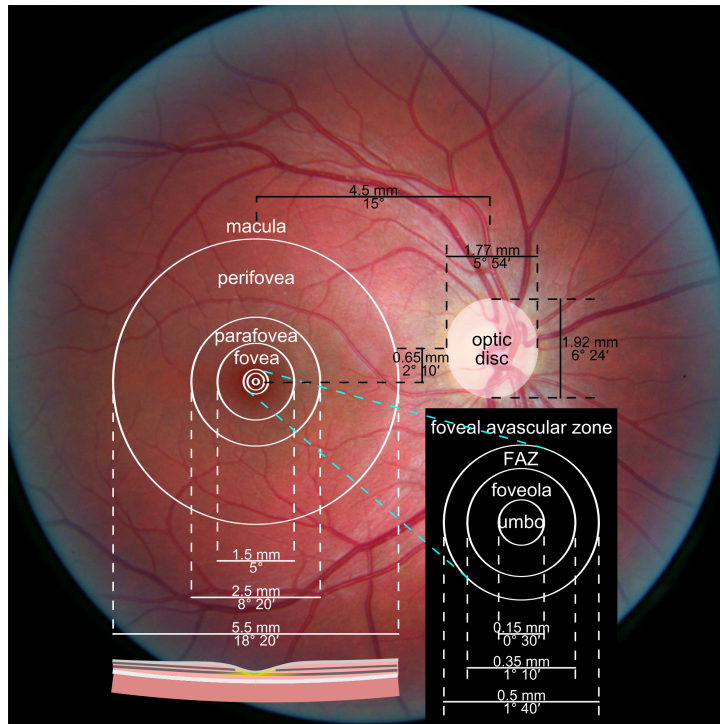


Figure 2.3: Location of fovea (within macular region) in relation with optic disc. (Hope, 2014)
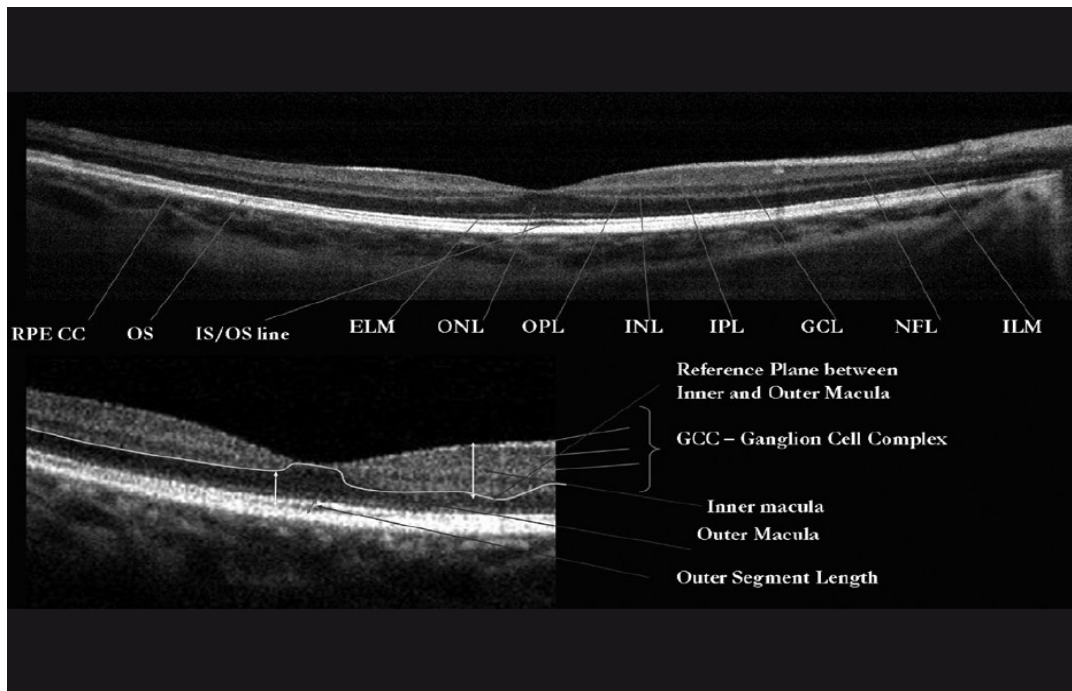
Figure 2.4: Macular RNF layer. (Sheth et al., 2012)

In a study to evaluate macular thickness and RNFL thickness using OCT, a significant difference was found between mean macular thickness in control subjects and patients with moderately advanced glaucoma. In addition, macular thickness and RNFL thickness were correlated with each other, indicating a loss of RGC and their axons (Greenfield et al., 2003a).

Bagga et al using time domain OCT and macular symmetry testing, found that localized macular thickness changes occur in glaucomatous eyes with sectional defect in the visual field. While they concluded that macular symmetry testing has potential to detect glaucomatous damage, the AUROC was only 0.76 to 0.84. Such an AUROC may be less than desirable for clinical use. The study was conducted using only four 5mm radial scans centred on the fovea, which could lead to low sensitivities and their controls were generated from 20 normal eyes, which were

not age matched (Bagga et al., 2005).

Another study investigating asymmetry in hemifield macular thickness among 114 healthy subjects, 103 glaucoma suspect and 74 glaucomatous eyes has been carried out by Um et al (Um et al., 2012) using a spectral domain OCT. Macular asymmetry analysis was conducted on 5 zones in the inferior and superior regions (similar to the GHT), they found that the sensitivity was significantly greater than that of RNFL measurement in the early glaucoma group. However, this study was limited in terms of control subjects, which were not age matched with the glaucoma group.

Yamada et al. also used spectral domain OCT to investigate whether discriminatory potential varied when different segmented layers where included in the calculations, e.g. RNFL+ganglion cell layer + inner plexiform layer. Result demonstrated that, in the 30x15° macular area, asymmetry index of the RGC layer had the best diagnostic performance, followed by asymmetry index of ganglion cell complex, the RNFL, and the total retina (Yamada et al., 2014).

However, Hwang et al 2015 reported that the diagnostic capability of macular RGC layer asymmetry performed better only in early stage disease, reducing in more advanced stages. The diagnostic performance appears to be sensitive to case mix within the POAG sample. This study used the Cirrus HD-OCT GCA algorithm while previous studies utilized the Spectralis OCT. The Spectralis OCT algorithm provides total retinal thickness values for an 8×8 grid positioned symmetrically to Bruch's membrane opening to the fovea axis with the central point of the grid at the fovea. In Hwang et al's study, the thickness map was located along the horizontal meridian.

While there are methodology differences between the different studies, all studies report good discriminating power for Sup/Inf hemifield macular thickness asymmetry (Bagga et al., 2005, Sullivan-Mee et al., 2013, Um et al., 2012, Yamada et al., 2014).

### 2.2.3. Sup/Inf asymmetry in VF

Glaucomatous functional damage usually respects the horizontal midline and the anatomy of the retinal nerve fiber layer, particularly at the early stages of the disease. The first serious discussions and analyses of patterns of glaucomatous visual field loss emerged in 1984, when Mikelberg and Drance published their review on the pattern of VF progression using static and kinetic perimetry. They reported that 70% of eyes had initial damage limited to a single hemifield. The most common pattern of field progression was deepening of an existing scotoma, detected with static perimetry (Mikelberg and Drance, 1984). The findings from this study where supported by Boden et al who found that early glaucomatous field loss rarely crosses the horizontal midline (Boden et al., 2002).

The widespread use of SAP has led to a quantitative data on the visual field. In the HFA, an asymmetry algorithm, GHT was incorporated in 1992 to help identify early glaucomatous field damage (Asman and Heijl, 1992b). This algorithm utilized an up-down mirror image method to compare clusters of test loci in the superior field with their corresponding mirror image in the inferior field. The main purpose of

GHT is to summarise the visual field status based on normal data of superior and inferior differences in the Statpac (Humphrey Instruments, San Leandro, Calif) probability maps and "to identify field with localized defect as abnormal". GHT involves 5 corresponding pairs of sectors that are based on the normal morphologic structure of the RNFL. Asman and Heijl used photographs of the normal RNFL to identify the normal arrangement, see Figure 2.5.
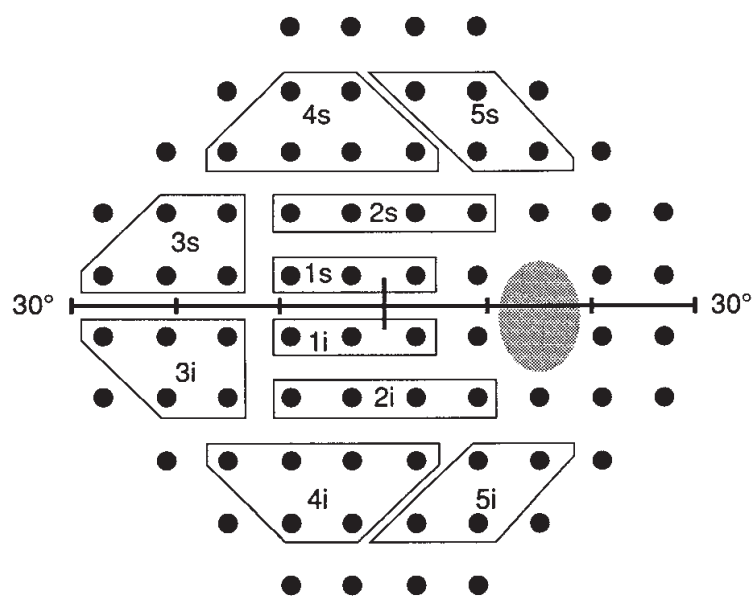


Figure 2.5: 10 sectors of Glaucoma Hemifield Test (from Asman and Heijl 1992)

The GHT algorithm utilizes the data given in the probability maps that represent significant deviation from normal values for age, corrected for overall sensitivity. It compares the sum of probability scores in the upper 5 sectors with the corresponding scores for the inferior sectors. GHT only includes test locations that fall within the 24-2 test pattern and excludes 3 points near the blind spot.

With the GHT algorithm, there are five possible outcomes:

     1. within normal limits;

     2. borderline;

     3. outside normal limits;

     4. general reduction in sensitivity;

     5. abnormally high sensitivity.

Figure 2.6 gives the steps used by Asman & Heijl to classify the asymmetry into one of the 5 outcomes.
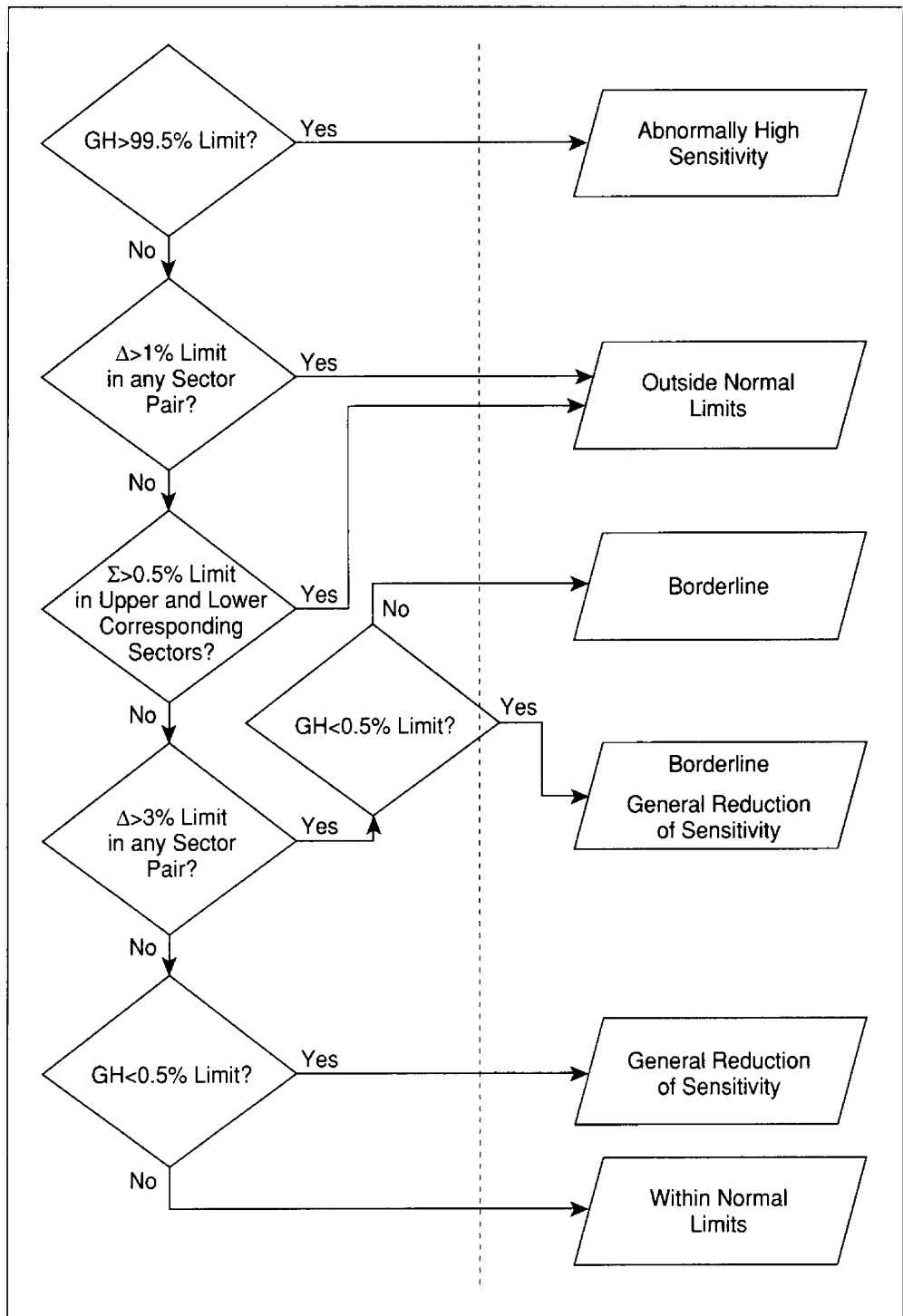
Figure 2.6: Flowchart used by Asman and Heijl to classify GHT outcomes

Based on the later report by (Asman and Heijl, 1992b), GHT was found to have a sensitivity of 78% with a specificity of 90% using 'outside normal limits' as the classifier. Katz et al examined the agreement of the GHT to other global visual field indices in 41 normal subjects, 407 ocular hypertension subjects and 95 glaucoma subjects all of whom were tested twice (Katz et al., 1995). Result indicates that, in patients with glaucomatous field loss, the specificity was improved from 81 to 90% with two versus one test. For the ocular hypertensive sample, specificity was increased from 84 to 89% if two normal tests were required. Katz et al concluded that there was a significant improvement in performance when agreement between two consecutives GHT results are used (Katz et al., 1995).

One question that needs to be asked, however, is whether the 5 fixed sector borders used in the GHT are ideal? Several studies have highlighted that the map of RGC axons varies significantly between individuals due to differences in ONH position, ONH dimensions, and the axial length (Denniss et al., 2014, Jansonius et al., 2012a). Inappropriate sector boundaries could lower the sensitivity when defects lie across sector borders. Further research needs to explore whether none sector based asymmetry analyses perform as well, if not better than GHT.

Future analyses should also consider alternative forms of output that include measures of probability similar to those of other global indices, i.e. outside the 5%, 2%, 1% or 0.5% limits.

## 2.3 R/L asymmetries in POAG

POAG is a bilateral disease and the onset of structural or functional damage often occurs in one eye before the other and remains asymmetric even when defects occur in both eyes. Evidence from large surveys performed in England (Poinoosawmy et al., 1998) and in Australia found that bilateral visual field loss is present in 25 to 50% of individuals with POAG (Lee et al., 2003b). Moreover, 7 to 25% of glaucoma patients with unilateral field loss at baseline will later experience visual field damage in the fellow eye (Caprioli et al., 1987, Quigley et al., 1982). In this section, literature investigating R/L asymmetry (also known as inter-eye asymmetry) is reviewed.

### 2.3.1 R/L Asymmetry in the ONH

Evaluation of the ONH structure is an important element of any clinical examination for glaucoma. However, detecting early glaucomatous change in a clinical setting is not always straightforward due to the wide overlap in ONH appearance between normal and glaucomatous eyes. Looking at asymmetries between the right and left eyes, which are usually closely matched, helps to increase the diagnostic power of ONH analysis.

Fishman undertook preliminary work on asymmetry of the ONH in normal eyes and individuals with ocular hypertension and OAG in 1970. He used the Halberg grading system to evaluate disc asymmetry and found that 5.6% of normal individuals, 30% of ocular hypertension patients and 36% of OAG patients have asymmetrical cupping of the optic disc (Fishman, 1970).

Several attempts have been made to quantitatively differentiate between normal and glaucomatous ONH parameters (volume, area and depth) based on photogrammetric analysis (Holm et al., 1972, Jonsas, 1972). Their results indicate that these parameters are highly symmetrical between the two eyes of normal patients. On the other hand, average volume, area and depth of optic cup were found to be larger in glaucomatous eyes than in normal eyes (Holm et al., 1972, Jonsas, 1972, Portney, 1975). Portney concluded that optic cup volume asymmetry between the two eyes was a sensitive photogrammetric measurement for differentiating normal subjects from glaucomatous patients (Portney, 1975). However, this study did not report sensitivity and specificity data.

In a large population based study in Australia, the eyes of 3654 participants (age range from 49 to 97 years) were examined to investigate the asymmetry in vertical optic disc parameters in three different groups (normal subjects, subjects classified as having ocular hypertension and subjects having open angle glaucoma). Measurements of optic disc parameters were obtained using stereo photographs and a stereo viewer with a plastic template (Picket circles 1203) placed under one of the stereo pair. Vertical cup/disc ratios were calculated from the optic disc and cup measurements, after excluding any peripapillary atrophy. Results from this study demonstrated that vertical optic disc parameter asymmetry alone has good discriminatory power to detect POAG (Ong et al., 1999).

Several investigators have explored other parameters of the ONH, e.g. the NRR area (Balazsi et al., 1984, Hitchings et al., 1983). The preliminary work on investigating the efficacy of rim area to disc area asymmetry (RADAAR) in

glaucoma patients has been made by Harasymowyz et. al (2005). Records of 140 randomly selected POAG, NTG and pseudoexfoliative glaucoma cases were evaluated from January 1996 to April 2000. HRT paramaters disc area, rim area, cup to disc area ratio, HFA data and IOP were recorded. The authors concluded that RADAAR was significantly correlated with the IOP and the severity of glaucoma. However, the ability of RADAAR to discriminate between normal and glaucomatous eyes was not reported due to the absence of normative data.

In 2005, the Bridlington Eye Assessment Project published data on normative RADAAR using a population-based sample of normal elderly subjects using the HRT II. Data from this study indicate that asymmetry analysis using rim to disc area ratio may improve discriminatory ability in identifying glaucomatous change (Hawker et al., 2006).

A recent cross-sectional population based study to investigate the symmetry of optic nerve head parameters between fellow eyes using HRT III in 1276 participants has shown that most ONH parameters in healthy subjects are symmetrical between the 2 eyes. Inter-eye asymmetry of cup to disc ratio greater than 0.2 can be considered as abnormal (Li et al.), see table 2.1. The results from this population based study were consistent with two other population based studies, the Tajimi Study (Abe et al., 2009) and The Bridlington Eye Assessment Project (BEAP) (Hawker et al., 2005), see table 2.1. In the Tajimi study the HRT II normal data was obtained from 1540 subjects aged ≥40 years of age. Twelve parameters were studied, disc area, cup area, rim area, cup-to-disc area ratio, cup volume, rim volume mean cup depth, maximum cup depth, height variation

contour, cup shape measure, mean retinal nerve fibre layer thickness and RNFL cross-sectional area. This study found that all HRT parameters were strongly or moderately correlated between right and left eyes (Pearson correlation coefficients=0.45-0.83, P<0.001).

**Table 2.1: Summaries of studies investigating inter-ocular optic disc asymmetries in healthy eyes**

| Study | Subjects | Instruments | Main Outcome |
| --- | --- | --- | --- |
| **Blue mountain Eye Study (BMES)** <br><br> **2013 (Li et al.)** | 1276 participants (mean age 71.9± 7.0 years) | HRT 3 | Most of the parameters measured by HRT 3 are symmetrical between right and left eyes in healthy subjects |
| **The Bridlington Eye Assessment Project (BEAP) 2005 (Hawker et al., 2005)** | 459 normal elderly (mean age was 72.6 years) <br><br> (Age range: 65.5-89.3) | HRT II | There are clinically insignificant differences in HRT parameters between right and left eyes. |
| **The Tajimi Japaneses population based study 2001 (Abe et al., 2009)** | 1540 normal subjects (aged 40 years an above) | HRT II | All HRT parameters between fellow eyes were significantly correlated (Pearson correlation coefficients ≥0.450, P<0.001) |

## 2.3.2. R/L asymmetry in RNFL thickness

Evaluation of circumpapillary RNFL thickness remains the primary structural investigation tool used in glaucoma diagnosis and management. Relatively little attention has been paid to the role of R/L RNFL thickness asymmetry in glaucoma diagnosis. To the best of our knowledge, only 2 studies (Field et al., 2014, Sullivan-Mee et al., 2013) have investigated R/L RNFL have been published.

Sullivan-Mee et al (2013) assessed R/L RNFL asymmetry of 50 subjects with early POAG and 50 healthy individuals. The results suggested R/L RNFL asymmetry could have an important clinical role in identifying early glaucomatous damage.

The capability of R/L asymmetry determined from the study done by Sullivan-Mee et al (2013) are in in-line with the findings in recent work of Field et al (2014), which evaluated 66 POAG and 40 age-matched normal subjects using spectral domain OCT. This study demonstrated the R/L RNFL asymmetry (global average) achieved the greatest statistical difference (P<0.001) between POAG (23.64± 14.90 $\mu$m) and normal eyes (3.58 ± 3.96 $\mu$m), with 6.60 times greater asymmetry in OAG eyes. The inferior quadrant was found to be the second best discriminator (3.91 times greater; P < 0.001) (Field et al., 2014).

In a study which looked at categorical agreement on defective locations of RNFL defects between fellow eyes of 154 patients with glaucoma, using OCT, the average absolute inter-eye difference in RNFL thickness for global average, the superior, temporal, and inferior quadrants, and all 4 sectors were statistically greater in OAG eyes. Their result suggested that glaucomatous RNFL damage in 1 eye is correlated with damage at corresponding locations of the fellow eye (Bertuzzi et al., 2009).

In a study to determine the limits of the normal R/L asymmetry in 108 normal volunteers, Budenz and colleagues measured the thickness of peripaillary RNFL using time domain OCT. Their result indicated that mean RNFL thickness between the 2 eyes of normal individuals did not differ by more than 9 to 12µm (Budenz, 2008). Asymmetry values that exceed this limit, suggest statistically abnormal asymmetry, which may be indicative of early glaucomatous optic neuropathy. This finding is consistent with a more recent study (Mwanza et al., 2011), which suggested that asymmetry value in average RNFL thickness should not exceed 9µm if measured with Cirrus OCT. Moreover, this later study reported that asymmetry between average RNFL thicknesses remained stable with increasing age, which suggested that aging evenly affects the RNFL of both eyes.

In a population-based study to determine R/L asymmetry value in RNFL thickness in 1172 6-year-old children, measurements of RNFL thickness obtained with Stratus OCT showed an insignificant difference of 0.4µm between the 2 eyes (Huynh et al., 2007)

The R/L asymmetry in RNFL thickness has also been studied using other imaging devices. Two studies utilized SLP to measure R/L asymmetry in RNFL thickness and found no difference between the right and left eye average RNFL thickness (Essock et al., 1999, Kurimoto et al., 2000). However, Essock et al (1999) reported that the RNFL thickness in superior retina of the left eye was significantly thicker, whilst Kurimoto et al reported that the left eye RNFL was thicker in only 2 nasal sectors and the right eye RNFL was significantly thicker in 4 temporal sectors. In another study (Gherghel et al., 2000) compared the RNFL thickness in 314 normal eyes of 117 subjects using CSLO, statistically significant R/L differences in the average and nasal RNFL thickness were found with the left eye having higher values. Using the

same approach in measuring RNFL thickness in 882 eyes of 1764 normal individuals, Hermann and associates (2004) found significantly higher right eyes average RNFL values than left eyes (Hermann et al., 2004).

The reason behind the right and left differences in RNFL thickness in healthy eyes is not clear. The observed asymmetry could be attributed to variations in the density of RGC, glial and Müller cells.

### 2.3.3 R/L Asymmetry in macular thickness

Evidences from previous studies have established that macular thickness is thinner in glaucomatous eyes than in healthy eyes and this could have an important clinical role in glaucoma detection, especially in the early stages of the disease (Hood et al., 2014, Hwang et al., 2015, Sung et al., 2014). Despite the potential importance of Sup/Inf hemifield macular thickness asymmetry, there remains a paucity of evidence on R/L asymmetry. Only 2 studies have reported on R/L asymmetry in macular thickness (Asrani et al., 2011, Sullivan-Mee et al., 2013). Sullivan-Mee et al (2013) compared R/L asymmetry in 50 healthy individuals and 50 subjects with early POAG over the age of 40 years. Results suggested that macular thickness exhibits remarkable symmetry between eyes in healthy subjects. These results match those observed in case studies (Asrani et al., 2011), which utilized a customized Sup/Inf hemifield and inter-eye asymmetry protocol.

In an asymmetry analysis of the RNFL and total retinal thickness around macula in a normal population of Iranians, Mahmudi reported that the normal upper limit of

R/L eye differences in mean RNFL thickness, measured with Topcon OCT, is between 0.78 and 2.4µm and total thickness between 2.6 and 12.08µm (Mahmudi, 2013).

### 2.3.4 R/L asymmetry in the visual field

Traditionally, there are 3 methods for detecting visual field abnormalities;

1. Comparison with previous data
2. Comparison with aged norm database
3. Comparison with unaffected part of visual field in same eye

To date, method that compares visual field abnormalities with fellow eyes has not been incorporated in any commercially available perimeters. In 1986, Brenton et al carried out a study investigating the symmetrical properties of right and left eyes in 20 normal subjects using the 30-2 test pattern of the HFA. The inter-ocular difference (IOD) value was calculated by subtracting the retinal sensitivity (decibels) value of the right visual field from the mirror location of the left visual field. The average IOD ranged from +1.9 to -0.7dB with a standard deviation of ±1.2 to ±3.1dB. They concluded that the threshold values of the 2 visual fields are not exact mirror image of each other (Brenton et al., 1986). However, this study suffered from several limitations including, small sample size and sampling bias. Feuer et al (1989) examined the visual fields of 10 normal subjects with the HFA, with one eye tested twice. Results from this study suggest that a 2dB difference in mean sensitivity between the eyes is suspicious, a 1.5dB difference is statistically significant if confirmed on a second test, and a difference as small as 1dB may be meaningful if shown consistently in a series of four examinations (Feuer and

Anderson, 1989)

Henson et al examined 115 normal subjects and 107 suspect/diagnosed early glaucoma patients using the FVFA. Using a scoring algorithm they reported that R/L asymmetry is very sensitive to early glaucomatous field loss (Henson et al., 1986)

(Wang et al., 2004) reported on the R/L asymmetry in 128 POAG and 102 PACG eyes using SAP and a 24-2 test pattern of the HFA. They found that the AGIS scores and global indices were higher in angle closure than in POAG. This finding is consistent with recent work by Huang and associates who found R/L asymmetry to be higher in closed angle glaucoma than NTG and POAG. In this study, R/L asymmetry scores were defined by the differences of the 3 parameters; (1) global indices; (2) local MDs of 6 predefined visual field areas; and (3) stage designated by glaucoma staging system (Huang et al., 2014).

Levine et al (2006) assessed whether R/L visual field asymmetries could predict the onset of POAG using OHTS data. They reported that R/L asymmetries in visual field data could assist in clinical evaluation of eyes at high risk of developing POAG (Levine et al., 2006). In this study 2 reliable Humphrey 30-2 Full Threshold baselines were obtained from 1618 OHTS participants. Mean prognosis (MP), which is a linear combination of the visual field test points, was used to predict the onset of POAG. This monocular index summarizes the prognostic information in each test point and compares it to baseline MD and PSD. Results from this study demonstrated that, among the 643 eyes with an asymmetric pair with depressed

sensitivity at one or more test point locations, 7.5% developed POAG. In addition, eyes from an asymmetric pair with reduced sensitivity had a 59% risk of developing POAG (*P*=0.0077).

Existing research recognizes the critical role of visual field R/L asymmetry in detecting early POAG. However, no single study exists which compares the diagnostic performance of R/L asymmetries with Sup/Inf hemifield asymmetry analysis. There is room for further research to determine whether R/L asymmetry analysis is superior to currently available GHT or new Sup/Inf hemifield indices.

### 2.3.5 R/L asymmetry in IOP

The dynamic balance of aqueous humor production and drainage in healthy eyes maintains the IOP, at approximately 15mmHg. Despite the importance of IOP lowering in the management of glaucoma, much uncertainty still exists about the relation between IOP asymmetry and the pathogenesis of glaucoma.

There are a number of papers investigating the discriminatory power of IOP asymmetry in POAG (Cartwright and Anderson, 1988, Crichton et al., 1989, Haefliger and Hitchings, 1990a, Lee et al., 2004, OHTS, 2008). Many of these papers focused on IOP asymmetry in NTG (Cartwright and Anderson, 1988, Crichton et al., 1989, Haefliger and Hitchings, 1990a) and report that the eye with higher IOP is at the greater risk of developing glaucomatous damage. In the study by Crichton et al (1989) the relationship existed in 22 out 32 patients, using a difference criterion of 0.5mmHg. However, when criterion was raised to ≥1mmHg, only 13 of 47 patients showed asymmetric visual field defects (Crichton et al.,

1989). More recently Levine et al (2006) investigated IOP asymmetry in OHTS participants and reported that baseline visual field asymmetry and IOP asymmetry could facilitate the detection of eyes at risk of developing POAG. Conversely, in a study by Greenfield et al, a different conclusion was reached, i.e. no relationship between IOP asymmetry and visual field loss (Greenfield et al., 2007) while Ong et al reported that IOP asymmetry is only significant for glaucomatous damage in patients with pressures more than 21mmHg (Ong et al 1999).

A more recent population–based cross sectional study evaluated the association of IOP asymmetry with undiagnosed POAG and concluded that IOP asymmetry of >3mmHg has limited capability in the detection of undiagnosed glaucoma. This study highlighted that low sensitivity, when coupled with the low prevalence, leads to a poor positive predictive value for this parameter. This study has suggested that the accuracy could be improved if the parameter can be combined with other indicators (Choudhari et al., 2013). Gugleta et al reported a thinning of RNFL in the eye with higher IOP (Gugleta et al., 1999).

In the studies reviewed there is no consistent definition of IOP asymmetry (see table 2.2), which could account for some of the differences in their findings. In addition, all the studies have linked IOP asymmetry to the presence or absence of visual field loss rather than the extent of loss.

**Table 2.2: Comparison of studies investigating asymmetry IOP in glaucoma patients**

| Study | Subjects | IOP Difference | Outcome |
|---|---|---|---|
| Cartwright and Anderson (1988) | 14 eyes<br><br>Mean age: 74.6±29 | >> 1mmHg | VF loss and cupping are demonstrated in the eyes with higher IOP |
| Crichton et al (1989) | 59 NTG patients | 0.5, 1.0 and 1.5 mmHg | VF defect is greater in the eye with higher IOP |
| Haelfiger and Hitchings (1990) | 60 NTG patients | N/A | 13 of 60 have greater visual field loss in the eye with higher IOP |
| Jonas et al (1998) | 98 eyes of NTG patients<br><br>17 NTG with high myopic eyes<br><br>36 eyes with POAG | N/A | Eyes with high IOP have pronounced optic nerve damage |
| Gugleta et al (1999) | 15 NTG patients | 0.3-4.0mmHg | RNFL thinning is demonstrated is the eye with higher IOP |
| Lee et al (2004) | 3252 patients aged > 49 years old | ≥ 3mmHg | Significant association between asymmetry IOP and undiagnosed glaucoma |
| Levine et al (2006) | 1618 OHTS participants | > 1 mmHg | IOP asymmetry increased the risk of POAG onset |

| | | | |
|---|---|---|---|
| Greenfield et al (2007) | 190 low pressure glaucoma patients | > 1 mmHg | No correlation between asymmetry IOP and VF asymmetry |
| Choudhari et al (2011) | 6310 subjects | > 3 mmHg | IOP asymmetry > 3 mmHg has limited ability in detectiong undiagnosed POAG |
| William et al (2011) | 326 glaucoma patients, 326 control | ≥ 1-3mmHg | There is correlation between asymmetry IOP and likelihood of getting POAG |

**2.3.6 R/L Asymmetry in Visual evoked Potential (VEP) response.**

For more than 40 years, the VEP has been reported as being abnormal in glaucoma. Using multifocal (mfVEP) techniques, several regions of the visual field can be recorded simultaneously.

In a study done by Graham et al to analyse the asymmetry of VEP perimetry between the two eyes in early glaucoma; 24 control subjects, 10 patients with glaucoma and 31 high-risk suspects were examined with the VERIS system (Electro-Diagnostic Imaging, Inc. San Francisco, CA). The visual stimulus was generated on a computer monitor with a repetition rate of 67Hz and 60 segments arranged in a dartboard configuration. Asymmetry analysis, known as between-eye relative asymmetry coefficient (RAC) was able to correctly identify patient with glaucomatous field loss and 10/31 patients who were at high risk of glaucoma with currently normal visual fields (Graham et al., 2000). Among the glaucoma patients, higher RAC values were often found in a perimetrically normal eye. The work has

been criticised for its small control sample and the lack of any optic disc examination to determine the presence of any congenital structural differences. In addition, pre-existing ocular diseases, such as cataract or macular degeneration, could interfere with the perimeter interpretation. Another limitation is the probability of progression was based on a limited reproducibility study.

An investigation of test-retest variability of mfVEP and threshold perimetry in glaucoma by Bjerre et al recorded mfVEP data of 74 glaucoma patients using AccuMap (Version 1.0; ObjectiVision Pty Ltd., Sydney, Australia) and 24-2 SITA SAP (HFA). Results indicated that test-retest variability was slightly higher for mfVEP and that while mfVEP took longer to perform the majority of patients preferred this test to conventional perimetry (Bjerre et al., 2004).

As for relative comparison with SAP perimetry, mfVEP provides an alternative measure for patients who produce unreliable or questionable SAP results. The mfVEP can be very helpful in cases where SAP does not match other clinical features (optic nerve head appearance) (Hood and Greenstein, 2003).

**2.3.7 R/L Asymmetry in Pupil Response**

Although SAP is recognized as the gold standard for glaucomatous visual field assessment, the technique suffers from large test-retest variability. Several attempts have been made to develop new and objective functional tests including the use of the pupillary light reflex (PLR) (Bergamin et al., 2003, Fankhauser and Flammer, 1989, Hong et al., 2001, Johnson et al., 1988, Loewenfeld and Rosskothen, 1974). The first pupil perimeters used infrared pupilometry to assess the visual field with supra-threshold stimuli. These tests took a long time to

perform (up to 40 minutes), produced defect patterns that were not well correlated with visual field results (Kardon, 1992) and had large within and between subject variability (Turtschi et al., 1994). Chen et al 2005 used a similar design to the 'swinging flashlight test' to look at differences between the superior and inferior retina in 11 normal eyes (Chen et al., 2005) and later (Chen et al., 2008) in 40 patients with glaucoma and 40 age-matched control subjects. They concluded that this was a rapid method for detecting and classifying visual field loss in glaucoma patients. Seventy per cent of the eyes with abnormal pupillary findings were found to have similar findings with perimetry.

Preliminary work using a multifocal stimulation technique (mfPOP) was carried out by Sutter and Tran in 1992 and further developed by Tan et al 2001 and Wilhelm et al 2000. Maddess and co-workers have reported high diagnostic accuracy of mfPOP in POAG and early stage diabetic retinopathy (Bell et al 2010; Maddess et al 2009a).

With regard to the correlation between afferent pupillary and visual pathways, while there might be minor differences these are thought to be insignificant. This view is consistent with data that demonstrates spatial agreement between the damage to visual RGCs or their axons with the damage to pupillary ganglion cells or their axons when afferent lesion lie in or distal to the optic tract.

# 3. New Superior-Inferior Hemifield Asymmetry Indices for Detecting POAG.

## Contribution:

The project was conducted under supervision of Prof David Henson. The dataset used was collected from patients attending the outpatient department of Manchester Royal Eye Hospital (MREH) as part of their routine management for suspect/diagnosed glaucoma. I extracted the data from the database, taking into account the inclusion/exclusion criteria, performed the data analysis and presented the work at conferences. The work has been published in a special glaucoma issue of the journal Eye.

## Publication

**Ghazali N**., Aslam T., Henson DB. (2015) New superior-inferior visual field asymmetry indices for detecting POAG and their agreement with the glaucoma hemifield test. Eye (Lond). Oct; 29(10):1375-82.

## Conferences

**Ghazali N**., Aslam T., Henson DB. (2015) Diagnostic performance of New superior-inferior and right left visual field asymmetry indices for detecting POAG. ARVO 2014 Annual Meeting, Orlando, FL, USA (poster)

# Abstract:

**PURPOSE**: To describe and measure the discriminatory performance of 3 new superior-inferior asymmetry indices for detecting Primary Open Angle Glaucoma (POAG) and to compare these with the GHT.

**METHODS**: 412 control and 247 POAG eyes were selected from a visual field database of patients attending Manchester Royal Eye Hospital. Age adjusted defect asymmetries were calculated for each of the 22 vertically mirrored test point pairs used in the GHT. The 3 new indices, Hemifield Mean Difference (HMD) and Hemifield Standard Deviation (HSD) of the asymmetry values along with the Number of test Pairs (NP) falling outside the 85% probability limits of the control population, were calculated. Receiver Operating Characteristic (ROC) curves of the indices and GHT were constructed. Agreement between the indices was explored with a proportional Venn diagram and 3x3 contingency tables. Cases of disagreement between the indices were reviewed.

**RESULTS**: The area under the ROC curves were HMD=0.75 (95% Confidence Interval (CI) 0.71-0.79), HSD=0.86 (95% CI 0.83-0.89), NP=0.86 (95% CI 0.83-0.89) and GHT=0.79 (95% CI 0.75-0.83). The Venn diagram and contingency tables highlighted the good agreement between HSD, NP and GHT. Agreement was 78% (HSD vs GHT) and 82% (NP vs GHT) in the control sample and 70% (HSD vs GHT) and 71% (NP vs GHT) in the POAG sample. 5 cases are presented where disagreement existed between the indices.

**CONCLUSIONS**: The new HSD and NP asymmetry indices perform better than GHT in differentiating between normal and POAG eyes in this dataset. GHT can fail to detect significant asymmetry, detected by HSD and NP, when an early defect crosses the GHT sector boundaries.

# Introduction

The results of threshold visual field tests are often subjected to a number of analytical methods that can be broadly classified as point-wise or global. Global methods reduce the visual field data to a single number that can be compared to normative databases and monitored over time to aid the clinician in making decisions regarding the management of new and existing patients. Most of the visual field global indices we use today have been specifically designed for the detection and monitoring of glaucoma. They recognize and focus on specific characteristics of glaucomatous loss; changes in overall sensitivity (Mean Deviation), localised defects (Pattern Standard Deviation) and asymmetry between the superior and inferior hemifields (Glaucoma Hemifield Test (GHT)) (Sommer et al., 1985, Sommer et al., 1987, Flammer, 1986).

The frequent asymmetry between the superior and inferior hemifields of glaucomatous eyes was first recognized in the 1980s when several research groups (Hart and Becker, 1982, Mikelberg and Drance, 1984, Drance, 1969) described the onset and evolution of glaucomatous visual field defects. In 1985 Duggan et al (Duggan et al., 1985) reported that high discriminatory power between normal and POAG eyes could be achieved by comparing the Sup/Inf hemifields. The diagnostic potential of Sup/Inf asymmetries was further developed by Asman and Heijl (Asman and Heijl, 1992b, Asman and Heijl, 1992a) who derived the GHT that is incorporated in the HFA. The GHT uses a subset (22 test locations in the superior/inferior hemifields) of the 24-2 test pattern. The 22 test locations in each hemifield are divided into 5 sectors on the basis of the mapping of retinal locations to the ONH. The inferior sectors being vertically mirrored copies of the superior

sectors. The GHT assigns a score to each test point based upon values presented in the pattern deviation probability maps and then calculates a sum for each sector. The sector differences are then compared to a database of controls. If any sector pair is beyond the 0.5% or 99.5% normal limits the test is classed as 'Outside Normal Limits'. If none of the sector differences is beyond these limits but they are beyond the 3% or 97% limits the field is classified as 'Borderline'. If neither of the limits are exceeded the field is classified as 'Within Normal Limits'. To capture symmetrical losses within each sector pair the GHT also looks at the total score for each of the 10 sectors

GHT has found wide acceptance within the glaucoma community. It has been shown to provide earlier discrimination of visual field loss than other global indices (Mean Deviation (MD); Pattern Standard Deviation (PSD)) especially when repeated measures show consistent asymmetry (Katz et al., 1995). Its high diagnostic performance has led to it being used in several major glaucoma trials including the Collaborative Initial Glaucoma Treatment Study (Musch et al., 1999) and the Early Manifest Glaucoma Treatment Study (Leske et al., 1999).

The GHT assumes a constant mapping of the retinal locations to the optic nerve head, which is now recognized as being incorrect (Denniss et al., 2014, Jansonius et al., 2012a). There is thus a danger that early loss could cut across the GHT sector boundaries and fail to show significant abnormality in either sector.

The use of 5 descriptive outputs from the GHT, rather than a continuous scale, as is found with other global indices (MD and PSD), is less than ideal. A continuous output scale could include probability estimates and allow asymmetry to be tracked over time.

The computation of the GHT output is based upon the values presented in the pattern deviation probability map and is thus difficult to reproduce outside of the HFA software as the probability limits are not in the public domain.

The aim of this study is to describe 3 new superior-inferior asymmetry indices for detecting visual field loss in POAG and to compare these with the GHT. Our objectives in developing these new indices are to avoid the use of sectors within each hemifield, to provide a continuous output scale with probability values and to use well defined and easily reproduced computational methods that can be incorporated in third party analytical software.

## Methods

All the data used in this study were obtained retrospectively from patients attending MREH between 2007-12. Visual field data came from the 24-2 test pattern using the SITA strategy of the HFA. Visual field data were exported from the HFA to Excel 2010 (Microsoft, Redmond, WA) for analysis. The stage of visual field loss was quantified with Glaucoma Staging System II (GSS 2) (Brusini and Filacorda, 2006). Selection took no account of the reliability indices produced by the HFA software.

### Patients

30,899 SITA 24-2 visual field records were initially extracted from the database. Eyes with GSS stage ≤1, were then randomly selected and, following a record review to ensure they meet the inclusion criteria, assigned to one of the following groups.

*Controls (n=412 eyes from 206 patients)*

All patients had normal visual fields in both eyes at 2 consecutive visits (GHT within normal limits and no clusters of three or more neighbouring locations with an age adjusted defect of ≥5dB). Each included eye had a corrected visual acuity of 6/9 or better in patients <50 years of age or 6/12 or better in patients >50 years of age, intraocular pressures (IOP) of <22mmHg (Goldmann applanation), refractive error of between -5 and +5 Diopters (spherical equivalent), no history of serious eye disease or trauma, a normal optic nerve head (clinical examination) and an absence of any abnormal ocular findings likely to affect the visual field.

*Primary Open Angle Glaucoma (n=247 eyes from 222 patients)*

All POAG eyes had an IOP history of >21mmHg open angles observed by gonioscopic examination and a clinical diagnosis of POAG. In some cases, the selected eye was the better of the 2 eyes and the diagnosis of POAG might have largely been made on the basis of the other eyes findings. These eyes were included to provide a significant challenge to asymmetry analyses.

## New superior/inferior asymmetry analysis

The new asymmetry analyses use the same test locations as the GHT. This is a subset of the 24-2 test pattern, (44/54) excluding locations at or near the blind spot, see Figure 3.1. Each test location in the superior hemifield was paired with

vertically mirrored location in the inferior hemifield resulting in 22 test pairs.
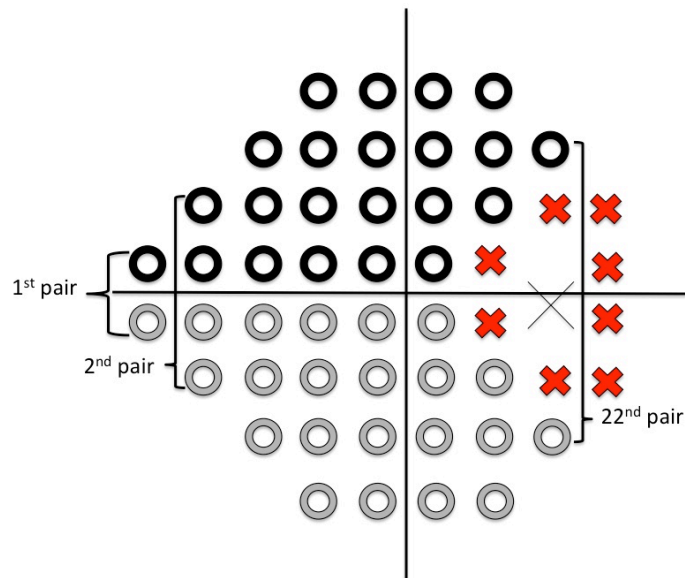


Figure 3.1: The 44 test points (black and grey annuli) of the 24-2 test pattern used in the analysis. Each point in the superior hemifield (black annulus) was paired with a vertically reversed point in the inferior hemifield (grey annulus) to provide 22 test pairs.

Figure 3.2 gives a flow chart of the analytical steps used in the new asymmetry analyses. The analysis is based on HFA defect values rather than a scoring of the values presented in the pattern deviation probability map, as used in the GHT, and does not pool data within any sectors. A bootstrapping procedure was used on the control sample (2000 samples of 412 eyes, randomly selected with replacement) from which the analysis empirically derived the normal limits for the Hemifield

Mean Difference (HMD) and the Hemifield Standard Deviation (HSD) of differences. HMD was a mean defect value calculated for all 22 pairs in each patient using this formula:

$$\text{HMD} = \frac{X_1 + X_2 + X_3 + \text{.......} + X_{22}}{22}$$

Where, x = asymmetry defect value in $n$ pairs

HSD was standard deviation value, obtained by using this formula:

$$\text{HSD} = \sqrt{\frac{(x_1 - \bar{x})^2 + (x_2 - \bar{x})^2 + (x_3 - \bar{x})^2 + \text{.....} + (x_{22} - \bar{x})^2}{22}}$$

Where, x = asymmetry defect value in $n$ pairs,

$\bar{x}$ = mean deviation value

HNP was obtained by calculating total number of asymmetric pairs that fall outside the 85% reference limits for each of the 22 test pairs in each patients. HNP more than 6 is classed as abnormal.

```
┌──────────────────────┐          ┌──────────────────────┐
│   412 control eyes   │          │    247 POAG eyes     │
└──────────┬───────────┘          └──────────┬───────────┘
           │                                 │
           ▼                                 ▼
┌──────────────────────┐          ┌──────────────────────┐
│  Calculate various   │          │ Transfer cut offs to │
│ confidence limits* for│─────────▶│     POAG sample      │
│  HMD, HSD  and NP    │          │                      │
└──────────┬───────────┘          └──────────┬───────────┘
           │                                 │
           ▼                                 ▼
┌──────────────────────┐          ┌──────────────────────┐
│ Calculate specificies│          │Calculate sensitivities for│
│  for HMD, HSD and NP │          │   HMD, HSD and NP    │
└──────────┬───────────┘          └──────────┬───────────┘
           │                                 │
           └────────────┬────────────────────┘
                        ▼
              ┌──────────────────────┐
              │ Generate ROC curves  │
              └──────────────────────┘
```
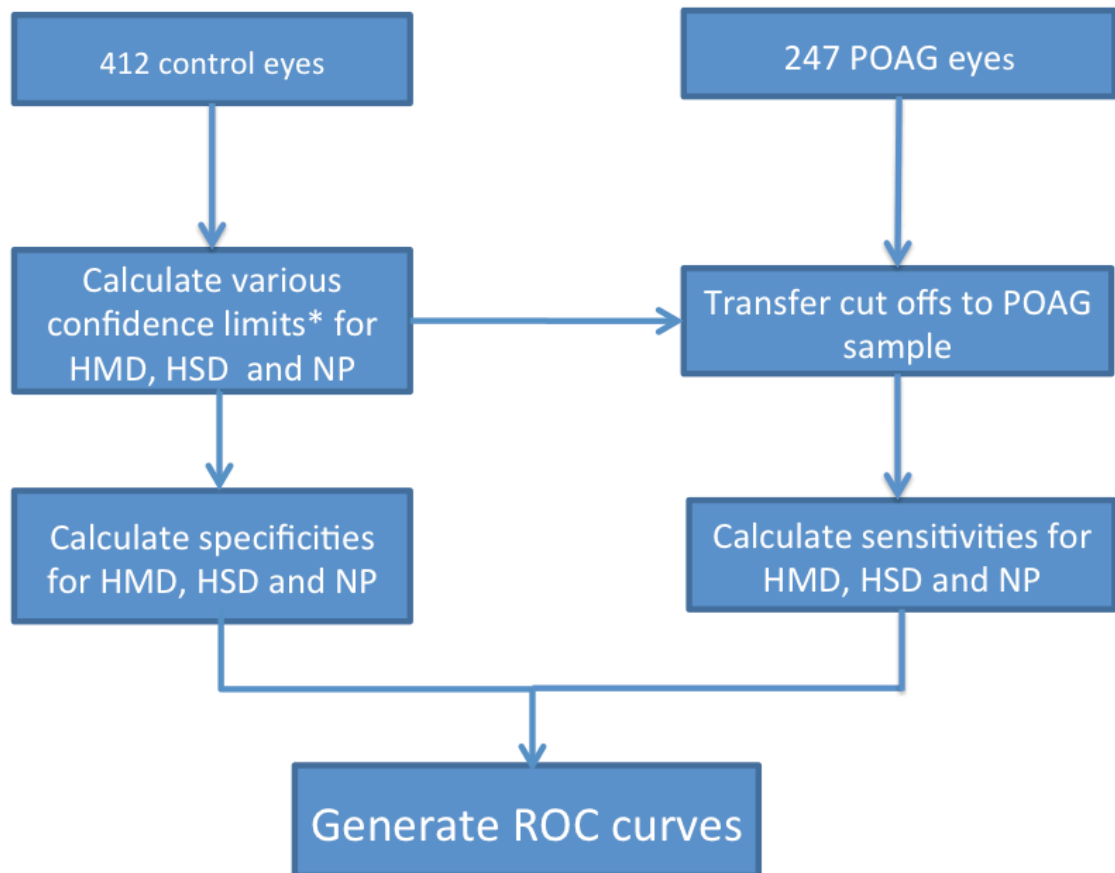
* 85% reference limits were determined using bootstrapping procedure (2000 samples of 412 eyes, randomly selected with replacement).

Figure 3.2: Flow chart of the analytical steps taken in the hemifield analysis. HMD-Hemifield Mean Difference; HSD-Hemifield Standard Deviation of differences; NP- number of pairs falling outside the 85% reference limits for each of the 22 test pairs.

The sensitivity and specificity of various cut off criteria were calculated from the control and POAG populations to derive ROC curves for HMD, HSD and Number of asymmetric Pairs (NP; outside 85% reference limits). The sensitivity and specificity

of the GHT analysis (values copied from charts) was also established when borderline value was classified as 'within normal limits' and 'outside normal limits'. The ROC curve areas were compared using a method derived by Hanley and McNeil (Hanley and Mcneil, 1983).

A proportional Venn diagram was constructed to graphically represent the agreement for the presence of a defect in the POAG eyes. The nature of disagreements were explored by visual inspection of the visual field charts.

3x3 contingency tables were constructed to further explore agreement between GHT and HMD and between GHT and HSD in both control and POAG eyes.

## Results

This study included POAG eyes with little or no visual field loss on the basis of GSS (41 in stage 0; 25 in stage Borderline; 181 in stage 1) and 412 control eyes (stage 0). Subjects with POAG were slightly older than controls, and the difference was statistically significant ($p<0.01$) with mean age (years) for Control and POAG samples being 60.4 ±10.6 and 71.7 ±13.2 respectively. Mean MD and mean PSD for Controls and POAG were also statistically significant. Mean MD was 0.31 ±0.85dB in Controls and -2.21 ±1.32dB in POAG; mean PSD in Controls and POAG were 1.63 ±0.32dB and 3.96 ±3.12dB respectively. Mean number of pairs (max 22) that fall outside various confidence limits derived from the control population were also calculated. The number of pairs for the POAG eyes that fall outside

various confident limits were, as suspected, significantly larger (P<0.01) than the controls.

Figure 3.3 gives the ROC curves for the new asymmetry indices along with the results from the GHT. The discriminatory power of NP and HSD as measured by the AUROC curve is significantly better than GHT, see table 3.1, but care needs to be taken when interpreting this finding as AUROC values for GHT are based on just 2 measures rather than a wide range of measures for the new indices and this could result in an under estimate of the AUROC measure for GHT.

**Table 3.1: Area under the ROC curves for the different Hemifield indices. NP=number of pairs outside the 85% CI of control sample; HSD=standard deviation of the hemifield differences; HMD=Mean hemifield difference**

|  | NP | HSD (dB) | HMD (dB) | GHT |
|---|---|---|---|---|
| **AUROC** | 0.86 | 0.86 | 0.75 | 0.79 |
| **95% confidence limits** | 0.83-0.89 | 0.83-0.89 | 0.71-0.79 | - |

The AUROC of NP used the 85% reference limit of the control group, which could have led to an over-estimation of diagnostic performance. Alternative probability limits (90, 95%) led to a slightly lower performance (AUROC 0.85, 0.85). At 95% specificity, the sensitivity value for HMD, HSD and NP were 39.2% (95% CI 36.4-42.1%), 55.5% (95% CI 52.5-58.4%) and 51.4% (95% CI 48.0-54.4%) respectively.
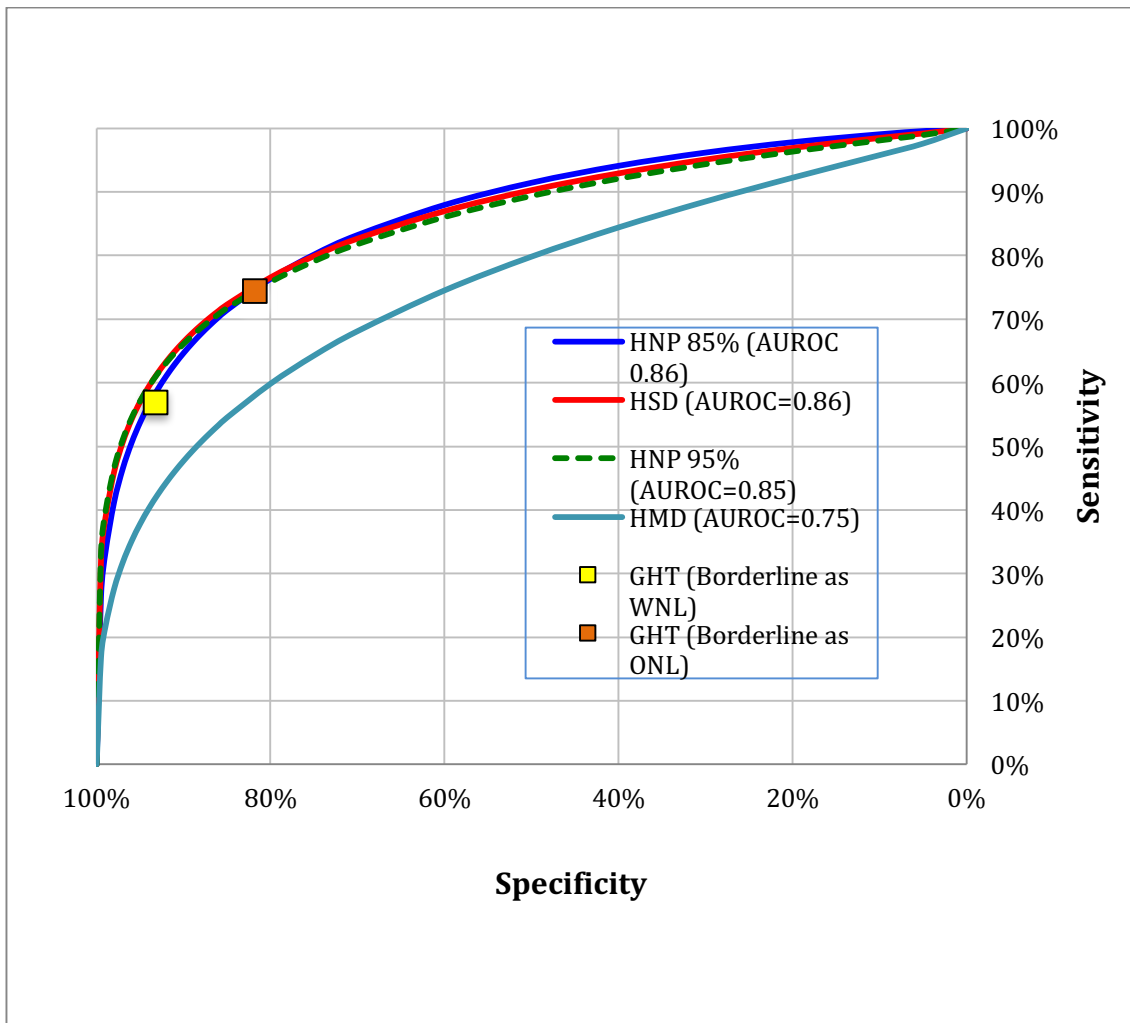
Figure 3.3: ROC curves for: GHT-(Glaucoma Hemifield Test) when borderline values are classified as within and outside normal limits; NP- number of pairs falling outside 85 and 95% reference limits; HMD- Mean Hemifield difference; HSD Hemifield Standard Deviation of differences; WNL-Within Normal Limits; ONL-Outside Normal Limits.

The Venn diagram in Figure 3.4 illustrates the good agreement for the presence of a defect in the POAG eyes between the indices HSD, NP and GHT. HMD has not been included due to limitations of proportional Venn diagrams and its relatively poor discriminatory performance. Complete agreement for presence of a defect

was found in 91 eyes (79%). Five examples where the GHT and new asymmetry analyses give different outcomes are given in table 3.2. The format of the new indices follows that of the MD and PSD indices, giving a measure of the asymmetry followed by a 'p' value if it falls <10%. Categories for p values being <10%, <5%, <2%, <1% and <0.5%. Comments are included in the table.

The 3x3 contingency tables, Figure 3.5, give a more complete analysis of agreement, including data on the control eyes and a borderline classification. For the POAG eyes complete agreement was 78% (HSD vs GHT) and 82% (NP vs GHT) in the control sample and 70% (HSD vs GHT) and 71% (NP vs GHT) in the POAG sample. For these tables cut off criteria for HSD and NP were chosen to match, as close as possible, the GHT values. The contingency tables again highlight the good agreement between GHT, HSD and NP. Contingency tables for HMD have again not been included due to its relatively poor discriminatory power as evidenced in the ROC curves.

## POAG sample

|      |   | GHT |   |   |
|------|---|-----|---|---|
|      |   | N   | B | D |
|      | N | 12  | 4 | 5 |
| HSD  | B | 5   | 3 | 7 |
|      | D | 2   | 7 | 55|

## Control sample

|      |   | GHT |   |   |
|------|---|-----|---|---|
|      |   | N   | B | D |
|      | N | 74  | 8 | 3 |
| HSD  | B | 7   | 2 | 1 |
|      | D | 1   | 1 | 2 |

## POAG sample

|      |   | GHT |    |   |
|------|---|-----|----|---|
|      |   | N   | B  | D |
|      | N | 12  | 2  | 4 |
| NP   | B | 3   | 2  | 5 |
|      | D | 4   | 10 | 57|

## Control sample

|      |   | GHT |   |   |
|------|---|-----|---|---|
|      |   | N   | B | D |
|      | N | 78  | 8 | 2 |
| NP   | B | 3   | 2 | 1 |
|      | D | 2   | 1 | 2 |

Figure 3.4: 3x3 contingency tables showing the percentage level of agreement between the 2 new indices HSD (Hemifield Standard Deviation) and NP (Number of pairs falling outside the 85% confidence limits) and GHT (Glaucoma Hemifield test), for the control and POAG sample populations. For HSD and NP cut offs were selected to match, as close as possible, the 2 GHT values.
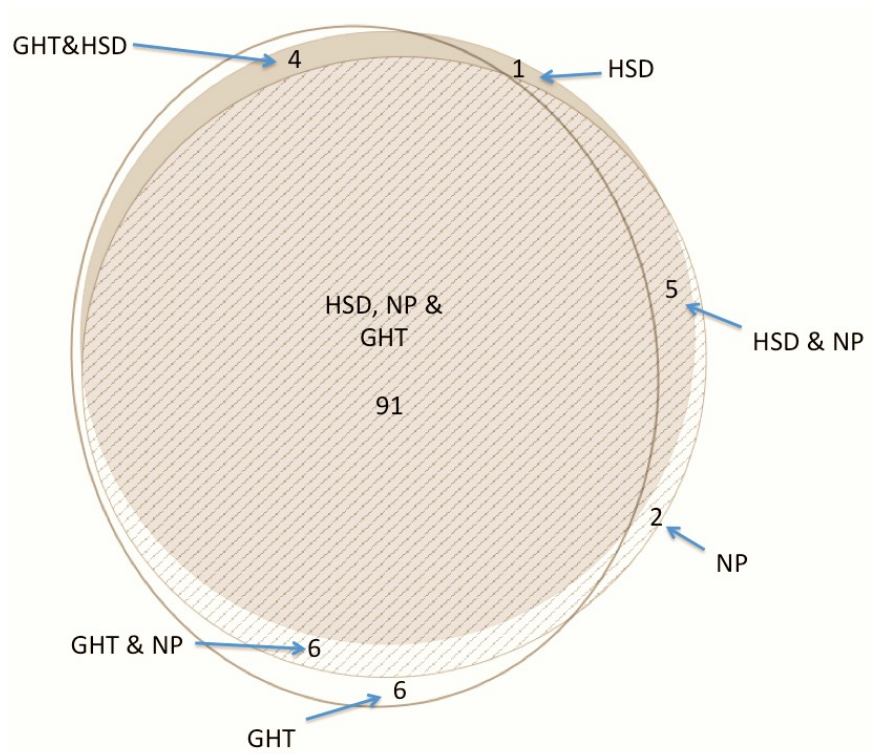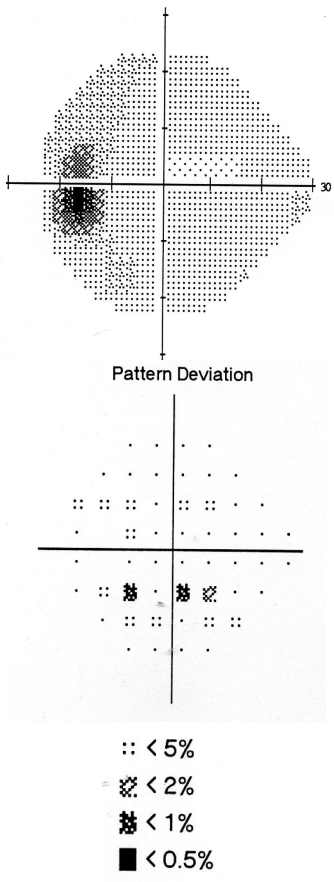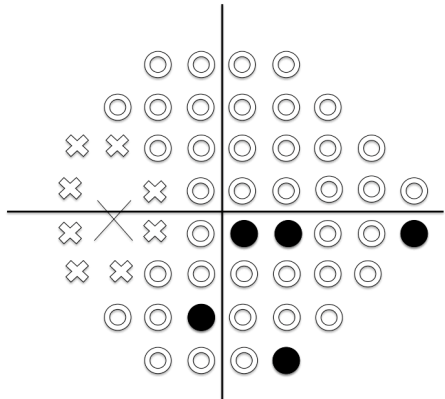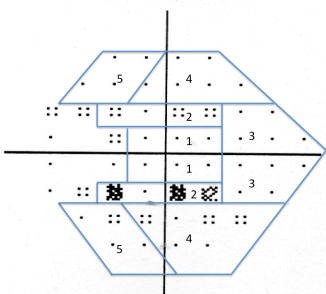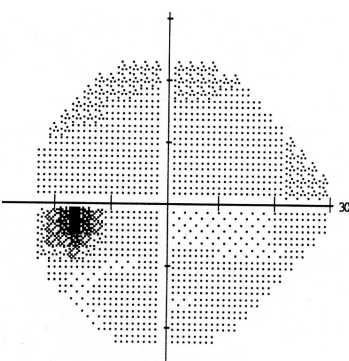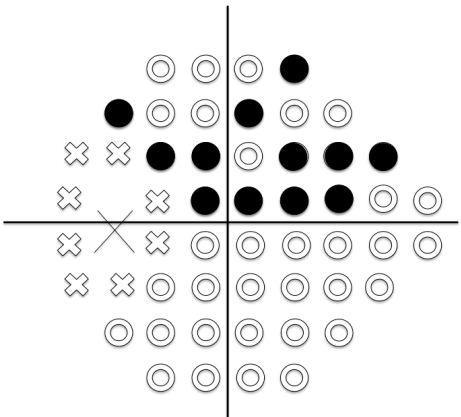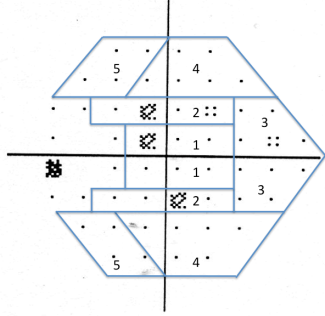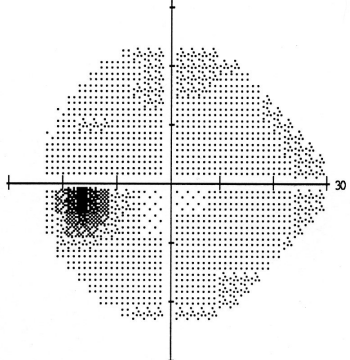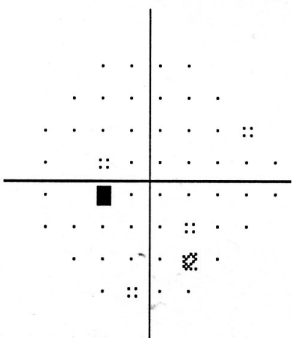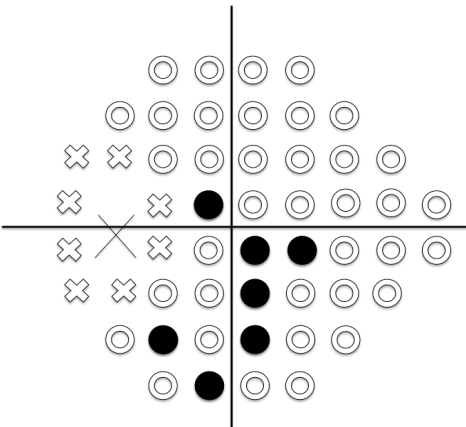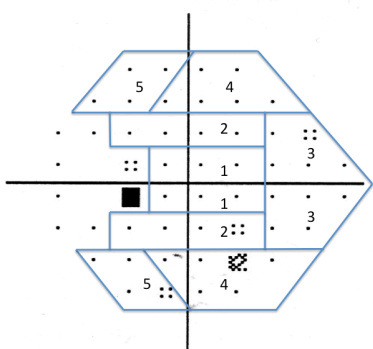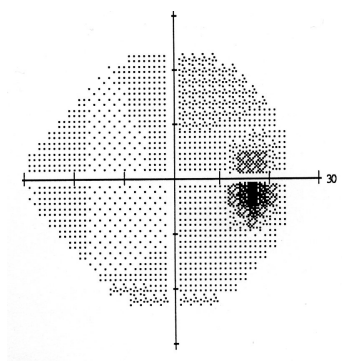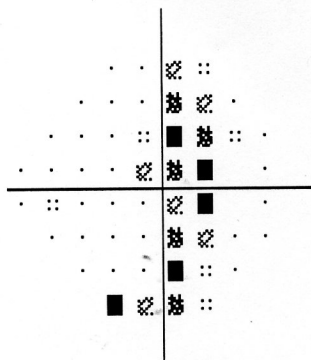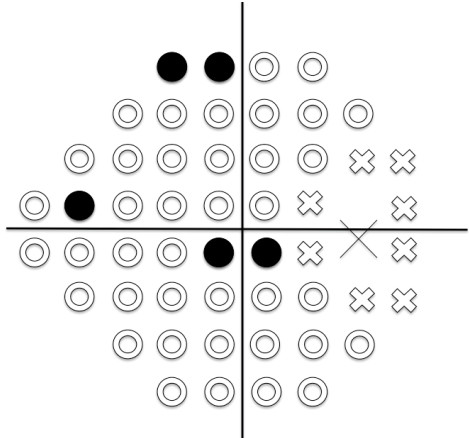
Figure 3.5: Venn diagram showing agreement for presence of a defect in POAG eyes. GHT-Glaucoma Hemifield Test; NP- number of points falling outside 85% reference limits; HSD-Hemifield Standard Deviation of differences. This figure only includes data where eyes fell within the normal or defect (no borderline) classification for all 3 indices (N=115). Diagram was reproduced using euler*APE* software
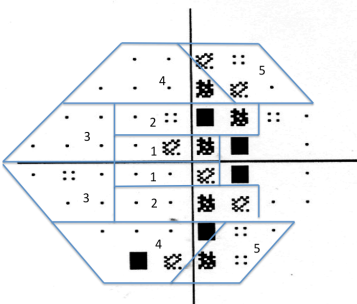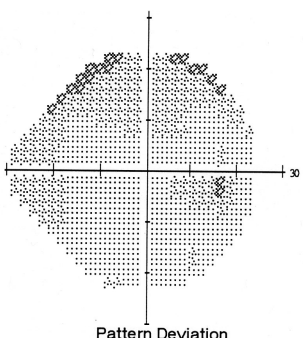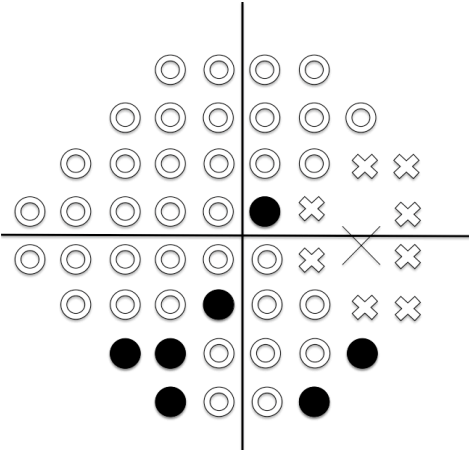
**Table 3.2: Clinical examples of comparison between the Glaucoma Hemifield Tests (GHT) and the new asymmetry indices. NP- number of points falling outside 85% reference limits (NP more than 6 is classed as abnormal); HMD-Hemifield Mean Difference; HSD-Hemifield Standard Deviation of differences.**

| Glaucoma Hemifield Test | Clinical Diagnosis | New Indices |
|---|---|---|
| **#128** <br><br> Pattern Deviation <br><br> :: < 5% <br> ⚌ < 2% <br> ▨ < 1% <br> ■ < 0.5% | POAG on treatment (Latanoprost nocte both eyes and Cosopt twice to both eyes) <br><br><br> Vision: 6/9 <br><br> Intraocular pressure: 14mmHg <br><br> Disc: cupped |  <br><br> NP: 5/44 (Normal) <br><br> HMD: -1.359 dB (P <15%) <br><br> HSD: 1.4dB <br><br><br> Comment: <br><br> This is the case where only GHT classed this field as defective (outside normal limits) while new indices (NP and HSD) classed as non-glaucomatous field loss |

Pattern Deviation

GHT
Outside Normal Limits

VFI    96%

MD    -3.09 dB  P < 2%
PSD   1.79 dB  P < 10%

---

**#178**



Pattern Deviation

1. POAG with treatment (Travatan od nocte both eyes)

2. Cataract

3. Previous trabeculectomy surgery R and L

Vision: 6/9

IOP: 16 mmHg



NP: 12/44 (defect)

HMD: -2.035 dB (P<2%)

HSD: 1.9 dB

Comment:

:: < 5%

⊠ < 2%

⊠ < 1%

■ < 0.5%

Pattern Deviation



GHT
Within Normal Limits

VFI    97%

MD    −2.95 dB  P < 2%
PSD    1.93 dB  P < 10%

This is the case where only NP classes the field as defective (points fall outside probability value are more than 6) while other indices classify (GHT and HSD) as normal

---

**#267**



Pattern Deviation



1.Pseudophakia

2. POAG on treatment (Latanoprost both eyes nocte)

Visual acuity: 6/9 both eyes

IOP: 13mmHg in both eyes

ONH: Thinning of the inferior rim



NP: 7/44

HMD: 1.123

HSD: 2.2


Comment:

This is the case where only NP

| | | classes the field as defective, while others (GHT and HSD) suggest normal field. |
|---|---|---|

:: ‹ 5%

✍ ‹ 2%

❄ ‹ 1%

■ ‹ 0.5%

**Pattern Deviation**



GHT
Within Normal Limits

VFI    98%

MD    -2.19 dB  P ‹ 5%
PSD    1.99 dB  P ‹ 10%

---

**# 217**



Pattern Deviation



1. POAG on treatment (Xalatan nocte both eyes)

Visual acuity: 6/7.5

IOP: 16mmHg

ONH: Cupped disc ratio of 0.9



NP: 5/44

HMD: 0.378 dB

HSD: 2.95 dB (P<5%)

Comments:

This is the case where only HSD

:: < 5%
※ < 2%
※ < 1%
■ < 0.5%

Pattern Deviation

GHT
Within Normal Limits

VFI    93%

MD    -2.45 dB  P < 5%
PSD    2.55 dB  P < 2%

classes the field as defective, while others (GHT and NP) suggest normal field.

---

# 91



Pattern Deviation

:: < 5%
※ < 2%
※ < 1%
■ < 0.5%

1. POAG on treatment ( Guttae Cosopt and guttae Xalatan in both eyes)

IOP: 17mmHg.

ONH: Cup/disc ratio is 0.8



NP:  7/44

HMD: -1.274 dB (P< 10%)

HSD: 2.89 dB (P< 5%)


Comments:

This is the case where new indices (NP and HSD) classed the field as defective while GHT classed as normal.

Pattern Deviation

GHT
Within Normal Limits

VFI    97%

MD    −4.00 dB  P < 1%
PSD    1.98 dB  P < 10%
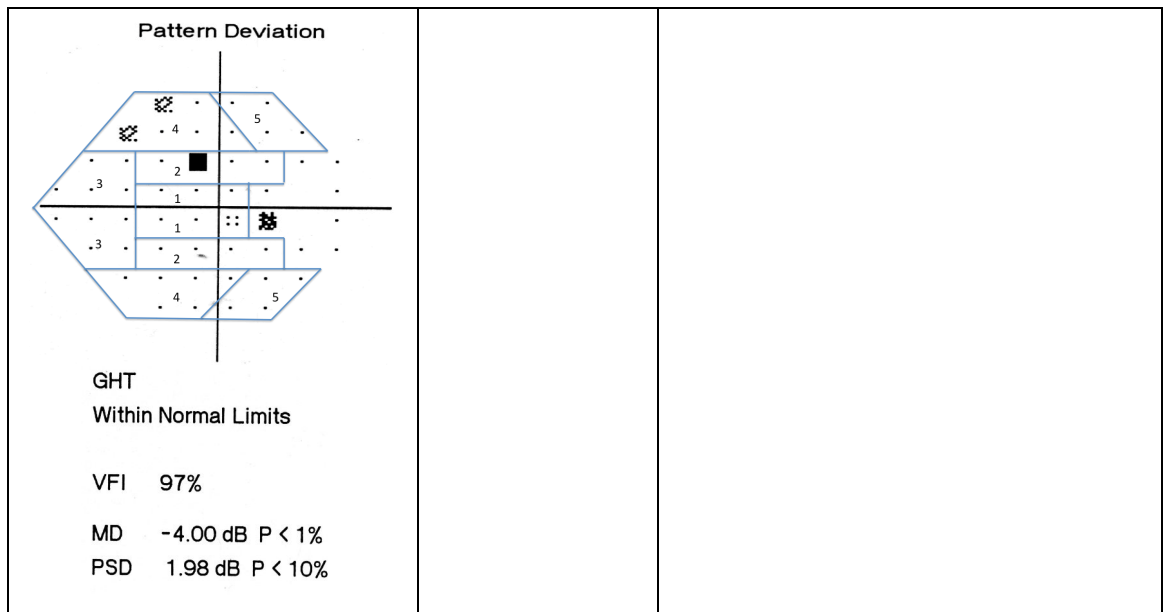
## Discussion

The detection of early glaucomatous changes in the visual field is hampered by the large range of values within the normal population. Thus while global indices MD and PSD are valuable when looking for change in the visual field over time their discriminatory power has never been very high. Global indices based on comparisons within an eye overcome between subject variability and have a much greater discriminatory potential.

In this paper we have looked at the discriminatory power of 3 new Sup/Inf hemifield indices and compared these to the well-established GHT analysis incorporated in the HFA.  A total of 659 eyes, classified on the basis of clinical diagnosis (Control, POAG), were used to derive estimates of discriminatory power.

The POAG sample was limited to eyes with little or no visual field loss measured by MD and PSD (GSS2≤1). In some cases the diagnosis of POAG seemed to be based more on the existence of POAG in the fellow eye. Including eyes where there is no apparent visual field/structural loss, but a high risk of loss, provides a diagnostic challenge to the new and established Sup/Inf hemifield analyses. However, the inclusion of these eyes will tend to depress the reported sensitivity estimates.

The inclusion criteria of 'GHT within normal limits' for the control group may have had the opposite effect, reducing variance in the control group and hence improving the performance of the hemifield analyses. While the reported sensitivity and specificity values are dependent upon the inclusion criteria this should not affect the relative performance of the indices as they are all based upon the same datasets.

In this study we did not exclude eyes on the basis of their reliability indices. This was for 2 reasons. First, we wished to establish performance on a representative clinical population where poor reliability is not exceptional and, second, the precision of these indices is poor (Bengtsson, 2000) especially the 'fixation' index which is often compromised by an error in locating the blind spot at the onset of the test.

Two of the outputs from the GHT are 'abnormally high sensitivity' and 'general reduction in sensitivity'. In this analysis we have ignored data that falls into these categories. Such classifications were rare comprising ~2% of eyes.

Our work looked at 3 different methods for quantifying the Sup/Inf asymmetry. The output from these indices has been designed to be familiar to perimetrists. HMD being similar to Mean Deviation, HSD similar to Pattern Standard Deviation and Number of asymmetric pairs similar to probability plots.

The discriminatory performance of HMD fell well below that of the other 2 indices, HSD and NP. This finding was not surprising given the relatively poor performance of Mean Deviation at discriminating between normal eyes and those with early glaucomatous loss. The poor performance of Mean Deviation is often ascribed to the local nature of early loss where a few locations can show significant loss but whose significance disappears when averaged with a large number of non-damaged locations. In contrast, HSD can be significant when only a small number of locations differ by moderate amounts.

The choice of pattern deviation probability values in GHT was based upon the work of Asman and Heijl who established, from an ROC analysis, that giving probability values a score that could be summed within each sector gave an improved performance over an analysis of defect values at sensitivity and specificity values above 90% (Asman and Heijl, 1992b). Our HSD and NP AUROC analysis, which does not involve summing scores within sectors and which use a similar bootstrapping procedure to that used by Asman & Heijl to provide empirical cut offs for each pair of test points, performs well at values above 90% and matches the performance of GHT at their cut off values.

Recent work on the structure function relationship (Jansonius et al., 2012b, Lamparter et al., 2013) in glaucoma has highlighted how anatomical variations impinge upon the mapping of the visual field to the optic nerve head. Although the possible benefit from using sector borders is to facilitate the detection of glaucomatous defect pattern, using fixed sectors for the pooling of visual field data introduces a risk that early defects may straddle sector boundaries and fail to reach significance within a sector. The last 4 cases in table 3.1 are examples of where the GHT failed to detect an asymmetry that was evident to the new indices because the defect straddled the GHT sector boundaries.

The use of continuous outputs and probability levels in a format similar to MD and PSD allows better tracking over time than can be achieved with the 5 output classes of the GHT. Asman and Heijl (Asman and Heijl, 1992b) point out that the GHTs performance, which included a borderline classification, was superior to earlier methods developed by Sommer et al (Sommer et al., 1985) which used a simple binary (defect/no defect) classification as many defects cannot be classified as either normal or pathological with any certainty. The new algorithms continuous scales and probability estimates improve further on this issue allowing a perimetrist to see movement within the sector boundaries of the GHT. The benefits of using a continuous scale are highlighted in the ROC analysis. The GHT analysis only allows 2 points on the ROC curve (when borderline cases are included in the 'outside normal limits' and 'within normal limits' categories). This is likely to result in an underestimate of what could be achieved with a continuous scale.

Importantly, the new indices are all based on simple well-defined methods that can easily be imported into third party software. The authors are happy to supply data on the probability limits needed for such calculations.

Bootstrapping is a re-sampling method for approximating the sampling distribution of a statistic. In this experimental chapter, the data is re-sampled with replacement and the statistic is computed. This process is repeated to produce a distribution of values for the statistic. Since the bootstrapping procedure is distribution-independent, it provides an indirect method to assess the properties of the distribution underlying the sample and the parameters of interest that are derived from this distribution.

In conclusion, our new Sup/Inf hemifield analysis techniques have been shown to have good diagnostic performance in the early stages of glaucoma. GHT can fail to detect significant asymmetry, detected by HSD and NP, when an early defect crosses sector boundaries. The new indices use methods and outputs that are familiar to clinicians working with glaucoma patients and can easily be adapted for use in third party software.

# 4. Right-Left Visual Field Asymmetry Indices for Detecting early POAG.

## Contribution:

The project was conducted under supervision of Prof David Henson. The dataset used here was collected from patients attending the outpatient department of MREH as part of their routine management for suspect/diagnosed glaucoma. I extracted the data from the database, taking into account the inclusion/exclusion criteria, performed the data analysis and presented the work at conferences. I also authored the paper.

## Publication

**Ghazali N**., Aslam T., Henson DB. (2015) Right-Left Visual Field Asymmetry Indices for Detecting early POAG. (Manuscript in preparation)

## Conferences

**Ghazali N**., Aslam T., Henson DB. (2015) Diagnostic performance of New superior-inferior and right left visual field asymmetry indices for detecting POAG. Accepted as a poster for presentation at ARVO 2016 Annual Meeting, Seattle, Washington, USA.

## Abstract:

**PURPOSE**: To investigate the performance of visual field indices based on R/L eye asymmetries at detecting early loss in POAG and to establish whether their performance is superior to uniocular hemifield indices.

**METHODS**: 206 control and 108 POAG patients (clinical diagnosis) were selected from a visual field database of patients attending Manchester Royal Eye Hospital. All POAG eyes had early glaucoma (GSS stage≤1). Age related defect asymmetries were calculated for each of the 44 test point pairs used in the Humphrey GHT. Two new indices were investigated: 1) R/L Standard Deviation (R/L SD) of differences; 2) Number of test Pairs (R/L NP) outside 95% CL of controls. Both indices were derived for whole field data (44 test pairs) and for hemi field data (2x22 test pairs). ROC curves were generated for the R/L indices along with those for 3 uniocular worse eye hemifield indices: 1) GHT; 2) Hemifield Standard Deviation (HSD) of differences; 3) Hemifield Number of asymmetric Pairs (NP; outside 95% CL) (HNP).

**RESULTS**: The control and POAG samples median MD was 0.29dB (Interquartile range (IQR) 1.07) and -2.4dB (IQR 1.55) while the median absolute MD differences between the two eyes were 0.47dB (IQR 0.61) and 0.99dB (IQR 1.21). Uniocular worse eye Sup/Inf hemifield indices performed better than the new R/L eye asymmetry indices. HSD worse eye and HNP worse eye have the highest

discriminatory power, followed by R/L SD and R/L NP (AOROC for HSD Worse eye=0.97; HNP Worse eye=0.94;  R/L SD=0.90;  R/L NP=0.90).

**CONCLUSIONS**: The new R/L asymmetry indices did not perform better than worse eye uniocular hemifield asymmetry indices and GHT in differentiating between normal and POAG eyes.

## Introduction

The diagnosis of POAG is based upon characteristic structural changes to the ONH (including the nerve fibre layer) and corresponding functional changes to the visual field. Raised IOP being a risk factor but not essential for the diagnosis. Over the last few years there have been tremendous developments in imaging technologies and the analytical methods used to extract and present the data needed for the detection and management of POAG. Comparatively speaking, there has been very little development in the techniques used to collect and present visual field data. The SITA algorithm of the HFA was introduced in 1997 (Bengtsson et al., 1997) and the Statpac analysis, which introduced probability maps and the single field analysis print out, was first produced in 1987 (Heijl et al., 1987b).

An important characteristic of structural and functional loss seen in early POAG is its asymmetry. Early loss is invariably more advanced in one eye than the other and within an eye is more advanced in either the superior or inferior hemifield. Asymmetry analyses, where comparisons are made within and between eyes of a patient, benefit from being a within subject design. Within subject designs do not include the errors that arise from variance between individuals and thus have an enhanced potential to detect early changes in the disease process. The GHT (Asman and Heijl, 1992b) which quantifies Sup/Inf hemifield asymmetry is a within subject design that has been shown to be valuable in detecting early POAG loss (Asman and Heijl, 1992a, Katz et al., 1995). GHT has been used in several of the major glaucoma trials to help identify patients with functional loss (Leske et al., 1999, Musch et al., 1999). One of the shortcomings of the GHT has been its reliance on fixed sectors within the superior and inferior hemifields. This

shortcoming has recently been addressed with the development of 2 new hemifield indices, Hemifield Standard Deviation (HSD) and a count of vertically paired locations that fall outside the normal 95% CI (HNP) (Ghazali et al., 2015).

R/L visual field asymmetry, which has been proposed as a valuable addition to the clinician's visual field analysis toolbox, has not so far been adopted within commercial perimeters (Henson et al., 1986, Feuer and Anderson, 1989, Levine et al., 2006). In contrast, R/L asymmetry analysis is widely available in imaging devices (OCT, HRT, GDx) and in electrophysiology to aid discrimination. (Asrani et al., 2011)

In this study, we investigate the diagnostic performance of R/L visual field asymmetry in early cases of POAG. This performance is then compared to that of uniocular analyses to see if the new indices offer superior discriminatory power.

## Methods

All the data used in this study was obtained retrospectively from patients attending MREH between 2007-12. 30,899 SITA 24-2 visual field records were exported from the HFA to Excel 2010 (Microsoft, Redmond, WA) for analysis. The stage of visual field loss was quantified with the GSS (Brusini and Filacorda, 2006). GSS classifies each 24-2 threshold test on the basis of the global indices MD and PSD into 7 stages (Normal, Borderline and 5 stages of loss). Selection took no account of the reliability indices produced by the HFA software as these are often unreliable

(Bengtsson and Heijl, 2000) and to make our results generalizable to clinical populations where good reliability indices are not always obtained.

**Patients**

Patients in whom both eyes had a GSS stage ≤1 (Normal, Borderline and early loss) were selected from the Excel database.  This ensured that the POAG cohort was limited to patients with little visual field loss in either eye and thus provided a challenging task to the new and established indices.  Following a record review to ensure each patient met the inclusion criteria they were assigned to one of the following 2 groups.

### Controls (206 patients)

All patients had normal visual fields in both eyes at 2 consecutive visits (GHT within normal limits and no clusters of three or more neighbouring locations with an age related defect of ≥5dB). Each included eye had a corrected visual acuity of 6/9 or better in patients <50 years of age or 6/12 or better in patients >50 years of age, IOP of <22mmHg (Goldmann applanation), refractive error of between -5 and +5 Dioptres (spherical equivalent), no history of serious eye disease or trauma, a normal ONH (clinical examination) and an absence of any abnormal ocular findings likely to affect the visual field.

*Primary Open Angle Glaucoma (108 patients)*

All patients had an IOP history of >21mmHg open angles observed by gonioscopic examination and a clinical diagnosis of POAG in one or both eyes.

**New R/L asymmetry analysis**

The new R/L asymmetry analyses use the same test locations as the GHT. This is a subset of the 24-2 test pattern, (44/54) excluding locations at or near the blind spot, sees Figure 4.1. Each test location in the right visual field was paired with a mirrored location in the left visual field. A bootstrapping procedure was used on the control sample (2000 samples of 206 patients, randomly selected with replacement) from which the normal limits for differences in defect values for each test pair were empirically derived.
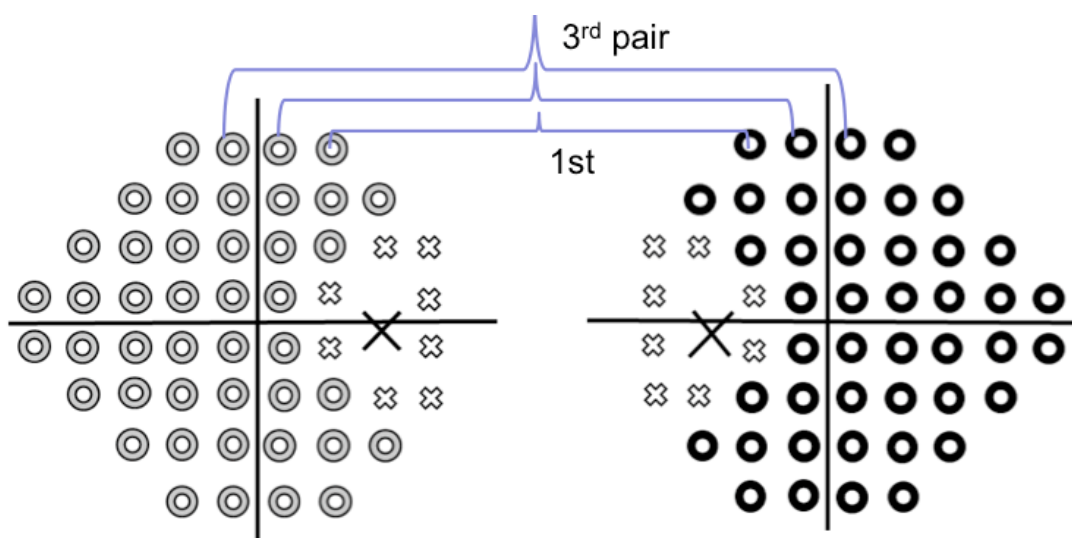


Figure 4.1: The 44 test points (black and grey annulus) used in the analysis. Each point in the
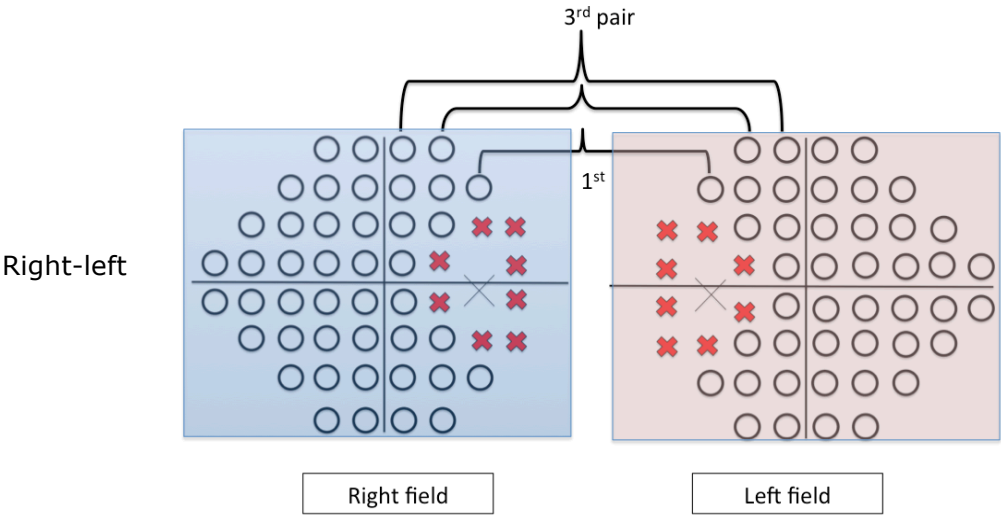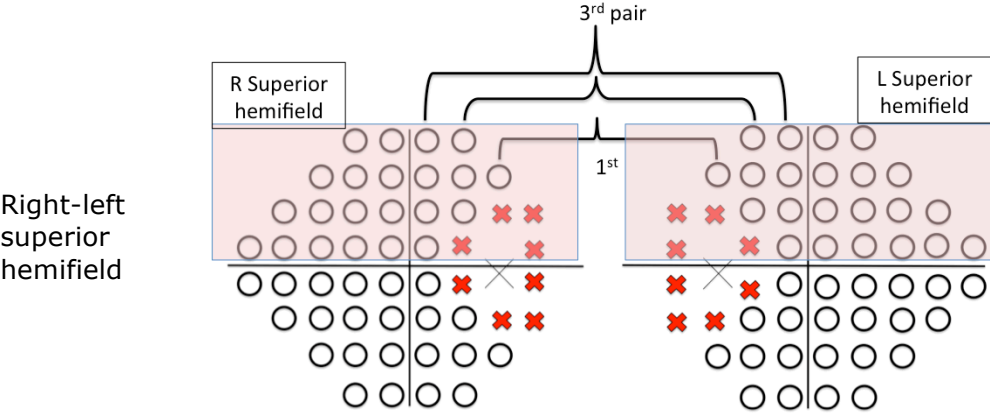
right field (grey annulus) was paired with a mirrored image point in the left field (black annulus) to provide 44 test pairs. Crosses represent 24-2 locations near the blind spot, which were excluded from the analysis.
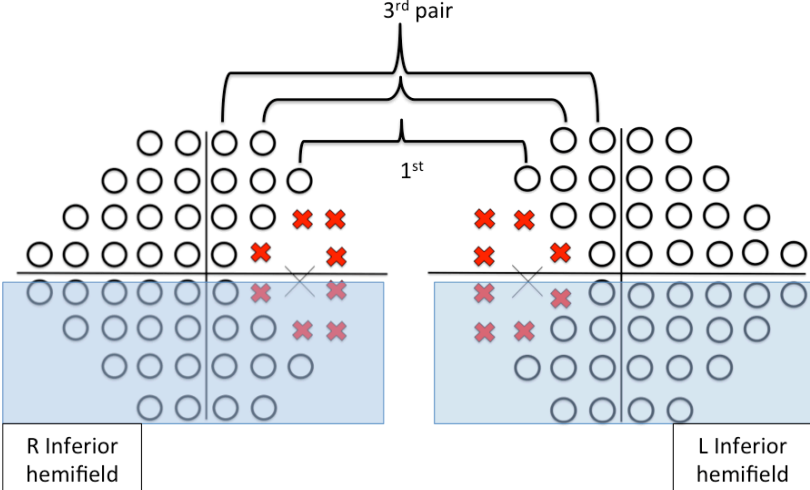
Four different R/L asymmetry analyses were investigated:

1. R/L whole field asymmetry (44 pairs),

2. R/L superior hemifield asymmetry (22 pair),

3. R/L inferior hemifield asymmetry (22 pairs),

4. R/L asymmetry of the worse hemifield (22 points).

Table 4.1 provides detail description of the R/L asymmetry indices and 3 Sup/Inf hemifield indices.

**Table 4.1: Description 11 indices for R/L asymmetry and 3 indices for hemifield asymmetry**

| Indices | Description |
|---------|-------------|
| Right-left |  |
| 1. **R/L MD** | The mean deviation of the differences for the 44 pairs (R/L MD). |
| 2. **R/L SD** | The standard deviation of the differences for the 44 pairs (R/L SD). |
| 3. **R/L NP** | The number of pairs that fall outside the 95% limits in 44 pair of points |
| Right-left superior hemifield |  |

| 4. | R/L MD Superior | Right-left mean deviation of the differences for the 22 pairs in superior hemifield |
|---|---|---|
| 5. | R/L SD Superior | Right-left standard deviation of the differences for the 22 pairs in superior hemifield |
| 6. | R/L NP Superior | The number of pairs that fall outside the 95% limits in 22 pair of point within superior |



| 7. | R/L MD Inferior | Right-left mean deviation of the differences for the 22 pairs in inferior hemifield |
|---|---|---|
| 8. | R/L SD Inferior | Right-left standard deviation of the differences for the 22 pairs in inferior hemifield |
| 9. | R/L NP Inferior | The number of pairs that fall outside the 95% limits in 22 pair of point within inferior hemifield |

| | | |
|---|---|---|
| **10.** | **R/L SD Worse Hemifield** | The worse value between R/L SD superior and R/L SD inferior |
| **11.** | **R/L NP Worse Hemifield** | The worse value between R/L NP superior and R/L NP inferior |



| | | |
|---|---|---|
| **12.** | **HMD Worse Eye** | Worse Hemifield Mean Deviation (HMD) between right and left eye |
| **13.** | **HSD Worse Eye** | Worse Hemifield Standard Deviation (HSD) between right and left eye |
| **14.** | **HNP Worse Eye** | Worse Hemifield Standard Deviation (HSD) between right and left eye |

Figure 4.2 gives a flow chart of the analytical steps used in the R/L asymmetry analyses.
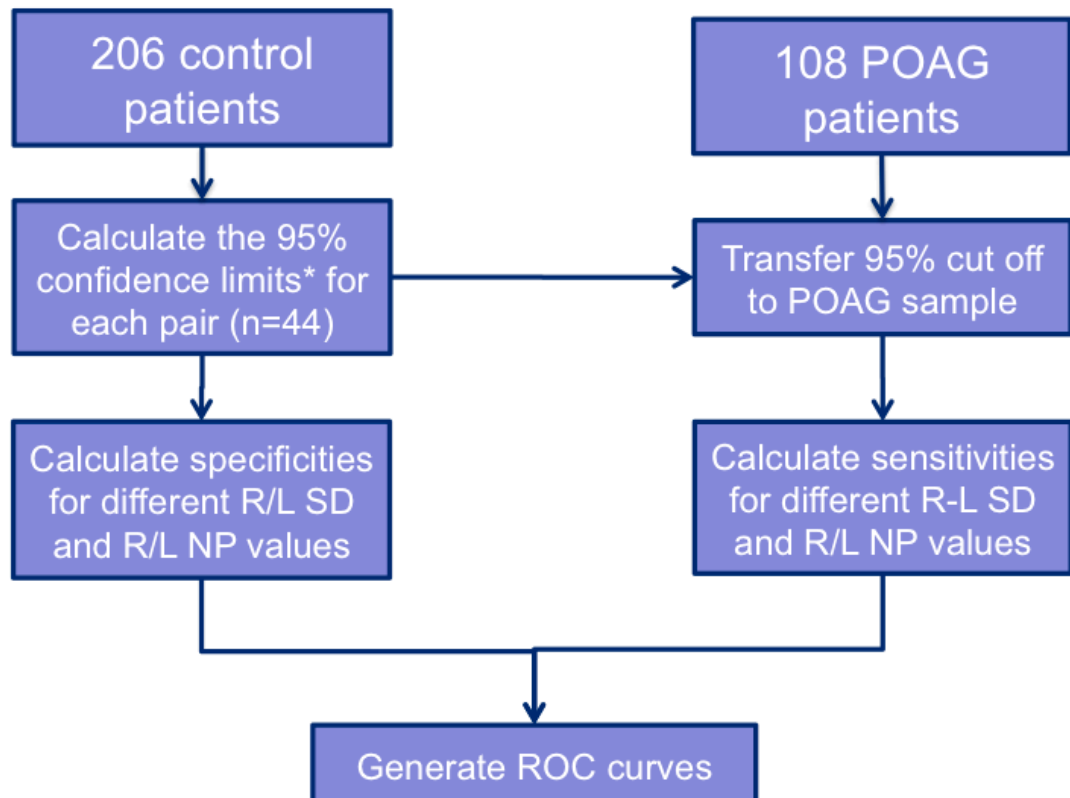


* The 95% reference limits were based upon a bootstrapping procedure (2000 samples of 412 eyes, randomly selected with replacement).

Figure 4.2: Flow chart of the analytical steps taken in the R/L analysis. R/L Standard Deviation of differences (R/L SD); number of test pairs falling outside the 95% confidence limits (R/L NP), (maximum 44).

The sensitivity and specificity of various cut off criteria were calculated from the control and POAG populations to derive ROC curves for all the 11 R/L indices. ROC curves were generated using jrocfit software, a web-based calculator for ROC Curves analysis (http://www.rad.jhmi.edu/jeng/javarad/roc/JROCFITi.html). For each AUROC, 95% confidence limits were calculated. AUROC was not calculated for GHT due to there being only 2 sensitivity/specificity estimates making comparisons inappropriate.

Sup/Inf hemifield indices, HMD, HSD and HNP (see chapter 3), were also calculated for each eye in the POAG and control groups. In this chapter, the inclusion criteria for the POAG and control samples were different to those used in chapter 3 which precluded the use of previous AUROC measures. The eye with the highest HMD, HSD or HNP was selected for comparison with the R/L indices.

The GHT results were extracted from the HFA charts and the eye with the worst GHT result was used for comparison with the R/L indices. Two sensitivity/specificity values were derived, one with Borderline values classed and Outside Normal Limits and one with Borderline values classed as Within Normal Limits.

## Results

The stages of visual field loss in the POAG cohort are given in table 4.2. All but 1 patient had a stage 1 defect in one or both eyes. Forty-eight (44%) had a GSS stage 1 in both eye while 59 (55%) had a stage 1 in just one eye.

**Table 4.2: GSS classification of right and left eyes from the POAG cohort of 108 patients.**

| | | Right eye | | |
|---|---|---|---|---|
| | | Normal | Borderline | Stage 1 |
| Left eye | Normal | 1 | 0 | 17 |
| | Borderline | 0 | 0 | 5 |
| | Stage 1 | 18 | 19 | 48 |

Patients with POAG were slightly older than controls (70.9 ±13.5 versus 60.4 ±10.6 years; p<0.01). The distribution of MD values for the POAG and control samples are given in figure 3. The mean MD for POAG patients was lower than controls (-2.2 ±1.22 versus +0.32 ±0.85 dB; p<0.001).
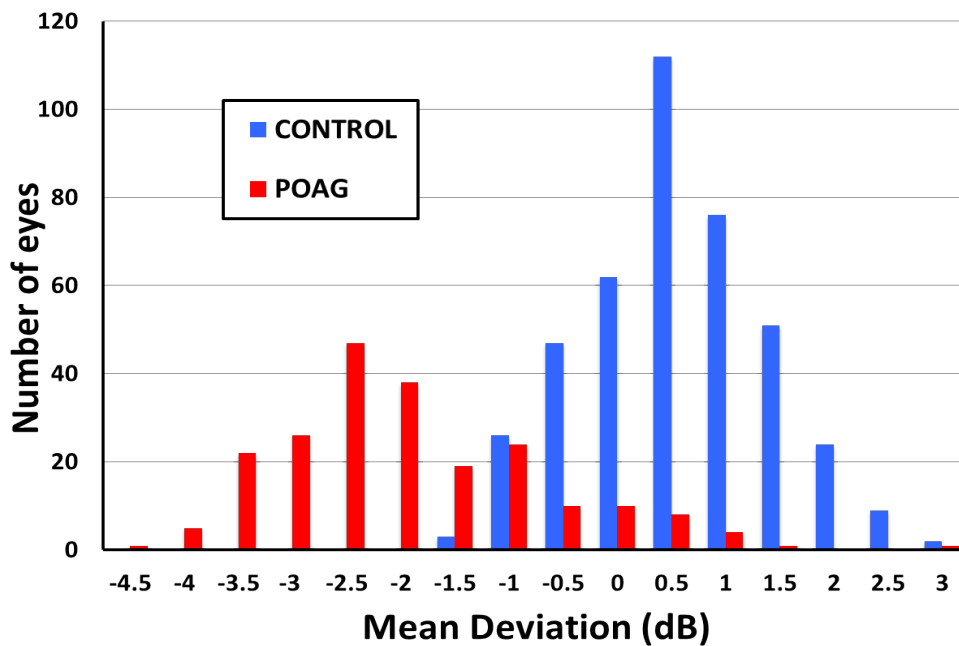
Figure 4.3: Distribution of MD in the POAG and control groups. The distribution of MD for each group was obtained in both eyes.

Figure 4.4 to 4.7 compare the ROC curves for; R/L (whole eye) asymmetry indices, R/L superior hemifield asymmetry indices, R/L inferior hemifield asymmetry indices and best R/L hemifield indices along with GHT. HSD worse eye and HNP worse eye have the highest discriminatory power, followed by R/L NP and R/L SD. The AUROC for all R/L and hemifield indices are presented in Table 4.3.

Table 4.4 provides the comparison of asymmetry analysis between R/L asymmetry (R/L NP), hemifield asymmetry (HSD worse eye) and GHT in 3 out of 6 cases where R/L indices gave a significant asymmetry while Sup/Inf hemifield indices did not. Non-POAG pathology; macula abnormalities, media opacities and amblyopia were found to be associated with these differences.
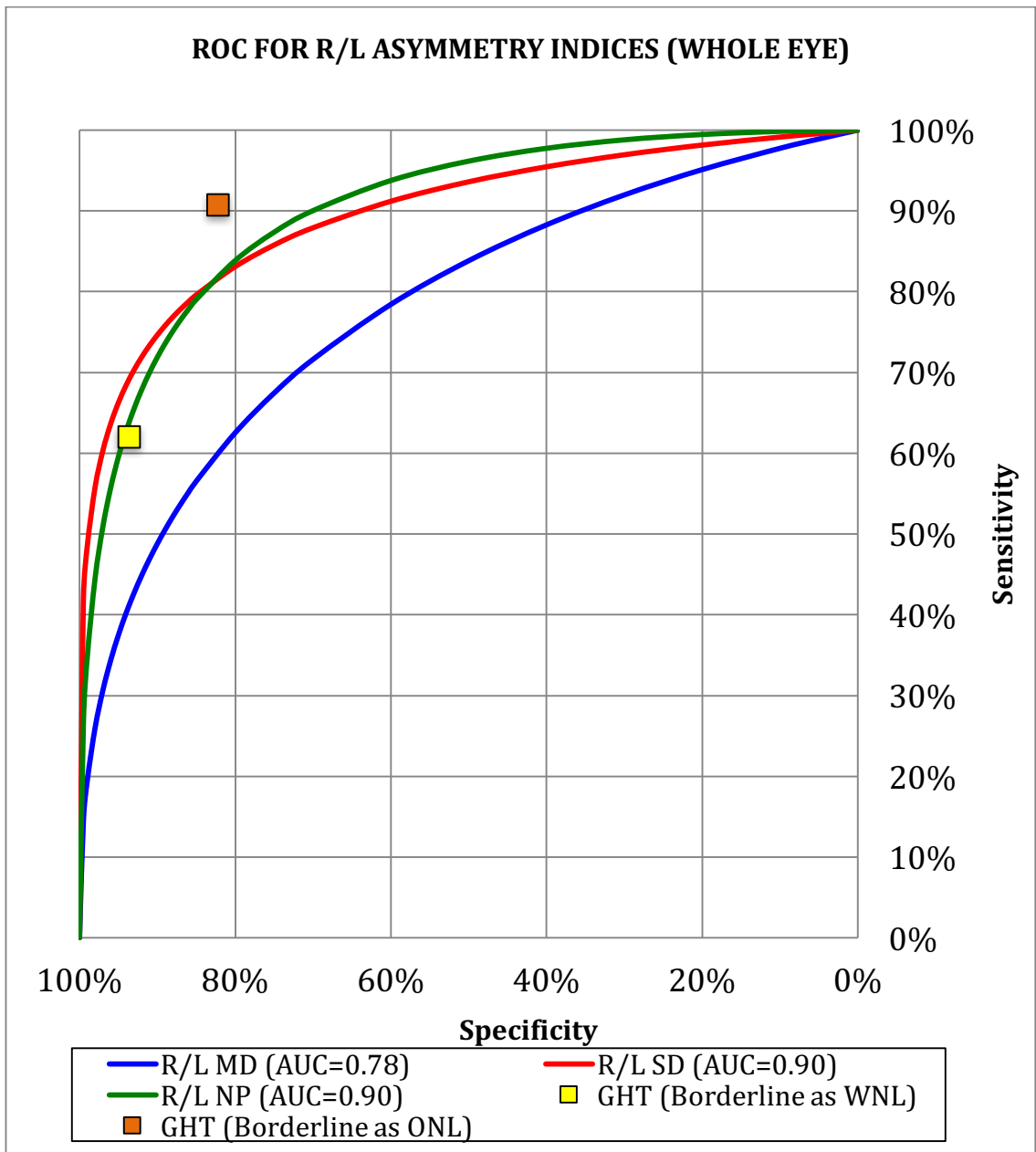
Figure 4.4: ROC for 3 whole eye R/L asymmetry indices and GHT. AUC=Area under ROC; WNL=Within Normal Limits; ONL=Outside Normal Limits.

**ROC FOR R/L SUPERIOR HEMIFELD INDICES**

Legend:
- R/L MD SUP HEMI (AUC=0.42)
- R/L SD SUP HEMI (AUC=0.87)
- R/L NP SUP HEMI (AUC=0.83)
- GHT (Borderline as WNL)
- GHT (Borderline as ONL)
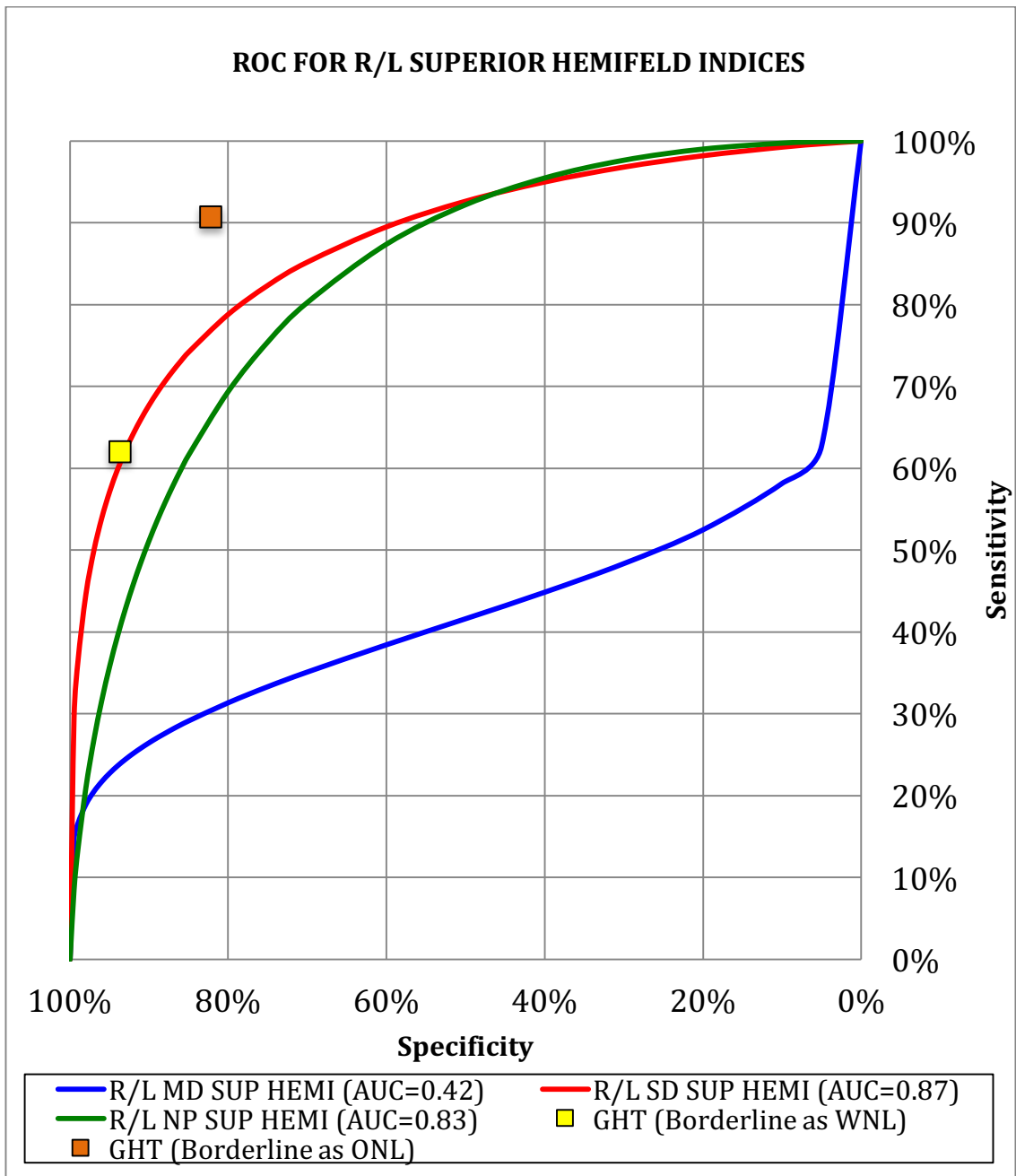
Figure 4.5: ROC for 3 R/L superior hemifield asymmetry indices and GHT. AUC=Area under ROC; WNL=Within Normal Limits; ONL=Outside Normal Limits.
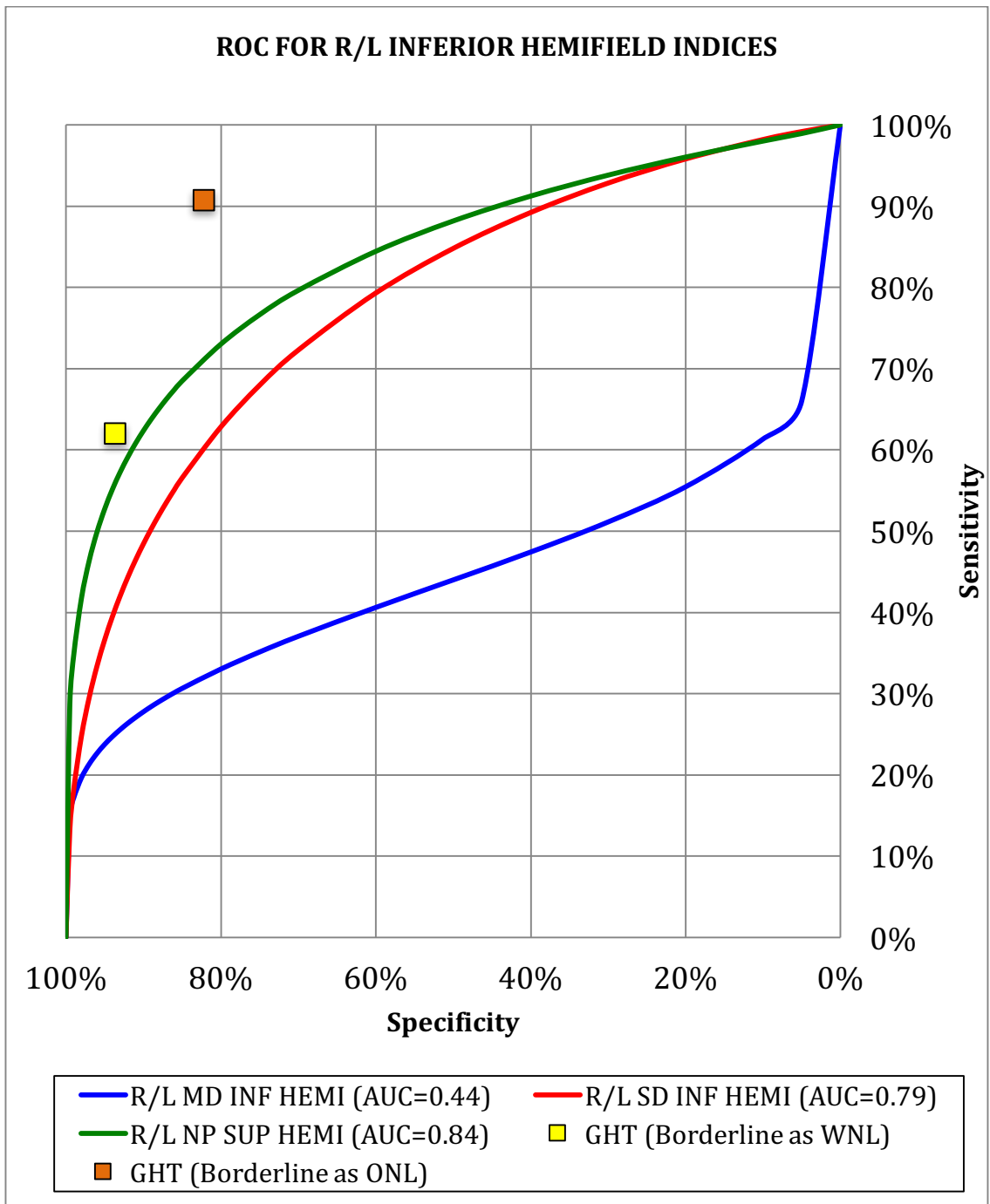
Figure 4.6: ROC for 3 R/L inferior hemifield asymmetry indices and GHT. AUC=Area under ROC; WNL=Within Normal Limits; ONL=Outside Normal Limits.
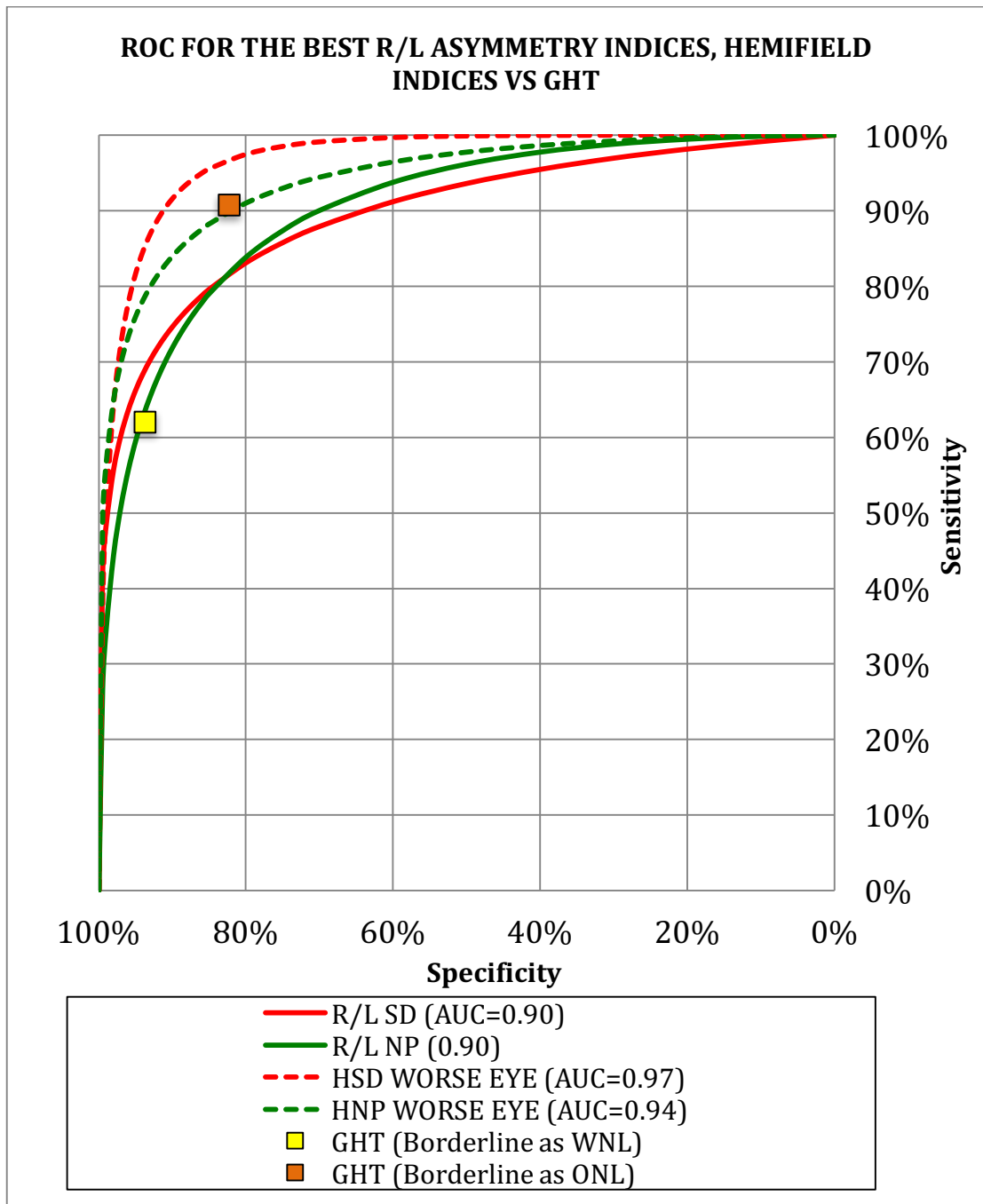
Figure 4.7: ROC for; 2 best R/L asymmetry indices; 2 best Sup/Inf hemifield asymmetry indices and GHT. AUC=Area under ROC; WNL=Within Normal Limits; ONL=Outside Normal Limits.

**Table 4.3: Area under ROC (AUROC) for R/L asymmetry indices, Sup/Inf hemifeld asymmetry indices and GHT in discriminating early POAG from healthy eyes**

| Asymmetry indices | AUROC | 95% Confidence interval | |
|---|---|---|---|
| | | Lower Bound | Upper Bound |
| HSD Worse Eye | 0.968 | 0.951 | 0.986 |
| HNP Worse Eye | 0.942 | 0.913 | 0.971 |
| R/L NP | 0.903 | 0.867 | 0.938 |
| R/L SD | 0.897 | 0.857 | 0.936 |
| R/L NP Worse Hemifield | 0.897 | 0.861 | 0.933 |
| R/L SD Worse Hemifield | 0.872 | 0.851 | 0.932 |
| R/L SD Sup | 0.875 | 0.827 | 0.922 |
| HMD Worse Eye | 0.870 | 0.826 | 0.913 |
| R/L NP Inf | 0.836 | 0.784 | 0.889 |
| R/L NP Sup | 0.832 | 0.785 | 0.879 |
| R/L SD Inf | 0.785 | 0.731 | 0.840 |
| R/L MD | 0.780 | 0.725 | 0.836 |
| R/L MD Inf | 0.443 | 0.364 | 0.522 |
| R/L MD Sup | 0.420 | 0.342 | 0.499 |

**Table 4.4: Comparison of 3 cases; classified as significant defect by R/L asymmetry (R/L NP) in comparison with hemifield asymmetry analysis (HSD worse eye) and GHT. (R/L NP is classed as defective when exceed 7 and more)**

| Cases | Clinical diagnosis | R/L Asymmetry Analysis |
|---|---|---|
| # AC<br><br>Right eye<br><br>    1. GHT: Within Normal limits<br>    2. VFI: 100%<br>    3. MD: -3.37 dB P< 2%<br>    4. PSD 1.25 dB<br><br>Left eye<br><br>    1. GHT: Within Normal limits<br>    2. VFI: 100%<br>    3. MD: -1.53 dB P< 2%<br>    4. PSD 2.22 dB P < 5% | 1. Left POAG<br>2. Right OHT<br>3. Bilateral pseudophakia<br>4. Right new macula hole (diagnose in 2011)<br>5. Left macula hole repair on 2009 | 1. R/L NP: 7/44<br>2. HSD Worse eye: 2.13 dB<br>3. GHT Worse eye: WNL<br><br>**Comments:**<br><br>This is an example where R/L asymmetry (RL NP) was significant while Sup/Inf hemifield asymmetry indices and GHT were not. The significance of R/L NP might be due to the non-POAG pathology (macula disturbances in both eyes). |
| # BF<br><br>Right eye<br><br>    1. GHT: Within Normal limits<br>    2. VFI: 97%<br>    3. MD: -2.94 dB P< 1%<br>    4. PSD 2.27 dB P < 5%<br><br>Left eye<br><br>    1. GHT: Within | 1. Bilateral early POAG<br>2. Left mild cataract<br>3. Left amblyopia | 1. R/L NP: 7/44<br>2. HSD Worse eye: 1.96 dB<br>3. GHT Worse eye: WNL<br><br>**Comments**<br><br>The superior/inferior asymmetry and GHT classed these cases as |

| | | |
|---|---|---|
| Normal limits<br>2. VFI: 94%<br>3. MD: -4.47 dB P<<br>1%<br>4. PSD 2.17dB P <<br>5% | | normal, while R/L NP was significant for defect.<br>The significance of R/L NP might be due to the non-POAG pathology; unilateral media opacities coupled with amblyopia. |
| # BH<br><br>Right eye<br><br>    1. GHT: Borderline<br>    2. VFI: 93%<br>    3. MD: -2.01 dB P< 5%<br>    4. PSD 2.06 dB P < 5%<br><br>Left<br><br>    1. GHT: Within Normal limits<br>    2. VFI: 94%<br>    3. MD: -3.64 dB P< 1%<br>    4. PSD 2.46 dB P < 2% | 1. Bilateral POAG<br>2. Bilateral ARMD (dry macula degeneration | 1. R/L NP: 9/44<br>2. HSD Worse eye: 2.03 dB<br>3. GHT Worse eye: Borderline<br><br>**Comments:**<br><br>The superior/inferior asymmetry and GHT classed these cases as normal, while R/L NP was significant for defect.<br>The significance of R/L NP might be due to the non-POAG pathology (ARMD) in both eyes. |

## Discussion

Asymmetries between eyes and Sup/Inf hemifields are recognised as an important diagnostic signs of early POAG. While clinicians often look for R/L visual field asymmetries there has been no systematic investigation of such asymmetries or the inclusion of R/L analyses in the outputs from perimeters. This is despite the recommendation that such indices may improve discrimination and the

use/presentation of R/L differences in structural measures, electrophysiological methods and in pupil perimetry.

This chapter investigates 3 methods R/L asymmetry within the whole field, R/L asymmetry with one hemfield and R/L asymmetry in the worse hemifield. Measures of discriminatory power are dependent upon the definition of POAG and upon the characteristics of the disease/control samples. In this paper we have used the clinical diagnosis of POAG to define whether or not an eye has POAG rather than a definition defined by organisations such as the National Institute for Health and Clinical Excellence (NICE) in its 2009 Glaucoma Guideline (2009). Most published definitions of POAG include the presence of a visual field defect and as such may not have included cases of 'pre-perimetric' loss and thus a more challenging task to the new indices. Clinicians will often take into account a wider range of factors, e.g. family history, the results from the other eye when making a diagnosis, and accept the concept of pre-perimetric glaucoma. Using a clinical diagnosis introduces more variability, as clinicians will have different diagnostic criteria. While variations between clinicians will influence overall measures of discriminatory power, comparisons between different analytical methods will still be valid.

Inclusion criteria for the POAG sample included a GSS result of ≤Stage 1 (Normal, Borderline or Stage1) in both eyes. Fifty-five percent of the patients included in the POAG sample had 1 eye classed as Normal with GSS while the other had a very early defect. This again ensured that our analyses were provided with a challenging task. Including more advanced cases would have increased the measures of discriminatory power and reduced the differences between analytical methods.

The control sample used in this study was taken from patients referred to MREH with suspect glaucoma. These patients are likely to have had some suspicious results, such as an elevated IOP. None had a clinical diagnosis of POAG or any visual field loss on repeated testing. While this sample might not truly represent the normal population they do represent the diagnostic challenge facing clinicians in an NHS eye clinic. The findings of this research are, therefore, pertinent to ophthalmologists and clinicians tasked with differentiating between true and false positive referrals.

In the POAG cohort of this study, very few cases were diagnosed with pre-perimetric glaucoma in both eyes. In most cases a bilateral diagnosis of glaucoma was made even when only one eye had glaucomatous visual field loss. This implies that, in some cases, clinicians were influenced by the diagnosis of glaucoma in the other eye leading to a change in their diagnostic criteria.

This results from this study match those observed in earlier studies (Henson et al., 1986, Feuer and Anderson, 1989, Levine et al., 2006), which highlight the potential of inter-eye comparison in detecting early POAG. Among the R/L indices, R/L NP has the highest AUROC followed by R/L SD, and RLNP. R/L indices did not perform better than Sup/Inf hemifield indices.

POAG is not the only condition that results in asymmetry between the right and left eyes. Early cataractous changes often occur in one eye before the other as do the retinal changes associated with diabetes and many other ocular pathologies. An examination of cases where R/L asymmetry was significant while Sup/Inf asymmetry was not identified cases where patients had non-POAG pathology in one

or both eyes. Non-POAG pathologies tended to have a greater effect upon R/L asymmetry indices than they did on Sup/Inf asymmetry indices.

This study was cross sectional and relied upon the clinical diagnosis of glaucoma to define the diseased cohort. A more robust design would have been to retrospectively look at the visual field records of group of patients who develop glaucomatous defects, without significant clinical findings (OHTS) and compare the inter-eye asymmetry properties with those who develop glaucomatous defect with significant clinical findings. Another ideal sample would be a group of patients who develop glaucomatous defects with significant clinical findings and establish at what stage the various indices flag significant asymmetry. Unfortunately, MREH records include very few cases where patients develop visual field loss. Most presenting cases either have establish field loss or no field loss and the majority of those with no loss show little change despite being monitored for long periods of time.

The analyses used in this study, with the exception of GHT, were based on defect values. The difference between the threshold measures and those from an age matched normal eye. The GHT output is based on a scoring of the values presented in the pattern deviation probability map. The use of defect values provides good performance from readily available data. In addition the new Sup/Inf hemifield and R/L indices do not pool data within sectors, as does the GHT. Variations in eyes (Denniss et al., 2014, Jansonius et al., 2012a) mitigate against the use of pre-defined sectors as was highlighted in chapter 3.

The indices developed in this chapter and in the earlier work on hemifield indices (chapter 3) give continuous outputs rather than a series of discrete textual outputs as seen in the GHT. Continuously scaled outputs allow better monitoring of change

and can be combined with probability estimates as found in the global indices of MD and PSD.

In this study each asymmetry index was looked at in isolation. Future work will combine indices in a discriminant analysis model to establish the contribution each make to the detection of early POAG.

# 5. Asymmetry Cluster Indices for Detecting early POAG

## Contribution:

The project was conducted under supervision of Prof David Henson. The dataset used here was collected from patients attending the outpatient department of MREH as part of their routine management for suspect/diagnosed glaucoma. I extracted the data from the database, taking into account the inclusion/exclusion criteria, performed the data analysis.

## Publication

**Ghazali N**., Aslam T., Henson DB. (2015) Asymmetry Cluster Indices for Detecting early POAG. (Manuscript in preparation)

## Abstract:

**PURPOSE**: To describe and measure the discriminatory performance of 2 indices, based on the clustering of locations where there are Superior/Inferior (Sup/Inf) hemifield asymmetries for detecting Primary Open Angle Glaucoma (POAG).

**METHODS**: 206 control and 160 POAG eyes (clinical diagnosis) were selected from a visual field database of patients attending Manchester Royal Eye Hospital. All POAG eyes had early glaucoma (GSS stage≤1). Age related sup/inf hemispheric defect asymmetries were calculated for each of the 22 test point pairs used in the GHT. Two new indices were investigated: 1) N clusters (≥2-missed locations at p-level <0.05 within 8.5 degrees of each other); 2) N clustered (number of pairs with asymmetries outside the 95% CI). ROC curves were generated for both indices. Selected cases where cluster analysis indicates significant defect not detected with other indices; HNP and GHT were reviewed.

**RESULTS**: Clusters of asymmetric defect locations were found in 13% of the controls eyes and 81% of the POAG eyes. The largest number of asymmetric pairs within clusters was 6 in controls and 16 in POAG. Glaucomatous eyes have larger cluster size with 65% having a cluster size of ≥3 test locations. Area under the ROC curve for N clusters was 0.92 (95% Confidence Interval (CI) 0.888-0.951) and for N clustered was 0.92 (95%CI 0.884-0.956). At 80% and 95% specificities, sensitivities for N clusters was 91 and 50% and N Clustered was 87 and 65% respectively.

**CONCLUSIONS**: Cluster analysis provides clinically useful information on early glaucomatous loss. In isolation, its diagnostic potential is no better than that of HSD and HNP in detecting early POAG loss.

## Introduction:

POAG is a progressive disease characterized by morphologic changes at the ONH and the NFL, accompanied by functional changes to the visual field. Early detection of POAG is important in reducing the visual morbidity associated with this disease. While structural measures are important in the diagnosis and monitoring of POAG, functional measurements quantify the patient's visual status and help evaluate the effectiveness of the treatment. Therefore, functional assessment by means of visual field testing is an important assessment in both the detection and monitoring of POAG.

Since large amounts of data are produced from a single visual field examination, several analytical techniques have been introduced to facilitate the interpretation of results. Heijl at al (1987) incorporated a series of global indices that were sensitive to generalised reduction in sensitivity (MD) and localised loss (PSD); however, these indices are spatially insensitive to the typical patterns of loss seen in POAG. The importance of incorporating spatial information in global indices was highlighted by Chauhan et al (1989) in a simulation experiment demonstrating the critical role of cluster analysis in assessment of glaucomatous field loss (Chauhan et. al, 1989).

Cluster analysis, an evaluation of the spatial relationship between defective test points, is widely used in the interpretation of visual field loss in glaucoma. In most cases the evaluation is undertaken by visual inspection of the field chart. However, there are a few reports of quantitative techniques. Henson and Dix, (1984) in a study of supra-threshold data obtained with a FVFA on 146 clinically normal eyes

reported that 13% of their sample had a cluster of two or more 4dB defects and that 0.7% had a cluster of three 4dB defects. This study evaluated clusters within a radius of 7.5 degrees across the whole visual field. None of their sample had a cluster of two or more defects of ≥6dB. In another study looking at the effect of changing the cluster radius on the number of clusters formed in both normal and glaucoma eyes, Chauhan et al., (1988) found similar findings with approximately 13% of normals having clusters. The majority had one cluster of two defects with most of the clusters due to physiological features of the eye e.g. variation in blind spot position and/or angioscotoma.

A few studies have investigated clusters within specific borders based on the normal RNFL anatomy (Asman and Heijl, 1993); Naghizadeh and Hollo, 2014). Asman and Heijl used 7 sectors and evaluated the number of depressed locations within each sectors. They compared the performance with a traditional cluster analysis (which was not based on any sectors) and concluded that cluster analysis using sectors performed better than non-sectoral analysis (Asman and Heijl, 1993). In more recent study of 2 cluster analyses, developed for the Octopus perimeter, (Corrected Cluster Trend Analysis (CCTA), which investigates the time-dependent change of the cluster defect corrected for diffuse change of the global visual field sensitivity and Cluster Trend Analysis (CTA) which investigates the time-dependent change of the absolute cluster defect without correction using 10 clusters sectors), results demonstrated that both methods were useful for recognizing early glaucomatous progression (Naghizadeh and Hollo; 2014).

We previously described several indices based upon Superior-Inferior (Sup/Inf) asymmetries (Chapter 3). None of these indices (HSD, HMD, HNP) took into account the spatial relationship of asymmetric pairs. There are no previous reports on the spatial relationships of asymmetric pairs.

The aim of this study is to report on the discriminatory power of 2 new indices that are based upon the clustering of asymmetric pairs of stimuli; 1) the number of clusters (N clusters) and 2) the total number of asymmetric pairs within clusters (N clustered).

## Methods

All the data used in this study was obtained retrospectively from patients attending MREH between 2007-12. 30,899 SITA 24-2 visual field records were exported from the HFA to Excel 2010 for analysis. The stage of visual field loss was quantified with GSS (Brusini and Filacorda, 2006). GSS classifies each 24-2 threshold test on the basis of the global indices MD and PSD into 7 stages (Normal, Borderline and 5 stages of loss). Selection took no account of the reliability indices produced by the HFA software as these are often unreliable (Bengtsson and Heijl, 2000) and to make our results generalizable to clinical populations where good reliability indices are not always obtained.

### Patients

Patients in whom both eyes had a GSS stage ≤1 (Normal, Borderline and early loss) were selected from the Excel database. This ensured that the POAG cohort

was limited to patients with little visual field loss in either eye and thus provided a challenging task to the new and established indices.  Following a record review to ensure each patient met the inclusion criteria they were assigned to one of the following 2 groups.

Control (n=206 eyes from 206 patients)

All patients had normal visual fields in both eyes at 2 consecutive visits (GHT within normal limits and no clusters of three or more neighbouring locations with an age related defect of ≥5dB). Each included eye had a corrected visual acuity of 6/9 or better in patients <50 years of age or 6/12 or better in patients >50 years of age, IOP of <22mmHg (Goldmann applanation), refractive error of between -5 and +5D (spherical equivalent), no history of serious eye disease or trauma, a normal fundus (clinical examination) and an absence of any abnormal ocular findings likely to affect the visual field.

POAG (n=160 eyes from 160 patients)

The POAG group consisted of 160 eyes from 160 patient's records with early visual field loss (GSS stage 1). The clinical records of all selected cases were reviewed and patients with ocular abnormalities other than glaucoma that could be expected to affect the visual field, apart from early cataract, were removed.

**Cluster definition**

The cluster definition was based upon the 22 vertically paired test locations used in the GHT. Paired locations whose difference fell outside normal limits (95%) were identified to create an asymmetry map, see figure 5.1. On this map a location is marked (filled in annulus) if its defect value is significantly below that of its mirrored location. Marked locations can therefore be in the superior or inferior half of the map. An asymmetric cluster is defined as 2 or more asymmetric locations within a ≤8.5° radius of each other (vertically, horizontally and diagonally) and within a single hemifield. To derive the normal limits for each vertically pair a bootstrapping procedure was used on the control sample (2000 samples of 206 eyes, randomly selected with replacement).
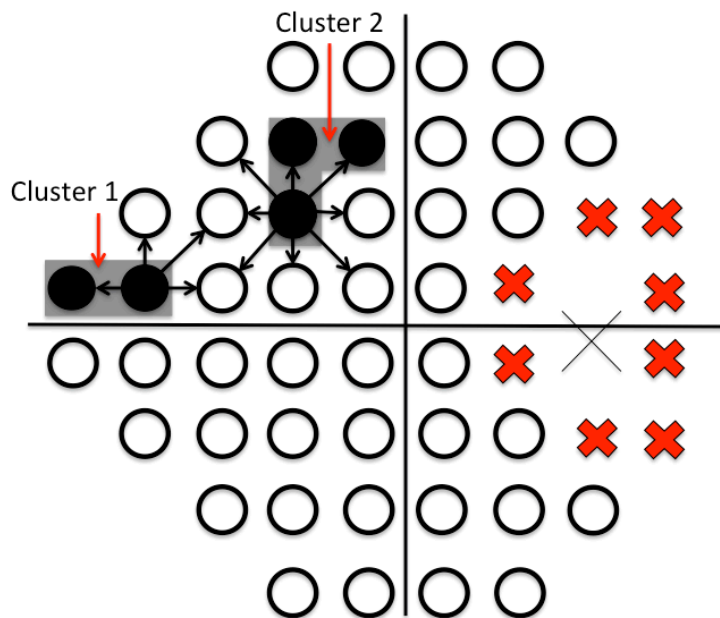


Figure 5.1: Schematic diagram of clusters formed by a group of abnormally depressed points (two or more points that fall outside 95% CI in control sample) (shaded areas).

**Quantification of cluster size**

The analysis reports on two cluster indices; 1) the N clusters and 2) the N clustered. Two clusters that sit next to each other within ≤8.5° radius will be count as one.
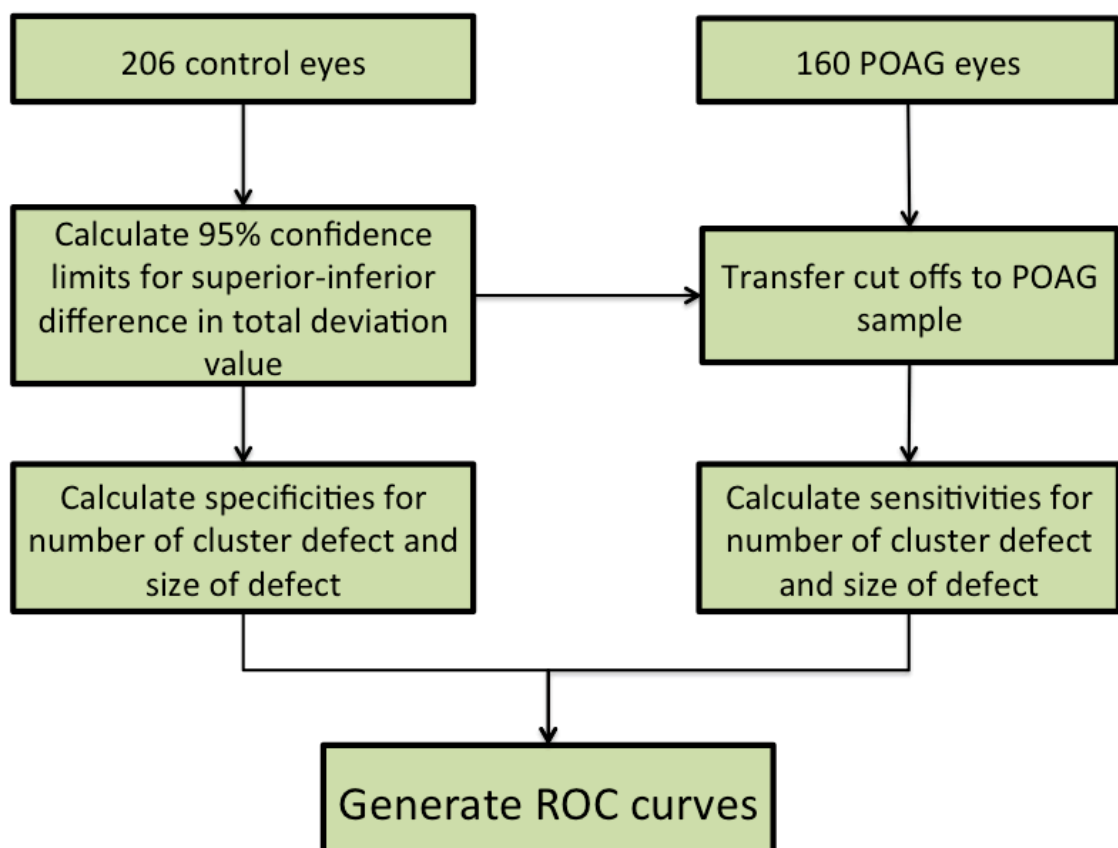


Figure 5.2: Analytical steps in evaluating cluster defect.

**Discriminating power of cluster analysis.**

To analyse the discriminant power of cluster analyses in separating between normal and POAG eyes, the AUROC was calculated. Sensitivities at 80% and 95% specificities were determined for both N clusters and N clustered. The analytical steps taken to derive the ROC curves are summarised in figure 5.2.

For comparison with Sup/Inf hemifield indices the AUROC was also established for HSD and HNP.

**Statistical Tools**

Statistical analyses were performed using statistical software (SPSS, v. 22.0; SPSS, Chicago, IL). The tests used to check the statistical significance of the difference of the parameters means between the two groups were two sample t-test, Kolmogorov-Smirnoff to test normality, Levene's test of equality of error variances to test homogeneity of variances, and an independent sample t-test (ANOVA). ROC curves and area confidence limits were derived with jrocfits (http://www.rad.jhmi.edu/jeng/javarad/roc/JROCFITi.html).

# Results

Descriptive statistics for initial evaluation of visual field parameters between control and POAG eyes are presented in Table 5.1. The mean age in control group (60.37

ranging from 24.5 to 85.8 years) was statistically different (p<0.001) from POAG group (mean age is 72.35 years; range from 43.30 to 93.30 years).

**Table 5.1: Visual field characteristics between Control and POAG eyes**

| Parameter | Control (N=206 eyes) | POAG (N=160 eyes) | P Value |
|---|---|---|---|
| Age (years) | 60.37 | 72.35 | P<0.001* |
| Standard Deviation (SD) | ±10.54 | ±11.51 | |
| Mean Deviation (MD)(dB) | 0.31 | -2.74 | P<0.001* |
| Standard Deviation (SD) | ±0.85 | ±0.93 | |
| Pattern Standard deviation (PSD) (dB) | 1.631 | 2.84 | P<0.001* |
| Standard Deviation (SD) | ±0.32 | ±0.77 | |
| GSS | All eyes are in stage 0 (0=Normal) | All eyes are in stage 1 (1= early defect) | P<0.001* |

* Significant difference between Control and POAG eyes (independent t-test P>5%)

GSS Glaucoma Staging System (Brusini and Filacorda, 2006).

**The distribution of the N clusters and N clustered.**

Figure 5.3 and 5.4 show the frequency distribution of N clusters and N clustered in the control and POAG eyes. Clusters (≥2 depressed points) were found in 13.1% of controls eyes and 80.6% of POAG eyes. The largest number of clustered pairs in

controls and POAG eyes were 6 and 16 respectively. 65% of the POAG eyes had 3 or more pairs within clusters. In the control sample only 6% had 3 or more asymmetric pairs within a cluster.

**Diagnostic potential of cluster analysis**

ROC curves for the N clusters and N Clustered are presented in Figure 5.5.

The N clusters has a similar AUROC to N clustered (The N clusters =0.92 (95% CI 0.888-0.952 and N clustered =0.92 (95%CI 0.884-0.956).

**Comparison of diagnostic performance of cluster analysis with Sup.Inf hemifield analysis**

Figure 5.6 provides comparison of performance of cluster analysis and 2 hemifield asymmetry indices HSD and HNP using the same data set. Cluster analysis did not perform better than hemifield indices. AUROC for HSD and HNP were 0.92 (95% CI 0.90-0.95) and 0.93 (95% CI 0.90-0.95), see Figure 5.7. At 80% and 95% specificities, sensitivities for N Clusters, N Clustered, HSD and HNP were 91% and 50%; 87% and 65%; 88% and 70% and 88% and 68% respectively, see figure 5.7.

**Assessment of cluster analysis in selected cases**

Cases where the cluster analyses classed a result as significant, while the hemifield indices classified it as within normal limits are reviewed in Table 5.2
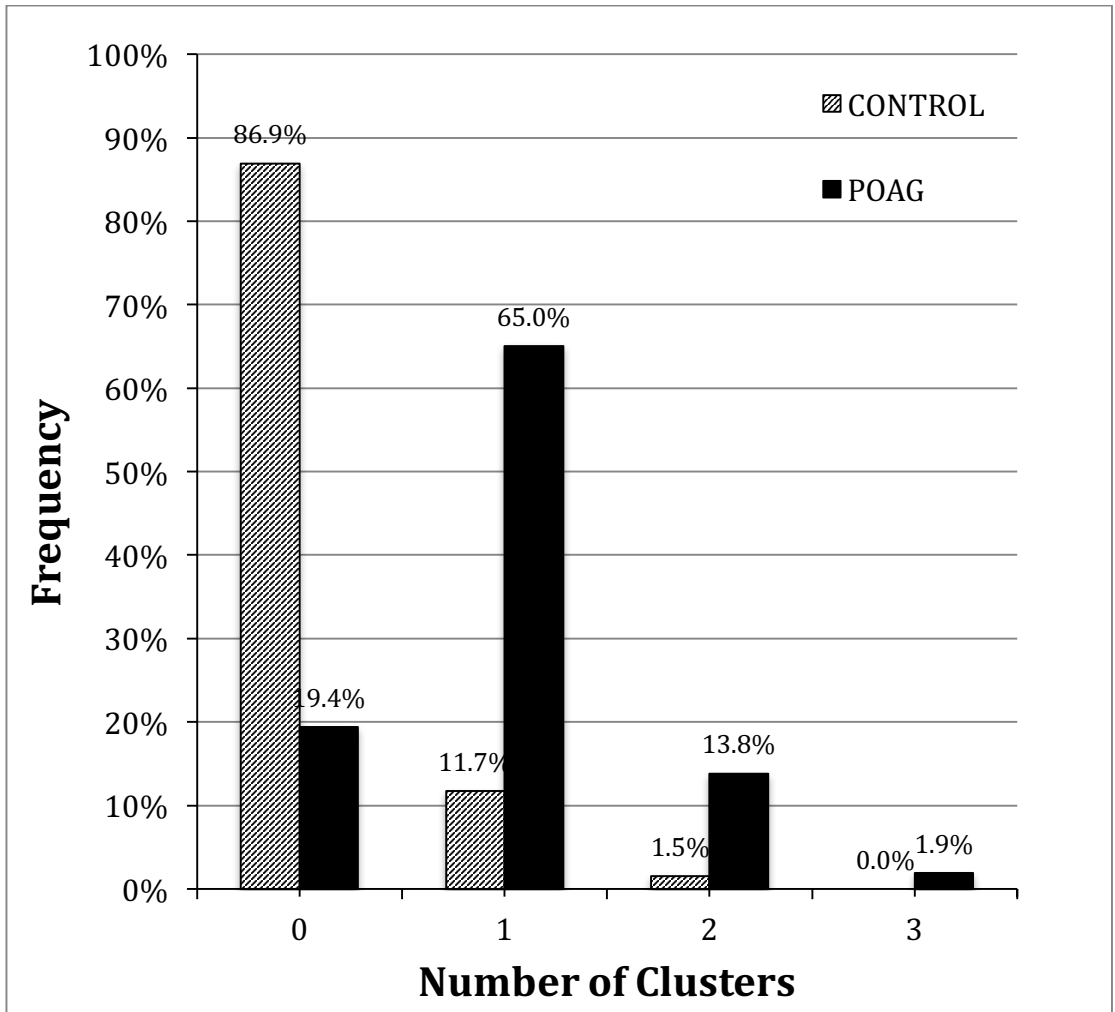
Figure 5.3: Frequency distribution of N clusters in controls and POAG eyes
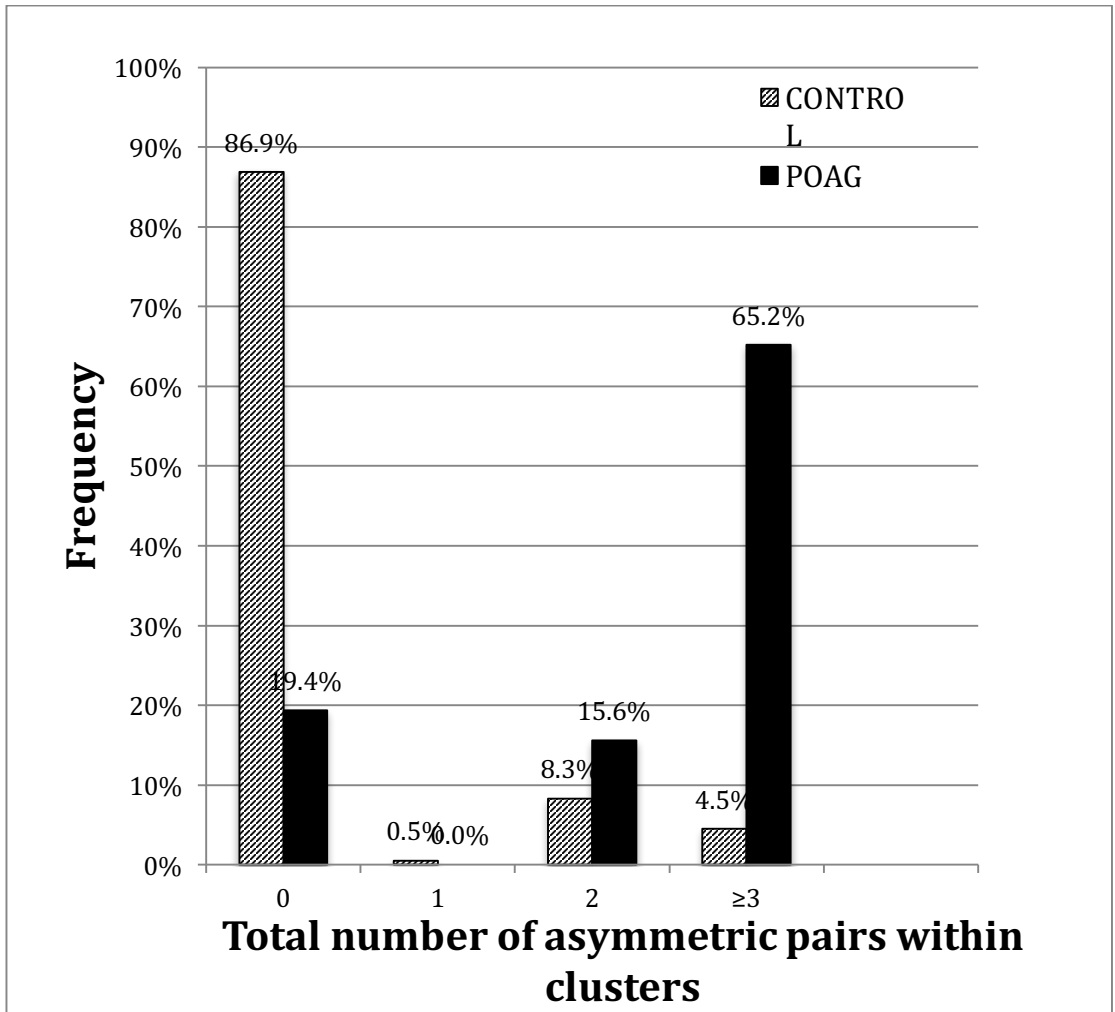
Figure 5.4: Frequency of N clustered within clusters in control and POAG eyes
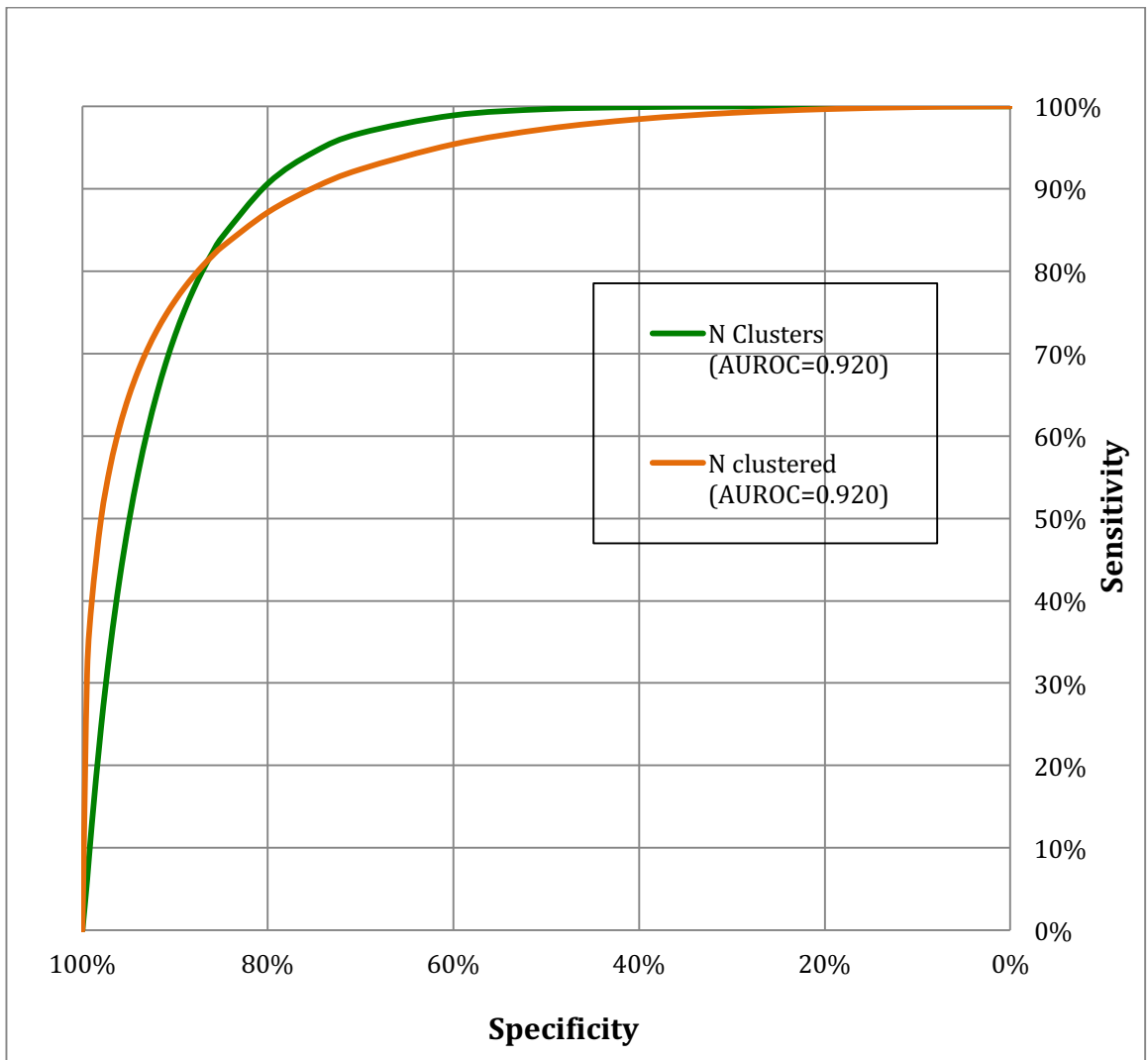
Figure 5.5: ROC for the 2 cluster indices; N Clusters and the N Clustered within clusters
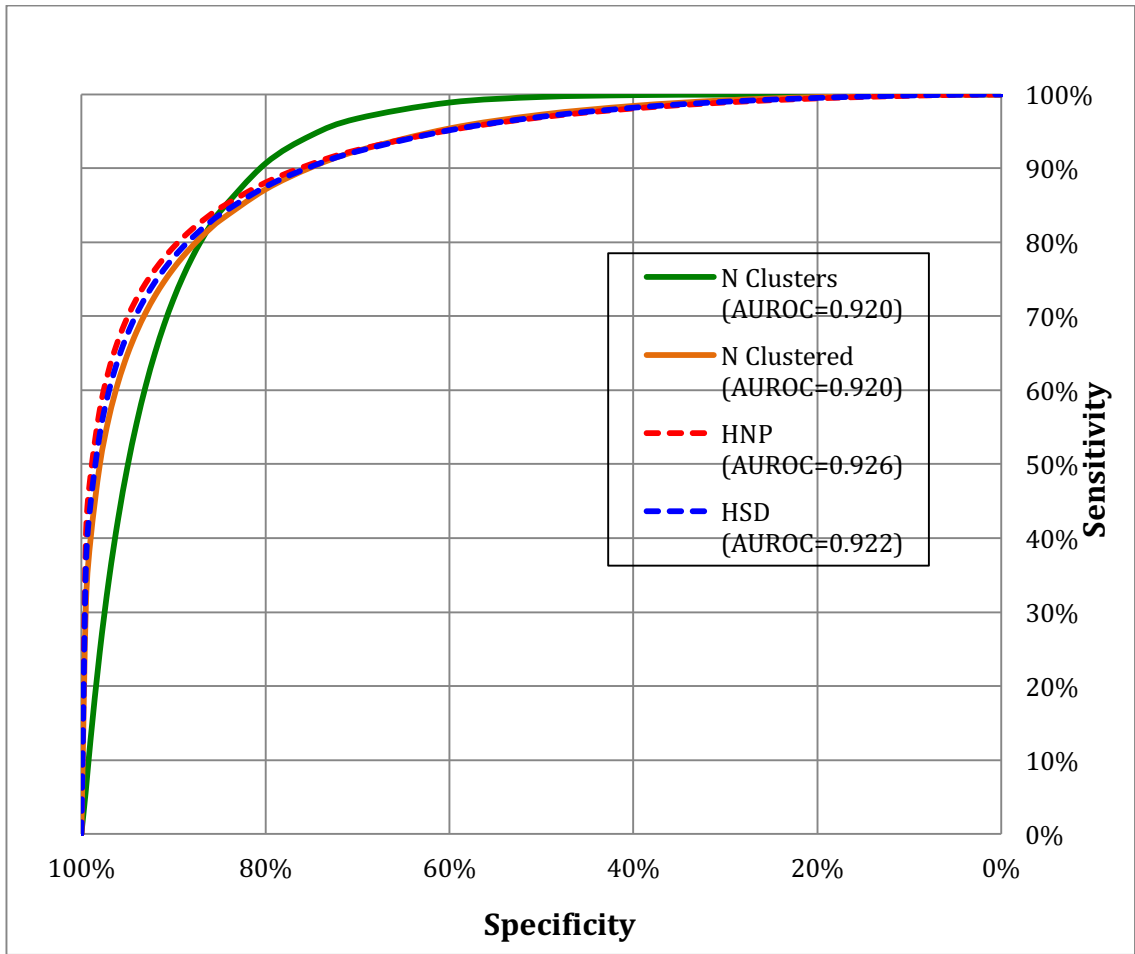
Figure 5.6: Comparison of ROC for cluster indices; N Clusters and N Clustered, and hemifield indices; HSD and HNP
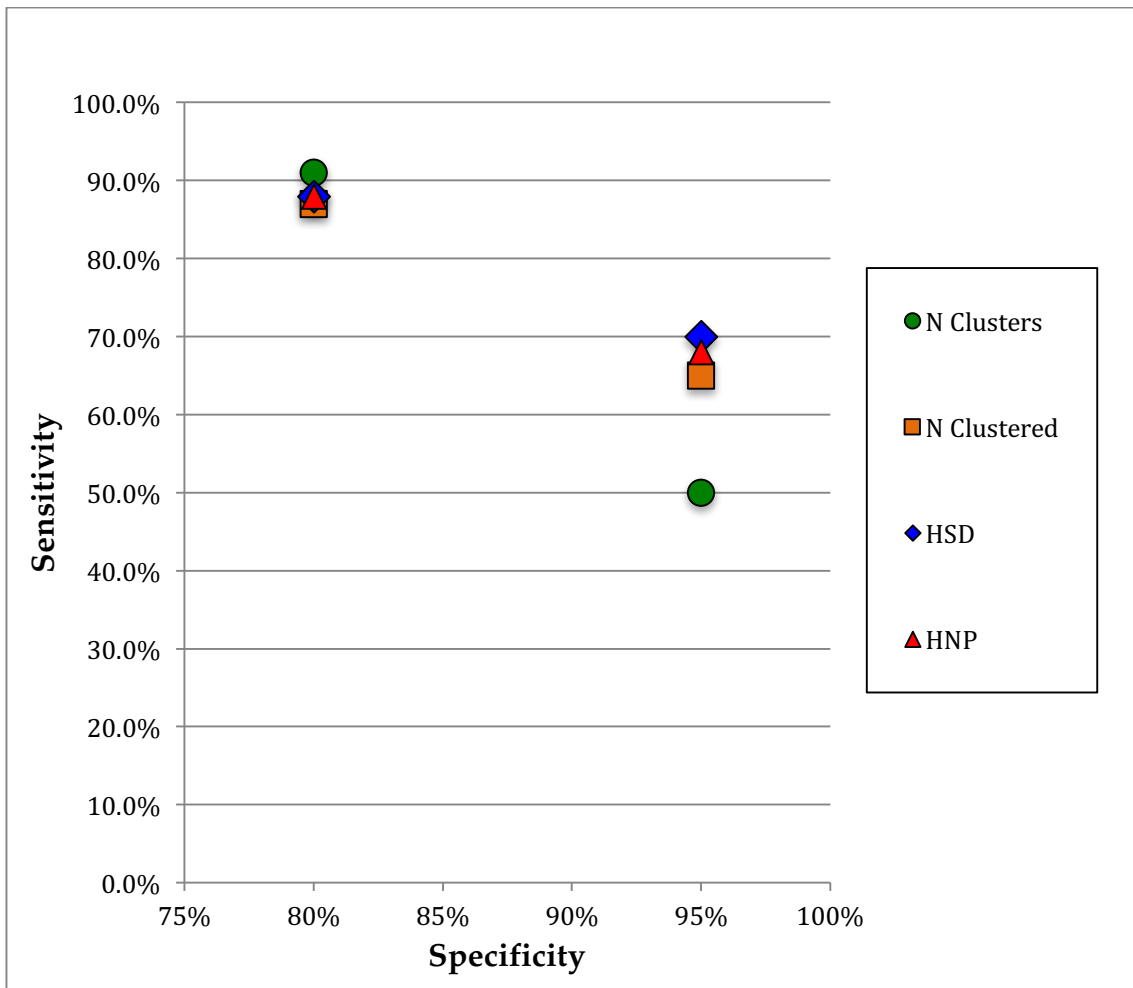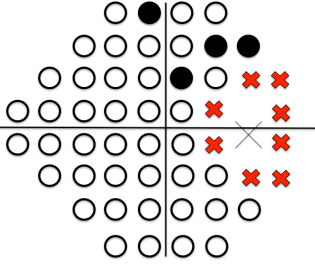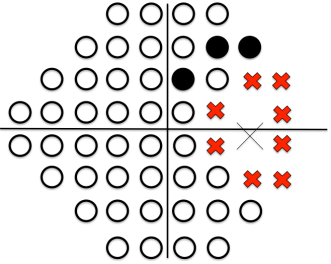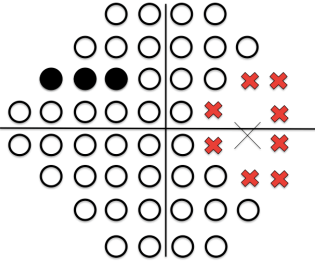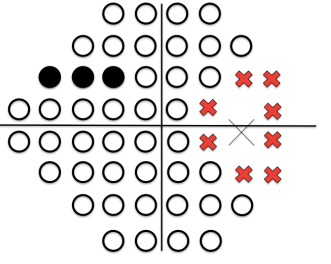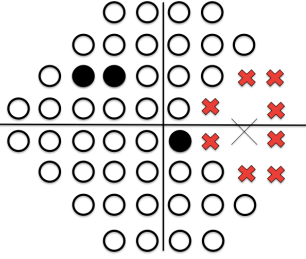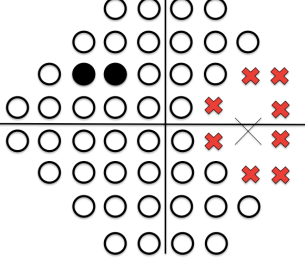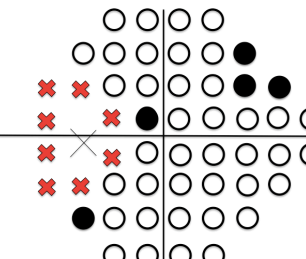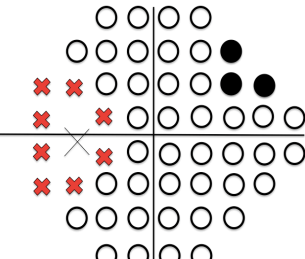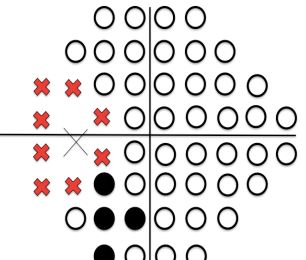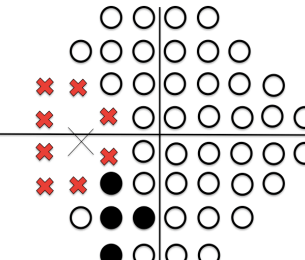
Figure 5.7: Scatter plot of sensitivities for cluster indices (N Clusters and N Clustered,) and hemifield indices (Hemifield Standard Deviation (HSD) and Hemifield Number of asymmetric Pairs (HNP) at two specificities (80% and 95%)

**Table 5.2: Example of cases classed by cluster indices as significant defect in comparison with GHT and HNP**

| Clinical diagnosis | GHT & Global Indices | HNP | Cluster asymmetric defect |
|---|---|---|---|
| #AN<br><br>POAG eye with treatment (Xalatan BE)<br><br>CDR : 0.85 | Within normal limit<br><br>VFI: 94%<br><br>MD: -4.31dB P < 0.5%<br><br>PSD 2.34 dB P< 5% | <br>HNP: 4/22 (within normal limits)<br><br>* Cut off criteria for classifying HNP as defect is >6 pairs of asymmetric points. | <br>Cluster analysis show cluster of 3 asymmetric pairs in the superior hemifield that do not conform to any recognisable pattern of glaucomatous loss.  The cluster is close to the BS and could be related to PPA or angioscotoma |
| #BC<br><br>Early POAG with treatment (Gt Xalatan od nocte both eyes | Borderline<br><br>VFI: 97%<br><br>MD: -3.18 dB P<1%<br><br>PSD 2.04 dB P< 5% | <br>HNP: 3/22 (within normal limits) | <br>Clusters analysis identified 3 asymmetric pairs indicative of a nasal step-defect pattern. |

| #BD<br><br>1. Bilateral POAG (on medication : guttae Azopt bd and guttae Ganforth mane to bothe eys<br>2. Post selective laser trabeculectomy | Within Normal limits<br><br>VFI: 98%<br><br>MD: -3.63 dB P<1%<br><br>PSD 2.52 dB P< 2% | <br><br>HNP: 3/22 (within normal limits) | <br><br>Clusters analysis identified 2 asymmetric pairs in superior hemifield. |
|---|---|---|---|
| # BB<br><br>1.Normal Tension Glaucoma<br><br>Mild NPDR | Borderline<br><br>VFI: 96%<br><br>MD: -3.03 P < 2%<br><br>PSD 2.54 dB P< 2% | <br><br>HNP : 5/22 (within normal limits) | <br><br>Cluster analysis identified a cluster of 3 asymmetric pairs which is outside the 95% CL. Pattern suggests an early nasal defect. |
| # AJ<br><br>1. Normal tension glaucoma<br><br>2. Bilateral cataracts | Borderline<br><br>VFI: 97%<br><br>MD: -3.28 P < 10%<br><br>PSD 1.84 dB P< | <br><br>HNP: 4/22 (within normal limits) | <br><br>Cluster analysis shows significant defect (4 |

| | 10% | | asymmetric pairs in inferior hemifield. |
|---|---|---|---|

## Discussion

In this study, we examined the performance of 2 indices based on the clustering of vertically asymmetric pairs in detecting early glaucomatous loss. The present study found a lower frequency of clusters in normal eyes than in POAG eyes, a finding that is similar to that reported by Chauhan et al who found that the frequency of clusters in normal eyes was approximately 13% (Chauhan et al., 1988). It is important to emphasize that while Chauhan was reporting on clusters of missed locations this research is reporting on clusters of asymmetric pairs. In addition, the data from Chauhan used an FVFA in which the location and number of stimuli differed significantly from the 24-2 test pattern used in this analysis (Chauhan et al 1998). In this evaluation of clusters, the spatial relationship among significant Sup/Inf asymmetric points (≥2 significant asymmetric points within 8.5 radius and within a single Sup/Inf hemifield) was explored. The calculation of the cluster indices in our analysis is constrained to within a single hemifield due to the fact that the early glaucomatous loss is normally confined to within one hemifield.

The highest number of clustered pairs in the control sample was 6, which is above that found by Chauhan (Chauhan et al., 1988). This result may be explained by the fact that the control sample used in this study included suspicious eyes (patients referred to MREH with suspect POAG). These patients are likely to have had some suspicious results such as an elevated IOP but did not meet our definition of POAG.

Furthermore, it might also be due to more variability in our control group which used retrospectively collected data collected within routine NHS clinics rather than by researchers undertaking a clinical trial.

Asman (1993) proposed using an arcuate cluster analysis pattern, which corresponds to the anatomy of the normal retinal nerve fiber layer. They found that when the cluster analysis took place within pre-defined sectors it performed better than traditional cluster analysis (which did not take cluster shape into account). Their results were based upon central 30 degrees static thresholds from 87 eyes of 87 normal subjects and 101 eyes of 101 patients with glaucoma (Asman and Heijl, 1993). Other researchers, however, have found that mapping structural fixed-sector borders to functional measures of visual field data is less than ideal due to: 1) small visual field defects can lead to insignificant findings when averaged across large sectors; 2) significant defect points that fall on the border between the 2 sectors do not clearly reflect the defect in either sector. Thus using fixed sectors might be advantageous in some eyes but not in others.

The present data indicate that diagnostic performance of cluster analysis (calculated from the value of AUROC) is slightly lower than Sup/Inf asymmetric analysis for detecting early loss. It is interesting to note here that, for POAG sample used in this study, we only looked at eyes with early loss (GSS stage 1) that have a clinical diagnosis of POAG. The diagnostic performance of cluster indices for moderate or advance stages of loss will be higher. Previous studies have reported that cluster analysis can provide additional diagnostic power in separating between normal and glaucomatous eyes. The inclusion of clustering criteria has been

incorporated in several of the major clinical glaucoma trials including the Collaborative Initial Glaucoma Treatment Study (CIGTS) (Musch et al., 2014) and Collaborative Normal Tension Glaucoma Study (CNTG) (Panarelli et al., 2015). In CIGTS the visual field score is based on clusters formed in total deviation probability maps while in CNTG, one of the criteria to define glaucomatous visual field loss was a cluster of at least 3 adjacent points depressed by at least 5dB from normal age values, with one of these points depressed by at least 10dB from normal values for age.

Comparison with R/L asymmetry indices is not included in this chapter as the sampling for cluster analysis involved unilateral rather than bilateral data. Direct comparison of the AUROC data from this study with that from the earlier chapters on hemifield asymmetry and R/L asymmetry is not appropriate as these were based on different samples and the effects of sampling are likely to be significant.

Our approach in quantifying clusters could provide additional clinically useful information on early glaucomatous loss.  As shown is our example of cases where only cluster analysis indicates significant loss. Early cases might present with insignificant findings for HNP but significant clustering. However, these data must be interpreted with caution as clustering of asymmetric pairs is not specific to POAG. Similar findings could result from conditions such as diabetic retinopathy.

The present study raises the possibility that cluster analysis could improve discriminatory power when used in combination with other asymmetry indices.

Therefore further research should be undertaken to investigate the diagnostic potential of combining cluster analysis with other asymmetry indices to quantify any additional benefits.

# 6. Multivariate Logistic Regression of asymmetry Indices for detecting early POAG

## Contribution:

The project was conducted under supervision of Prof David Henson. The dataset used here was collected from patients attending the outpatient department of MREH as part of their routine management for suspect/diagnosed glaucoma. I extracted the data from the database, taking into account the inclusion/exclusion criteria, performed the data analysis after receiving statistical advice in multivariate regression analysis from the statistics support group at Manchester University/CMFT.

## Publication

**Ghazali N**., Aslam T., Henson DB. (2015) Multivariate Logistic Regression of asymmetry Indices in detecting POAG. (manuscript in preparation)

## Abstract:

**PURPOSE**: To describe and measure the performance of a discriminant analysis incorporating global indices based upon: Sup/Inf hemifield asymmetry; R/L asymmetry and clustering of hemifield asymmetric locations, for detecting POAG and to determine the best combination of asymmetry indices for future inclusion in perimetric analytical software.

**METHODS**: 412 eyes from 206 control and 340 eyes from 170 patients with a diagnosis of early POAG were selected from a visual field database of patients attending MREH. Age adjusted defect asymmetries (outside 95% confidence limits of control population) were calculated for each of the 22 vertically mirrored test point pairs (for Hemifield Standard Deviation (HSD), Hemifield Number of Pairs (HNP) and Hemifled Mean Deviation (HMD) analyses) and for 44 right-left mirrored test point pairs (for total, superior and inferior R/L Mean Deviation (R/L MD), R/L Standard Deviation (R/L SD) and R/L Number of Pairs (R/L NP analyses) used in the Glaucoma Hemifield Test. Number of Sup/Inf hemifield clusters (N Clusters) and number of hemifield asymmetric pairs within clusters (N Clustered) were also calculated based on numbers of significantly asymmetric pairs. The best model for combination of all asymmetry indices (14) was determined using a logistic regression analysis.

**RESULTS**: For individual asymmetry indices, the largest area under the receiver operating characteristic (AUROC) were R/L NP = 0.892 (95% Confidence Interval

(CI) 0.869-0.915) and R/L SD AUROC= 0.876 (95% CI 0.852-0.901). The multivarible logistic regression analysis model identified 6 significant asymmetry indices; HNP, R/L SD, R/L SD Inferior, R/L NP, R/L NP Inferior and R/L SD Superior as being independently related to a diagnosis of early glaucomatous field loss (p<0.05) This model correctly classified 80% of POAG cases and 88% of controls and performed better than GHT and all single asymmetry analyses.

**CONCLUSIONS**: A model based on 6 asymmetry indices performed best for discriminating between early POAG and normal visual field data. This combination of analyses was superior to GHT and all single asymmetry analyses.

## Introduction

Early detection of glaucoma is paramount in helping to prevent future visual impairment. Visual field assessment plays an important role not only in detecting early functional loss but also in monitoring the effectiveness of treatment. SAP, using the 24-2 pattern of test locations, is the most widely used functional assessment in glaucoma. The first threshold algorithm introduced in SAP was the Full Threshold algorithm in 1970. While this algorithm delivered accurate threshold estimates, it suffered from extended test times. To address this limitation, new threshold algorithm was developed (Fast Pac and Fast Threshold). While being faster they were found to be less accurate than the Full Threshold algorithm. King-Smith et al., (1994) described a new threshold algorithm, known as ZEST (Zippy Estimation by Sequential Testing), which used a more efficient Bayesian approach to derive threshold estimates. Most perimetric threshold algorithms used today are based upon King-Smith's work including SITA (HFA II), ZATA (Zippy Adaptive Threshold Algorithm; Henson 9000) and Fast Threshold (Medmont M700) (Turpin et al., 2003).

In 2002, Foster and associates proposed a standardized scheme for defining glaucomatous visual field loss which included; "*The Glaucoma Hemifield Test (GHT) graded "outside normal limits" and a cluster of three contiguous points at the 5% level on the pattern deviation plot, using the threshold test strategy with the 24-2 test pattern of the Zeiss-Humphrey Visual Field Analyzer 2*".

In chapters 3-5 we have described and investigated 3 classes of asymmetry indices: Sup/Inf hemifield, R/L and cluster. The new Sup/Inf hemifield indices were based on individual mirrored imaged pairs, rather than pooled data within fixed sectors, and defect values rather than PDP values as used in the GHT. The findings indicated that the new Sup/Inf asymmetry indices HNP and HSD performed slightly better than GHT at discriminating between healthy and glaucomatous eyes especially when an early defect crosses GHT sector boundaries. The diagnostic potential of using asymmetry between the right and left eyes has also been explored in chapter 4. R/L asymmetry did not perform (AUROC) significantly better than the Sup/Inf hemifield indices HNP and HSD. However, these results need to be interpreted with caution as this analysis was based on the data obtained from a pre-selected population of patients in which almost half had similar GSS staging in both eyes. This may have inadvertently lowered the performance of R/L asymmetry indices.

While the overall performance of an asymmetry index might not be superior to another there is a possibility that these indices could improve performance when used in combination. Multivariate Logistic Regression (MLR) allows the combination of a series of indices to predict a dichotomous output (POAG or Normal). MLR will also allow us to establish which indices are making a significant contribution to the discrimination between POAG and controls. This analysis provides a coefficient 'b' which measures each independent asymmetry indexes contribution to the overall diagnostic performance using the most parsimonious model.

The aim of the final study undertaken for this PhD is to describe and measure the discriminatory performance of an MLR analysis incorporating global indices based upon: Sup/Inf hemifield asymmetry; R/L asymmetry and clustering of hemifield asymmetric locations, to correctly predict the probability of having glaucoma for individual eyes for future inclusion in perimetric analytical software.

## Methods

All the data used in this study was obtained retrospectively from patients attending MREH between 2007-12. 30,899 SITA 24-2 visual field records were exported from the HFA to Excel 2010 for analysis. The stage of visual field loss was quantified with GSS (Brusini and Filacorda, 2006). GSS classifies each 24-2 threshold test on the basis of the global indices MD and PSD into 7 stages (Normal, Borderline and 5 stages of loss). Selection took no account of the reliability indices produced by the HFA software as these are often unreliable (Bengtsson and Heijl, 2000) and to make our results generalizable to clinical populations where good reliability indices are not always obtained.

### *Control (n= 412 eyes from 206 patients)*

All control subjects had normal clinical findings and visual field results with GSS Stage 0 in both eyes. All control eyes had visual acuity of 6/9 or better, refractive error ≤5.0D (spherical equivalent), IOP less than 22mmHg and no history of systemic and ocular disease that might influence the visual field.

183
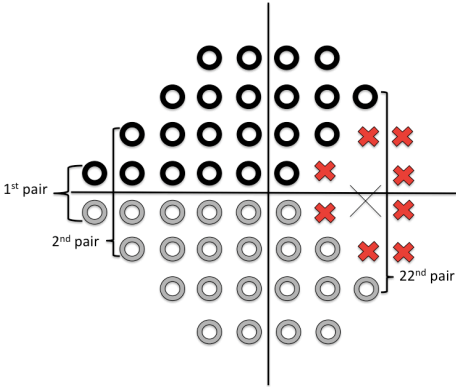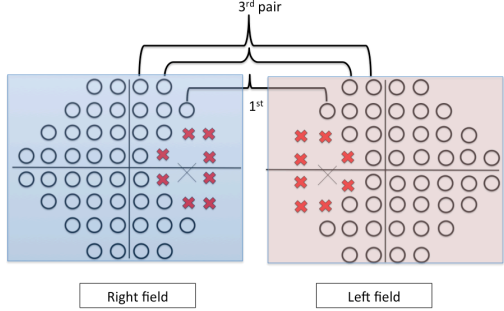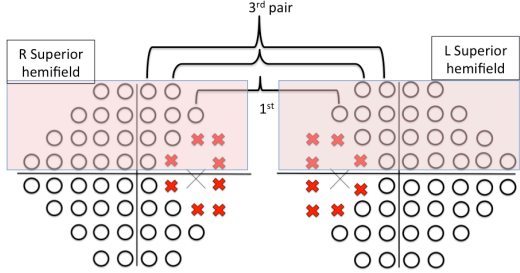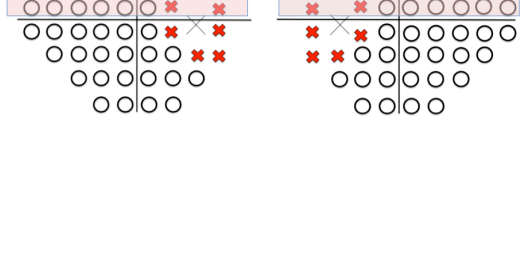
### *POAG (n=340 eyes from 170 patients)*
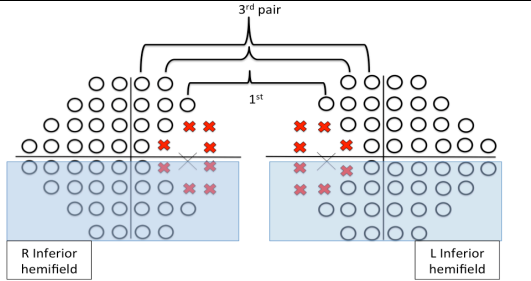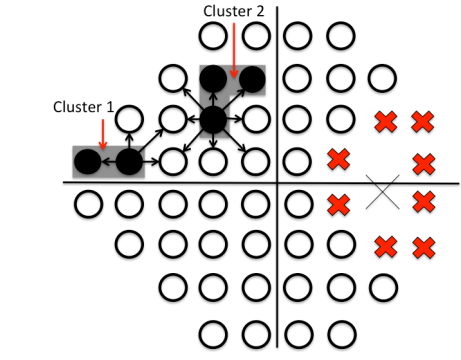
The POAG sample consisted of 170 patient's records with a clinical diagnosis of POAG in both eyes. The distribution of GSS stages in the POAG eyes was: stage 1=180, stage 0.5 or borderline=80 and stage 0 or normal=80. Patients with ocular abnormalities other than glaucoma that could be expected to affect the visual field, apart from early cataract, were removed.

## Cluster, Sup/Inf hemifield and R/L asymmetry analysis

The diagnostic performances of 14 indices are considered within this chapter. See Table 6.1 for details. In the cluster, and hemifield indices the same test locations are used, which is a subset of the 24-2 test pattern (44/54), excluding locations at or near the blind spot. Each test location in the superior hemifield was paired with vertically mirrored location in the inferior hemifield resulting in 22 test pairs. In the R/L whole field indices the same subset of the 24-2 test pattern (44/54) was used which is paired with a mirrored location in the other eye resulting in 44 test pairs. In the R/L hemifield indices (superior and inferior) there are only 22 test pairs. As diagnostic performance in this chapter is based on individual eyes, the hemifield worse eye indices (HMD, HSD and HNP worse eye) used in chapter 4 are not included in this analysis.

**Table 6.1: Description of asymmetry indices used in this study**

| Asymmetry Analysis | Index | Description |
|---|---|---|
| Sup/Inf | 1. HMD<br>Hemifield Mean Deviation.<br><br>2. HSD<br>Hemifield Standard Deviation.<br><br>3. HNP<br>Number of pairs (maximum 22) that fall outside the 95% confidence limits. |  |
| Right/Left | 4. R/L SD<br>R/L Standard Deviation for the wholes field 44 pairs.<br><br>5. R/L SD-Superior<br>R/L Standard Deviation of the superior hemifield 22 pairs.<br><br>6. R/L SD-Inferior<br>R/L Standard deviation of the inferior hemifield 22 pairs.<br><br>7. R/L NP<br>R/L number of pairs (max 44) that fall outside the 95% confidence limits<br><br>8. R/L NP-Superior<br>R/L number of pairs in the |  |

| | | |
|---|---|---|
| | superior fields (max 22) that fall outside the 95% confidence limits. |  |
| | 9. R/L NP-Inferior<br><br>R/L number of pairs in the inferior fields (max 22) that fall outside the 95% confidence limits. | |
| | 10. R/L MD<br><br>R/L Mean Deviation. | |
| | 11. R/L MD-Superior<br><br>R/L Mean Deviation of the 22 pairs in the superior hemifield | |
| | 12. R/L MD Inferior<br><br>R/L Mean Deviation of the 22 pairs in inferior hemifield | |
| Cluster | 13. N Clusters<br><br>Number of clusters of asymmetric pairs, radius 8.5° |  |
| | 14. N Clustered<br><br>Total number of asymmetric pairs within clusters, radius 8.5° | |
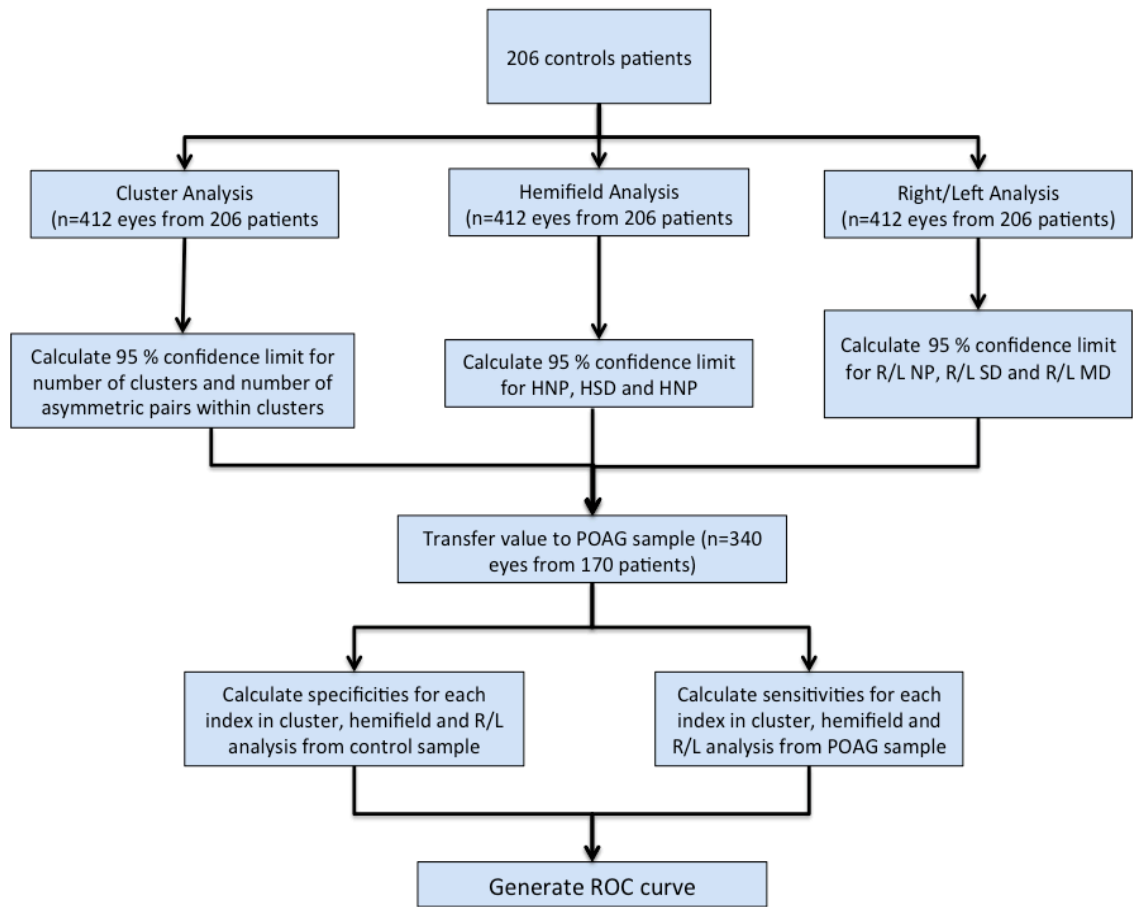
Figure 6.1: Analytical steps used in cluster, hemifield and R/L asymmetry analyses

Figure 6.1 gives a flow chart of analytical steps used in cluster, hemifield and R/L asymmetry analyses

**Statistical Tools**

Statistical analyses were performed using SPSS (SPSS, v. 22.0; SPSS, Chicago, IL). The tests used to check the statistical significance of the difference of the parameters means between the two groups were one-sample Kolmogorov-Smirnoff to test normality, Levene's test of equality of error variances to test homogeneity of variances, and an independent sample t-test (ANOVA).

AUROC with 95% CI for each asymmetry indices were generated using jrocfits (http://www.rad.jhmi.edu/jeng/javarad/roc/JROCFITi.html). Sensitivities at 80% and 95% specificity were determined for each index for comparisons.

MLR was performed using the forward stepwise Likelihood Ratio (LR) method. Forward selection begins with an empty equation. Asymmetry indices are added one at a time beginning with the index with the highest correlation with the POAG diagnosis. Asymmetry indices of greater theoretical importance are entered first. For the final model, the 'goodness of fit' ($X^2$ P>0.05 and Hosmer-Lemshow P>0.05) and the significance of each index (Wald test P<0.05) are included. Finally, the formula of probability of having glaucoma will be constructed based on a constant value and coefficients calculated from the MLR model. MLR will model the chance of an outcome based on individual characteristics. Because chance is a ratio, what will be actually modelled is the logarithm of the chance given by:

$$\mathrm{Log}\left(\frac{\pi}{1-\pi}\right) = \beta_\theta + \beta_1 \chi_1 + \beta_2 \chi_2 + \ldots \beta_n \chi_n$$

where $\pi$ indicates the probability of having POAG, $\beta\theta$ is the constant value calculated from regression analysis; $\beta 1$ are the regression coefficients associated with the x(1..n) explanatory variables (asymmetry indices).

To validate how well the proposed model correctly classifies cases, the AUROC of the proposed model will be compared with the GHT indices and the best single asymmetry indices (R/L NP).

## Results

The mean age in this control group (60.37 range 24.5-85.8 years) was statistically different (p<0.001) from POAG group (71.50 years range 30.1-92.3 years).

A cluster of defective locations (outside 95% CI) was found in 14% of controls eyes and 60% of POAG eyes. In control eyes, the largest numbers of clusters was 2 (1.2%) and the highest N Clustered was 6. For POAG eyes, 40.3% has no cluster while 43.2% have cluster size ≥3 with the largest involving 16 asymmetric pairs. Figure 6.2 and 6.3 gives the frequency distribution of N Clusters and N Clustered in control and POAG eyes. Comparison of N Clustered in POAG eyes with early loss (GSS 1) shows a significantly higher number of asymmetric pairs than the eyes

with stage 0 or borderline (GSS 1 VS GSS 0.5 p<0.001); (GSS 1 VS GSS 0.5, p<0.001), see figure 6.4

The discriminatory power (AUROC) of all 16 asymmetry indices is given in Table 6.2 along with their 95% CI and the sensitivity of each index at specificities of 80 and 95%. R/L NP (whole eye) and R/L SD have the highest AUROC. Comparison of AUROC for all 14 indices in the present study with previous studies which used different samples (chapters 3-5) are given in Table 6.3

To determine the best MLR model, we first performed the Pearson correlation test on all indices. HMD, R/L MD, R/L MD Superior and R/L MD Inferior were excluded from the MLR due to their weak correlation to a diagnosis of POAG and low AUROC leaving 10 indices. For every included index, univariate analysis using enter method of binary logistics was done to explore their association with glaucoma diagnosis as a single predictor. Forward stepwise Likelihood Ratio (LR) was performed until we reached a final model with significant asymmetry indices. Variables (asymmetry indices) of greater theoretical importance are entered first. Once in the equation, the variable remains there.

Final model identified 6 significant asymmetry indices; HNP, R/L SD, R/L SD Inferior, R/L NP, R/L NP Inferior and R/L SD Superior as being independently related to a diagnosis of early POAG field loss (p<0.05). The coefficient, the Wald Statistic and significant value are presented in table 6.4.

The Hosmer–Lemeshow test (Chi Square=11.648, 8 degrees of freedom and $P = 0.168$) indicates that the numbers of glaucomatous eyes are not significantly different from those predicted by the model and that the overall model fit is good. Furthermore, the Nagelkerke $R^2$ value for the final model was 0.704, suggesting that there is a strong relationship between asymmetry indices and the prediction of eyes with POAG field loss. The Wald criterion demonstrated that all indices in the proposed model; HNP, R/L SD, R/L SD Inferior, R/L NP, R/L NP Inferior and R/L SD Superior contribute significantly to the prediction of eyes with POAG field loss ($p<0.05$).

From Table 6.4 the fitted model for predicted Glaucoma Asymmetry Test value is:

P (Glaucoma Asymmetry Test) = −5.82 + (0.492 × HNP)
+ (4.908 × R/L SD)
+ (-2.486 × R/L SD Inferior Hemfield)
+ (0.214 × R/L NP)
+ (0.272 × R/L NP Inferior Hemifield)
+ (-1.233 × R/L SD Superior Hemifield)

Validation of the performance of the proposed model, known as Glaucoma Asymmetry Test (GAsym Test), correctly predicts 80.3% POAG cases and 89.3% normal cases with an AUROC of 0.94 (95% CI 0.924–0.95). This value is significantly higher than that for GHT 0.84 (95% CI 0.80–0.87) and R/L NP 0.89 (95% CI 0.87-0.91). Again, care needs to be taken when providing AUROC values for GHT due to it being derived from just 2 measures. At 80% and 95% specificities the sensitivities for proposed model are 90 and 74% while those for R/L NP are 82 and 56% and for GHT 70 and 9%, see figure 6.5 and table 6.5. Mean value for GAsym Test in control eyes is significantly different from POAG eyes (p=0.001) with

GAsym Test for control is -2.06 while for POAG eyes, mean GAsym Test value is 3.18, see figure 6.6.

Example of cases where only the proposed model classified the eye as POAG while GHT and R/L NP did not are given in Table 6.6
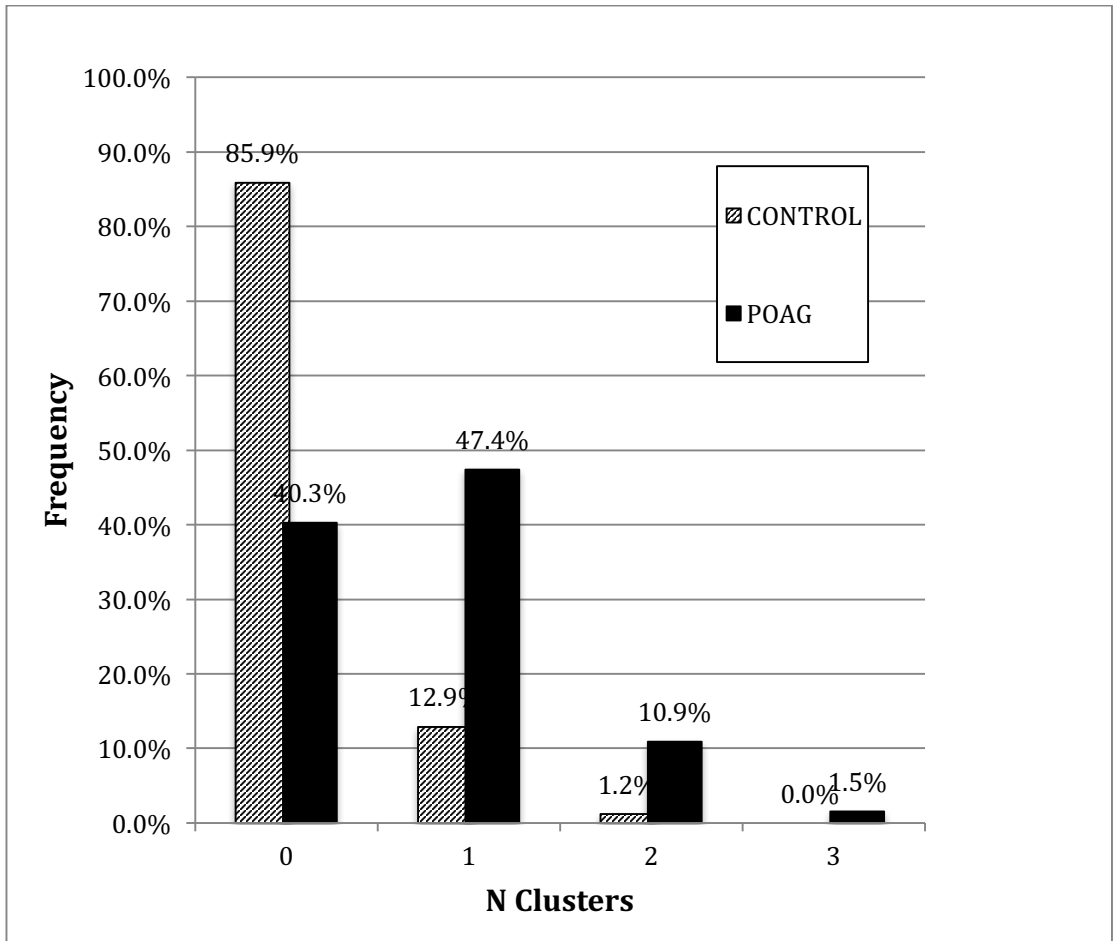
Figure 6.2: Frequency of N Clusters in the control and POAG eyes.
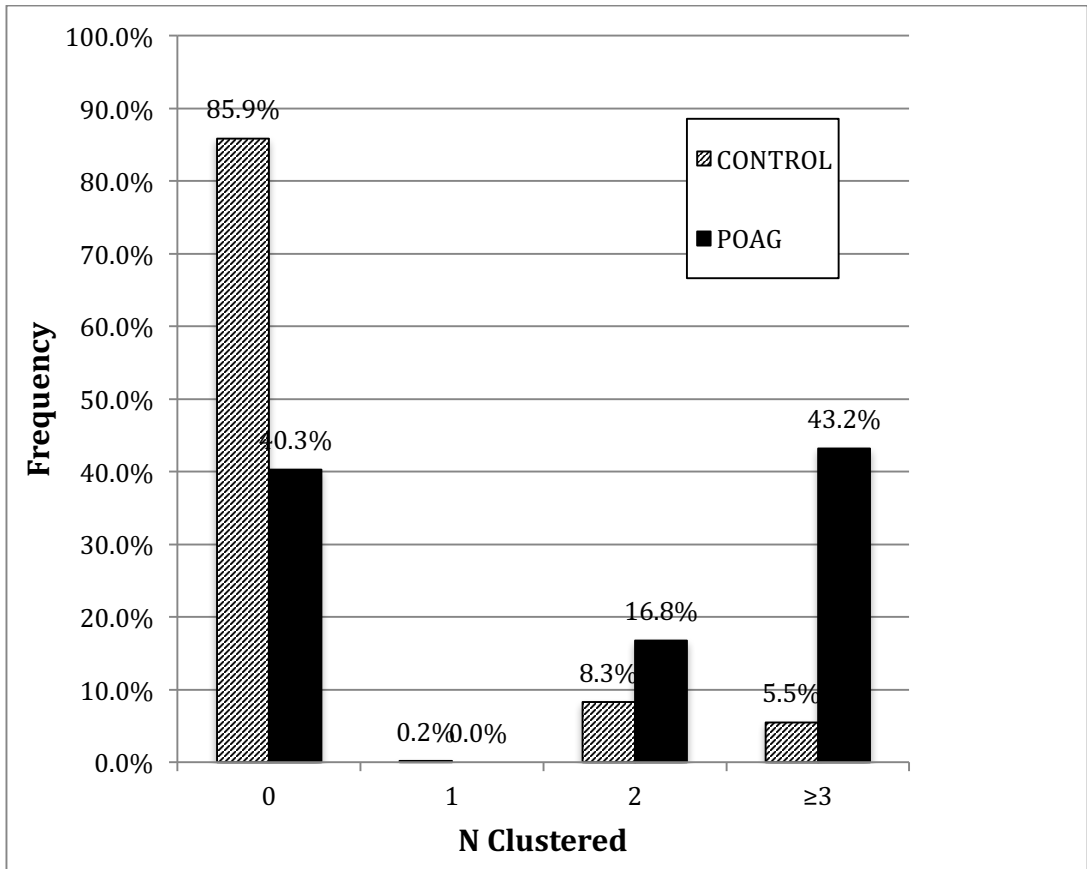
Figure 6.3: Frequency of the N Clustered for all the control and POAG eyes.
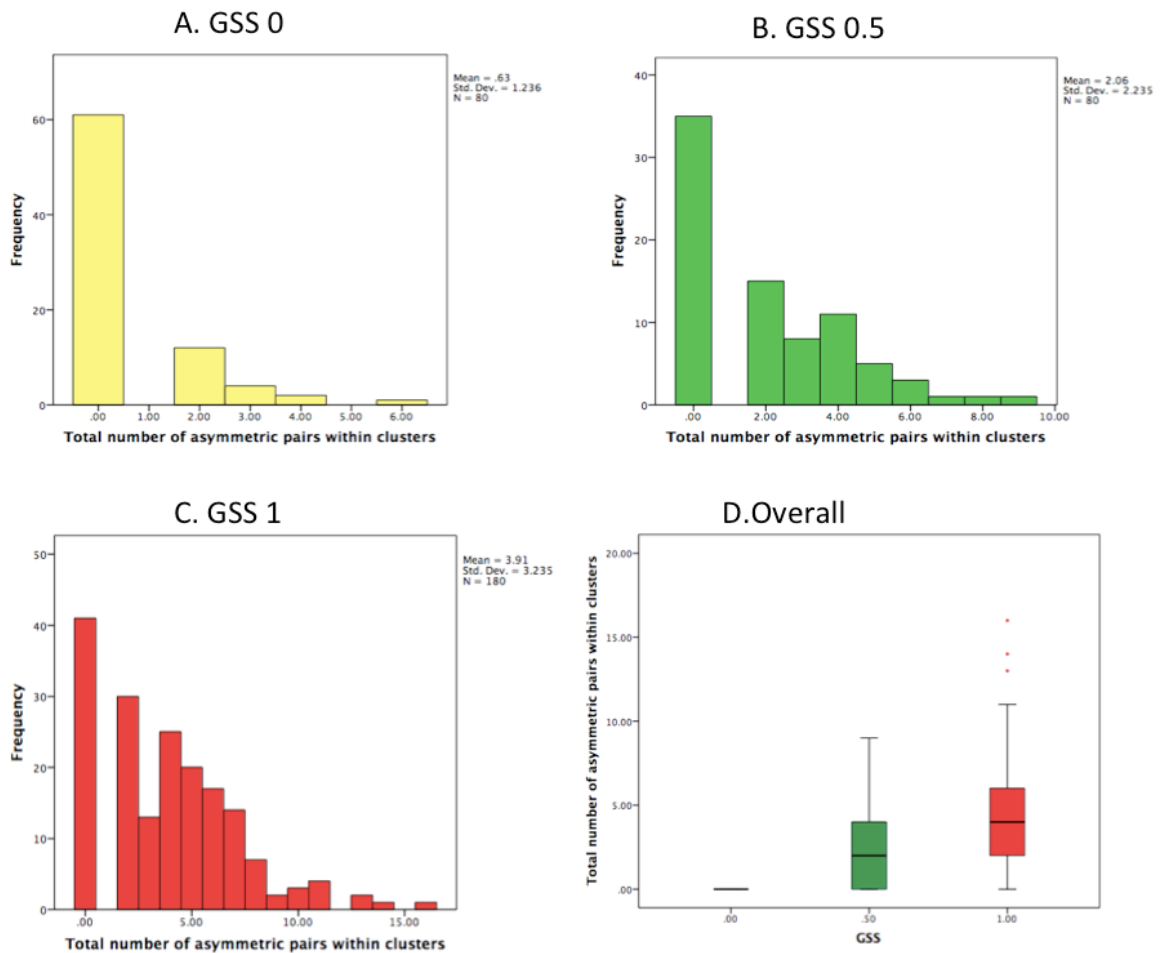
Figure 6.4: Comparison of N clustered within clusters in A. GSS=0; B. GSS=0.5; C. GSS=1 in POAG eyes and D. Overall comparison. Mean N clustered for GSS 0=0.63, GSS 0.5=2.06 and GSS 1 =3.9.

**Table 6.2: Diagnostic performances of all 14 asymmetry indices for differentiating early POAG from normal. Area under Curve (AUROC). 95% confidence limits of the AUROC**

| Asymmetry indices | AUROC | 95% Confidence Interval | | Sensitivity at 80% specificity | Sensitivity at 95% specificity |
|---|---|---|---|---|---|
| | | Lower limits | Upper limits | | |
| R/L NP | 0.891 | 0.868 | 0.914 | 82% | 56% |
| R/L SD | 0.876 | 0.852 | 0.901 | 79% | 58% |
| R/L SD Superior | 0.848 | 0.821 | 0.876 | 74% | 52% |
| R/ L NP Inferior | 0.840 | 0.810 | 0.870 | 73% | 52% |
| GHT | 0.837 | 0.803 | 0.870 | 70% | 9% |
| N clusters | 0.835 | 0.791 | 0.879 | 70% | 34% |
| HSD | 0.830 | 0.801 | 0.859 | 74% | 52% |
| R/ L NP Superior | 0.829 | 0.800 | 0.859 | 69% | 35% |
| HNP | 0.827 | 0.796 | 0.858 | 71% | 47% |
| N Clustered | 0.796 | 0.741 | 0.850 | 66% | 43% |
| R/L SD Inf | 0.757 | 0.723 | 0.791 | 58% | 31% |
| R/L MD Inferior | 0.610 | 0.568 | 0.652 | 46% | 41% |
| R/L MD | 0.600 | 0.558 | 0.643 | 46% | 33% |
| R/L MD Superior | 0.569 | 0.526 | 0.611 | 42% | 28% |
| HMD | 0.459 | 0.416 | 0.502 | 31% | 19% |

**Table 6.3: Comparison of AUROC of 14 indices found in the present study with the earlier studies**

| Present study | | | | Chapter 3 | Chapter 4 | Chapter 5 |
|---|---|---|---|---|---|---|
| Asymmetry indices | AUROC | 95% Confidence Interval | | Sup/Inf indices | R/L indices | Cluster indices |
| R/L NP | 0.891 | 0.869 | 0.915 | - | 0.903 (95% CI 0.867-0.938) | - |
| R/L SD | 0.876 | 0.852 | 0.901 | - | 0.897 (95% CI 0.857-0.936) | - |
| R/L SD Superior | 0.848 | 0.821 | 0.876 | - | 0.875 (95% CI 0.827-0.922) | - |
| R/ L NP Inferior | 0.840 | 0.810 | 0.870 | - | 0.836 (95% CI 0.784-0.889) | - |
| N clusters | 0.835 | 0.791 | 0.879 | - | - | 0.920 (95% CI 0.888 - 0.951) |
| HSD | 0.830 | 0.801 | 0.859 | 0.864 (95% CI 0.833-0.894) | - | 0.922 (95% CI 0.895-0.950) |
| R/ L NP Superior | 0.829 | 0.800 | 0.859 | - | 0.832 (95% CI 0.785-0.879) | - |
| HNP | 0.827 | 0.796 | 0.858 | 0.853 (95% CI 0.819-0.886) | - | 0.926 (95% CI 0.899-0.953) |
| N Clustered | 0.796 | 0.741 | 0.850 | - | - | 0.920 (95% CI 0.884- |

| | | | | | | |
|---|---|---|---|---|---|---|
| | | | | | | 0.956) |
| R/L SD Inf | 0.757 | 0.723 | 0.791 | - | 0.785 (95% CI 0.731-0.840) | - |
| R/L MD Inferior | 0.610 | 0.568 | 0.652 | - | 0.780 (95% CI 0.725-0.836) | - |
| R/L MD | 0.600 | 0.558 | 0.643 | - | 0.780 (95% CI 0.725-0.836) | - |
| R/L MD Superior | 0.569 | 0.526 | 0.611 | - | 0.420 (95% CI 0.32-0.499) | - |
| HMD | 0.459 | 0.416 | 0.502 | 0.745 (95% CI 0.705-0.786) | - | - |

**Table 6.4: The best combination of 6-asymmetry indices as proposed by multivariate logistic regression.**

| Asymmetry indices | Coefficients | Wald | P value | Exp (B) |
|---|---|---|---|---|
| HNP | 0.492 | 51.25 | <0.001 | 1.872 |
| R/L SD | 4.908 | 16.71 | <0.001 | 1.424 |
| R/L SD Inferior | -2.486 | 14.378 | <0.001 | 0.301 |
| R/L NP | 0.214 | 9.057 | 0.003 | 1.423 |
| R/L NP Inferior | 2.72 | 6.054 | 0.014 | 1.630 |
| R/L SD Superior | -1.233 | 4.026 | 0.045 | 0.972 |
| Constant | -5.820 | 95.541 | <0.001 | - |
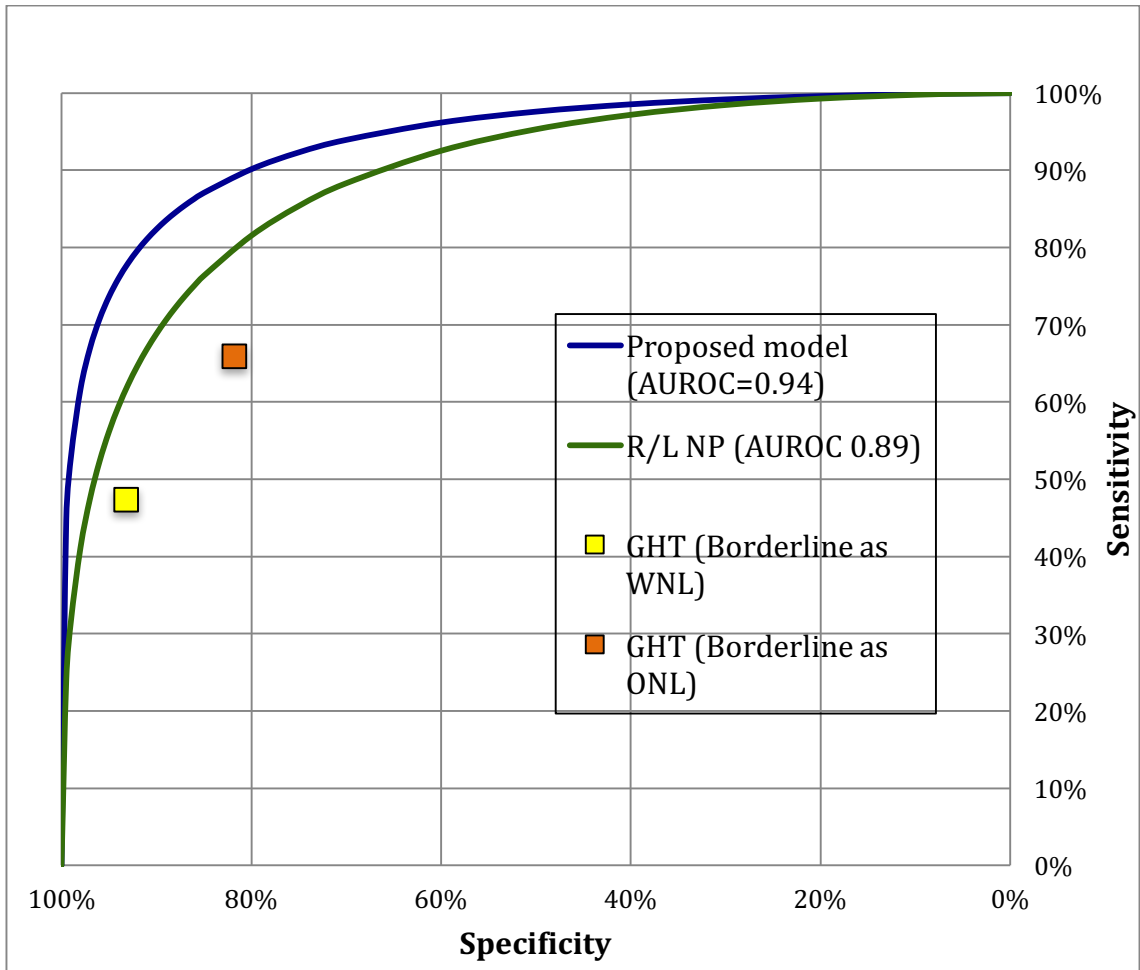
Figure 6.5: Comparison of ROC produced by final model proposed by multivariate logistic regression (combination of 6 significant indices), GHT and R/L NP.WNL=Within Normal Limits; ONL=Outside Normal Limits.
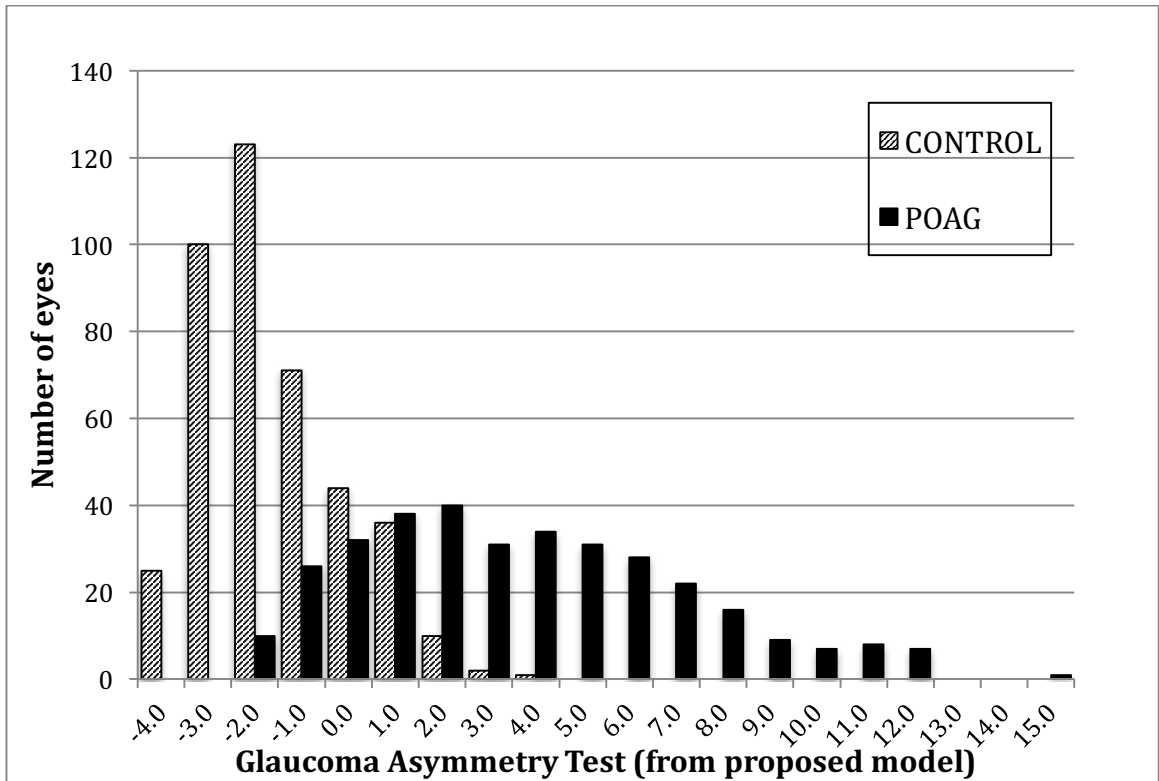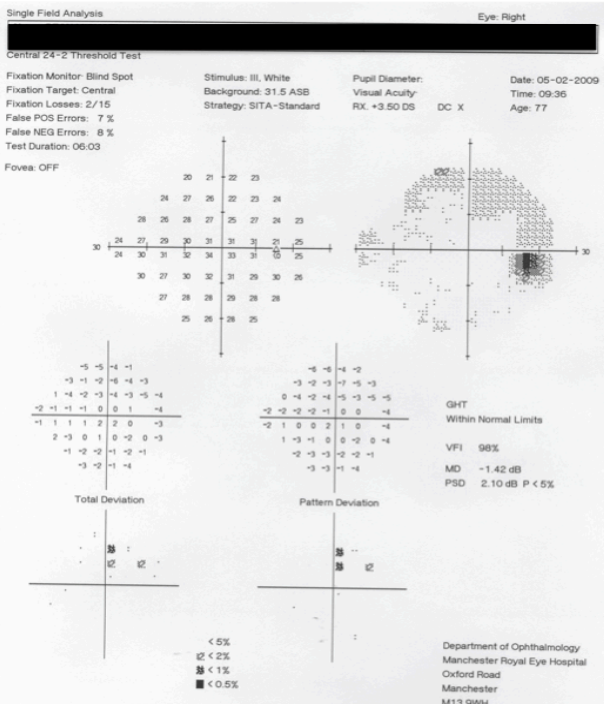
Figure 6.6: Glaucoma Asymmetry Test (GAsymT) value (from proposed model) in POAG and control eyes. Mean GAT value for control eyes is -2.05 and for POAG eyes is 3.10.

**Table 6.5: Example of 4 cases where our proposed model shows significant defect while individual indices (GHT and R/L NP) (the highest AUROC) did not**

| Clinical Diagnosis | GHT | Proposed model | Comments |
|---|---|---|---|
| #DM<br><br>RE<br><br>1. POAG with treatment; Travatan od nocte to both eyes and timolol 0.25% bd to both eyes |  | Glaucoma Asymmetry test (GAsymT) =2.25 | Proposed model indicative for POAG while other individual indices (GHT, R/L NP, HNP have finding within normal limits. |

| | | | |
|---|---|---|---|
| #CF<br><br>LE<br><br>Bilateral POAG with treatment (Timolol 0.25% daily for RE only) |  | Glaucoma Asymmetry test (GAsymT) 3.07 | This patient is within normal limits finding for GHT, R/L NP. HNP but proposed model indicates that this eye have 3.07 probability of having POAG. |

| #DP<br><br>LE<br><br>1.POAG with treatment; Gt Betoptic 0.25% bd both eyes |  | Glaucoma Asymmetry test (GAsymT) 2.25 | Proposed model indicates POAG, while single indices (GHT, R/L NP, HNP) report within normal limits. |
| --- | --- | --- | --- |

| #EW LE 1. POAG both eyes with treatment; Gt Timolol 0.25% bd both eyes, Gt travatan nocte bothe eyes |  | Glaucoma Asymmetry test (GAsymT) =4.28 | This patient has a within normal limits finding for GHT, R/L NP. HNP but proposed model indicates that this eye have 4.28 probability of having POAG. |
| --- | --- | --- | --- |
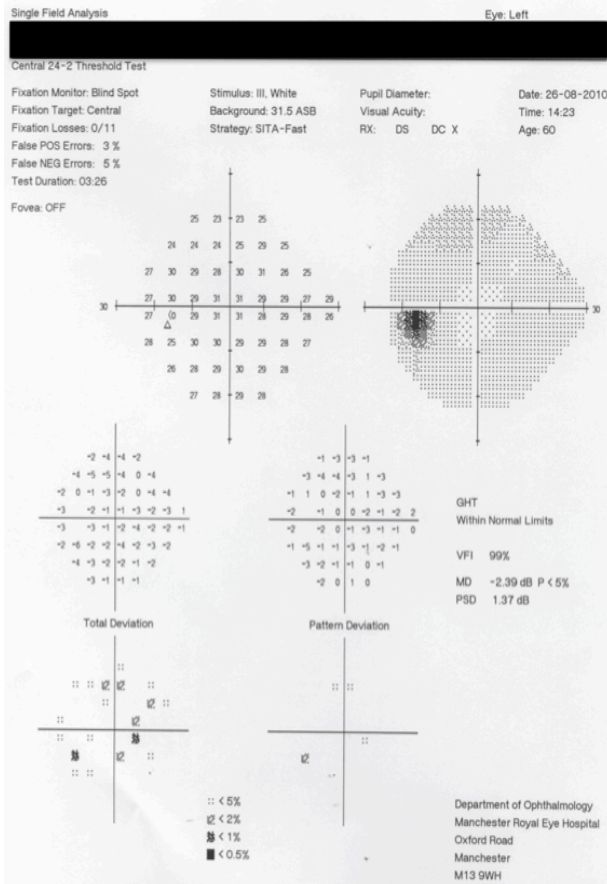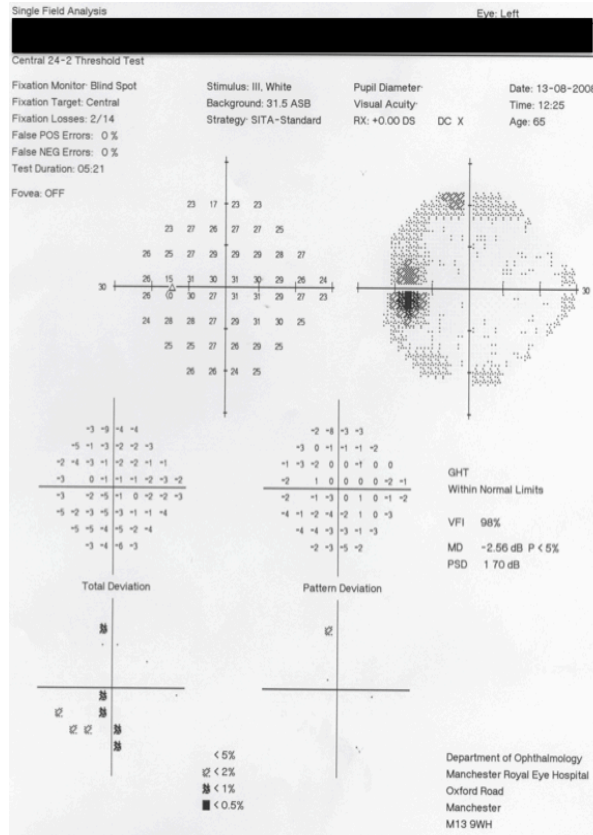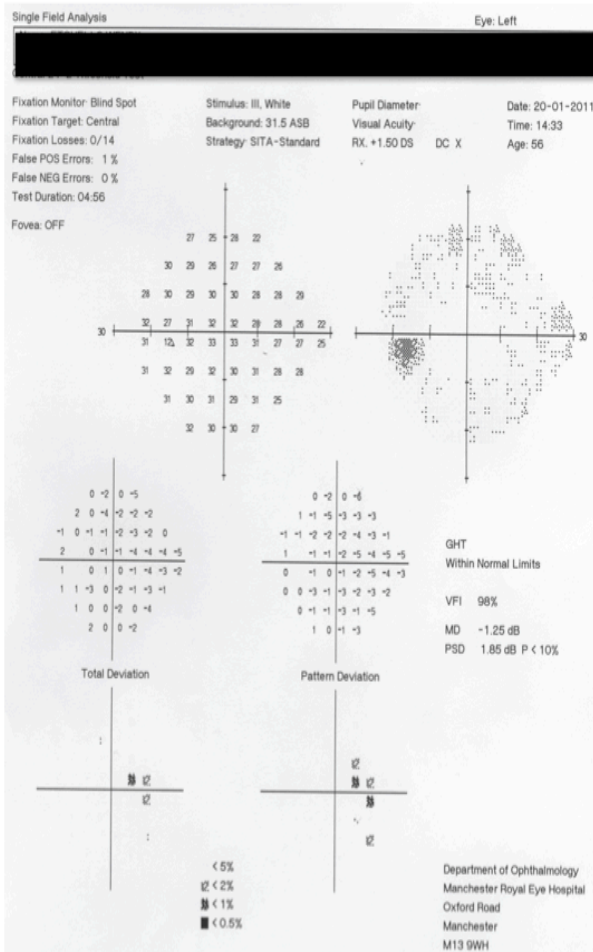
## Discussion

Recognition of early glaucomatous field loss and differentiation from defects caused by other ophthalmic conditions e.g. media opacities, diabetic retinopathy and early macula pathology, remains a challenging task. To address this issue, various indices has been introduced to both aid the decision process and provide a simple means to track change over time.

Previous chapters have explored the diagnostic potential of Sup/Inf hemifield asymmetries, R/L asymmetries and also clusters of Sup/Inf hemifield asymmetries in different POAG samples. The results of all these analyses are highly dependent upon the sample population. Sup/Inf hemifield asymmetry analyses in Chapter 5 used 247 POAG eyes from 222 patients and all POAG eyes had an IOP history of >21mmHg open angles observed by gonioscopic examination, a clinical diagnosis of POAG and early glaucoma (GSS stage≤1). In some cases, the selected eye was the better of the 2 eyes and the diagnosis of POAG might have largely been made on the basis of the other eyes findings. POAG samples for R/L asymmetry analyses in chapter 4 used 108 POAG patients (n=216 eyes) all eyes had early glaucoma (GSS stage≤1). For cluster asymmetry analyses, there were 160 POAG eyes included in the study all of which had early glaucoma (GSS stage=1). It is important to note here that all POAG eyes selected in the current and previous chapters had a clinical diagnosis of POAG rather than one based upon structural imaging or functional measures. The sample used for the MLR was different from that used in the previous studies/chapters. It was designed to provide an extremely challenging task to the indices with 40% of cases having a GSS≤0.5 (Normal and Borderline). Many of these cases have a diagnosis that is based more upon the results from the other eye rather than upon other measures. To have correctly identified 80.3%

POAG cases and 89.3% normal cases highlights the enormous potential of asymmetry analyses and emphasises how well functional measures can perform when new methods of analysis are used.

In the current study, the AUROC for most asymmetry indices are within 95% CI of the results found in the earlier studies (chapters 3 and 4). For cluster indices, N Clusters and N Clustered, the AUROC found for the MLR study was lower than that found in chapter 5. This difference is most likely due to a change in the POAG inclusion criteria. Having more POAG eyes with early loss (GSS=1) might have increased the performance of cluster indices in chapter 5. This can be seen from figure 6.4, where the N Clustered in POAG eyes with early loss (GSS=1) is significantly higher than those eyes with normal or borderline loss. The different distribution of GSS grades might also explain the higher AUROC value found in current study for HSD.  MD indices; (HMD, R/L MD, R/L MD Superior, R/L MD Inferior), were found to be significantly lower than in previous chapters, but were found to have a similar ranking on the basis of AUROC (the lowest among all indices). This suggests that MD indices have a weak correlation with glaucoma diagnosis.

Hemifield worse eye indices were not included in this study as these indices were generated for the purpose of comparison between R/L and Sup/Inf asymmetry indices in the earlier chapter (chapter 4). For the MLR study, the analysis was done on the basis on individual eyes rather than patients; therefore, the hemifield worse eye and worse hemifield index were not applicable.

A model proposed by MLR analysis identified 6 indices; HNP, R/L SD, R/L SD Inf, R/L NP, R/L NP Inf, R/L SD Sup as being independently related to a diagnosis of

early glaucomatous field loss. Forward stepwise method (LR) was used rather than backward selection because backward selection is often less successful than forward selection. The first step of a backward selection model is more likely to result in a complete or quasi-complete separation of response values. Other indices that have higher performance based on AUROC but not included in the final model are due to the fact that these indices are not significantly improve the performance of the model when used in combination.

The final model derived from a combination of the 6 indices outperformed GHT and the best single asymmetry analyses (R/L NP), correctly identifying 85.2% of all cases. This finding highlights the gain in discriminatory power obtained when indices are combined. While some indices might have lower AUROC than others this does not mean that, in combination, they cannot lead to an improved performance.

Our results suggest that asymmetry parameters have significant potential for aiding diagnosis of early glaucoma when a combination of asymmetry indices is used.

# 7. General discussion and future work

Early glaucomatous damage in either structure or function often remains localized to either side of the horizontal meridian and corresponds to the spatial organization and arrangements of the RNFL and the horizontal raphe (Mikelberg and Drance, 1984).

The GHT was designed to recognise any Sup/Inf hemifield asymmetry and has been shown to be a sensitive method for discriminating between normal and those with early POAG (Asman and Heijl, 1992b, Susanna et al., 1994). However, GHT suffers from a few limitations including the use of fixed sector borders, which assumes a constant mapping of the retinal locations to the optic nerve head. GHT also uses 5 categorical outcomes, rather than a continuous scale. The work in Chapter 3 introduced 3 new Sup/Inf hemifield asymmetry indices; HMD, HSD and HNP, for detecting early POAG (Ghazali et al., 2015). The new indices were found to have good discriminatory performance and agreement with GHT. Their outputs are on a continuous scale rather than discrete which provides improved facility for monitoring in a manner that is familiar to clinicians working with glaucoma patients.

Glaucomatous damage commonly occurs in one eye before the other and numerous studies have validated the structural and functional importance of R/L asymmetry in POAG (Asman and Heijl, 1992b, Asrani et al., 2011, Bagga et al., 2005, Cartwright and Anderson, 1988, Essock et al., 2005, Fansi et al., 2011, Feuer and Anderson, 1989, Greenfield et al., 2007, Gugleta et al., 1999, Gupta et al., 2011, Haefliger and Hitchings, 1990b, Harasymowycz et al., 2004, Henson et al., 1986,

Huang et al., 2014, Hwang et al., 2015, Kim et al., 2009, Lee et al., 2004, Levine et al., 2006, Liu et al., 2011a, Nakatani et al., 2010, Sullivan-Mee et al., 2013, Um et al., 2012, Wang et al., 2004, Williams et al., 2011). Despite the wide use of R/L asymmetry analysis in imaging devices (OCT, HRT, GDx) and in electrophysiology, there remains a paucity of studies establishing its discriminatory power for visual field data. The experimental work on chapter 4 advanced our understanding of visual field R/L asymmetry and sheds light on how its discriminatory performance compares to Sup/Inf hemifield indices. While R/L asymmetry indices had good discriminatory power none exceeded that of the best Sup/Inf hemifield indices.

In chapter 5, we introduced 2 indices based on the clustering of Sup/Inf asymmetric pairs, N Clusters and N Clustered. The results of this investigation found that the performance of these indices was similar to that of the Sup/Inf asymmetry indices.

In chapter 6 MLR was used to establish the best combination of indices in characterizing functional loss from POAG. Out of total of 19 indices used in chapter 3, 4 and 5, only 10 were selected from the earlier chapters. Indices based on 'worse' eye were not included along with those that did not show a significant correlation with the diagnosis. The MLR found that 6/10 indices made a significant difference to diagnostic performance and that in combination these 6 indices outperformed all single indices.

It is important to emphasize here that the results from all of these analyses are dependent upon the population sample. This can be seen from the findings of cluster asymmetry analysis where inclusion of different type of visual field loss in POAG eyes changes the AUROC measures found within the different chapters.

Inclusion of 160 POAG eyes defined by clinical diagnosis and with GSS =1 provides AUROC for number of cluster of 0.920, while inclusion of POAG eyes with mixture of stages 0, 0.5 and 1 (stage 1=130, stage 0.5 or borderline=26 and stage 0 or normal=17) reduces the AUROC for same indices to 0.835. The selection of patients was slightly different in chapters 5 and 6. The analysis in chapter 5 was based on single eyes rather than a comparison of the right and left eyes.

It is important to highlight here that all the POAG eyes had a clinical diagnosis of POAG and that this diagnosis was not based upon a restrictive number of structural or functional measures. Selection is likely to have included cases of pre-perimetric POAG and some non-POAG eyes. Clinical diagnoses are based upon a wide range of structural (e.g. disc hemorrhages) and functional predictors that are not usually incorporated in studies of diagnostic performance. Demographic factors may also have had a role to play in the clinical diagnosis. It is interesting to note here that, in all studies, there were significant differences in ages between the control and POAG samples. This was consistent across samples and it can thus be suggested that younger referred cases are less likely to have glaucoma. Furthermore, in all studies, the selected POAG samples would have excluded cases of significant asymmetry from other common age related pathologies, e.g. diabetes, cataract. Inclusion of such cases would weaken the potential of R/L indices.

In all our studies, the control samples came from the same source, MREH outpatient clinics. By selecting the control group from same source we ensured that the quality of the perimetric data is the same for controls and cases of POAG. While this sample might not truly represent the normal population they do represent the diagnostic challenge facing clinicians in an NHS eye clinic. The findings of this

research are, therefore, pertinent to ophthalmologists and clinicians tasked with differentiating between true and false positive referrals.

In each dataset in all experimental chapters, we applied bootstrapping technique to estimate the standard deviation. Bootstrapping provides a nonparametric approach to statistical inference when distributional assumptions may not be met. More accurate standard errors, confidence intervals, and even hypothesis tests for more complex samples can be derived using these methods. However, for future work, it may worth considering the alternative method for accuracy estimation other than bootstrapping which is known as "stratified ten-fold cross-validation" for model selection. This is due to fact that stratification is generally a better scheme, both in term of bias and variance. Bootstrap has low variance, but extremely large bias on some problems (Kohavi, 1995).

Furthermore, obtaining matched control and early POAG samples from different sources is difficult. Our approach is a pragmatic one.

Our data suggest that asymmetry analysis is potentially a better discriminator in diagnosing early POAG due to the fact that it removes inter subject variability. The introduction of GHT a few decades ago has significantly enhanced the diagnostic potential of visual field measures and the findings of this research suggests that this can be taken further with modifications the methods used and the addition of other asymmetry indices (e.g. R/L).

R/L analyses have added value but require shifts in current VF practices, which are eye specific and currently ignore data from the 'other eye'. The MLR analysis highlights the lost potential of retaining an eye only approach. While developments in the analysis of imaging data have undergone massive amounts of change, VF analyses has been stable for over a decade. There is a need to move forward and begin to utilize the power of combining asymmetry indices.

This research provides a framework for further exploration of visual field databases. Since most hospitals have been using HFAs for many years and saving records, the wealth of information obtained in visual field datasets will serve as a base for future studies for analysis of change in POAG.

# 8. Appendix

**Ghazali N**., Aslam T., Henson DB. (2015) New superior-inferior visual field asymmetry indices for detecting POAG and their agreement with the glaucoma hemifield test. Eye (Lond). Oct; 29(10):1375-82.

**Ghazali N**., Aslam T., Henson DB. (2015) R/L Visual Field Asymmetry Indices for Detecting early POAG. (Manuscript in preparation)

**Ghazali N**., Aslam T., Henson DB. (2015) Asymmetry Cluster Indices for Detecting early POAG. (Manuscript in preparation)

**Ghazali N**., Aslam T., Henson DB. (2015) Multivariate Logistic Regression of asymmetry Indices in detecting POAG. (Manuscript in preparation)

## List of conference contributions

**Ghazali N**., Aslam T., Henson DB. (2015) New superior-inferior and R/L visual field asymmetry indices for detecting POAG. ARVO 2013 Annual Meeting, Orlando, FL, USA (poster)

**Ghazali N**., Aslam T., Henson DB. (2015) New superior-inferior and R/L visual field asymmetry indices for detecting POAG. Institute Human Development Postgraduate Showcase 2014 University of Manchester (poster)

**Ghazali N**., Aslam T., Henson DB. (2015) R/L Visual Field Asymmetry Indices for Detecting early POAG. UKEGS 2015. UK and Eire Glaucoma Society Meeting,

Leceiseter 2015. (paper)

**Ghazali N**., Aslam T., Henson DB. (2015) R/L Visual Field Asymmetry Indices for detecting early POAG. ARVO 2016 Annual Meeting, Seattle, WA, USA (poster)

# 9. References

2009. *Glaucoma: Diagnosis and Management of Chronic Open Angle Glaucoma and Ocular Hypertension.* London.

ABE, H., SHIRAKASHI, M., TSUTSUMI, T., ARAIE, M., TOMIDOKORO, A., IWASE, A., TOMITA, G. & YAMAMOTO, T. 2009. Laser scanning tomography of optic discs of the normal Japanese population in a population-based setting. *Ophthalmology,* 116**,** 223-30.

AIRAKSINEN, P. J., MUSTONEN, E. & ALANKO, H. I. 1981. Optic disc haemorrhages precede retinal nerve fibre layer defects in ocular hypertension. *Acta Ophthalmol (Copenh),* 59**,** 627-41.

ALENCAR, L. M. & MEDEIROS, F. A. 2011. The role of standard automated perimetry and newer functional methods for glaucoma diagnosis and follow-up. *Indian J Ophthalmol,* 59 Suppl**,** S53-8.

ANTON, A., ZANGWILL, L., EMDADI, A. & WEINREB, R. N. 1997. Nerve fiber layer measurements with scanning laser polarimetry in ocular hypertension. *Arch Ophthalmol,* 115**,** 331-4.

ARTES, P. H., O'LEARY, N., HUTCHISON, D. M., HECKLER, L., SHARPE, G. P., NICOLELA, M. T. & CHAUHAN, B. C. 2011. Properties of the statpac visual field index. *Invest Ophthalmol Vis Sci,* 52**,** 4030-8.

ARVANITAKI, V., TSILIMBARIS, M. K., PALLIKARIS, A., MOSCHANDREAS, I., MINOS, E., PALLIKARIS, I. G. & DETORAKIS, E. T. 2012. Macular retinal and nerve fiber layer thickness in early glaucoma: clinical correlations. *Middle East Afr J Ophthalmol,* 19**,** 204-10.

ASMAN, P. & HEIJL, A. 1992a. Evaluation of methods for automated Hemifield analysis in perimetry. *Arch Ophthalmol,* 110**,** 820-6.

ASMAN, P. & HEIJL, A. 1992b. Glaucoma Hemifield Test. Automated visual field evaluation. *Arch Ophthalmol,* 110**,** 812-9.

ASMAN, P. & HEIJL, A. 1993. Arcuate cluster analysis in glaucoma perimetry. *J Glaucoma,* 2**,** 13-20.

ASRANI, S., ROSDAHL, J. A. & ALLINGHAM, R. R. 2011. Novel software strategy for glaucoma diagnosis: asymmetry analysis of retinal thickness. *Arch Ophthalmol,* 129**,** 1205-11.

ASRANI, S., ZEIMER, R., WILENSKY, J., GIESER, D., VITALE, S. & LINDENMUTH, K. 2000. Large diurnal fluctuations in intraocular pressure are an independent risk factor in patients with glaucoma. *J Glaucoma,* 9**,** 134-42.

BADLANI, V., SHAHIDI, M., SHAKOOR, A., EDWARD, D. P., ZELKHA, R. & WILENSKY, J. 2006. Nerve fiber layer thickness in glaucoma patients with asymmetric hemifield visual field loss. *J Glaucoma,* 15**,** 275-80.

BAGGA, H., GREENFIELD, D. S. & KNIGHTON, R. W. 2005. Macular symmetry testing for glaucoma detection. *J Glaucoma,* 14**,** 358-63.

BALAZSI, A. G., DRANCE, S. M., SCHULZER, M. & DOUGLAS, G. R. 1984. Neuroretinal rim area in suspected glaucoma and early chronic open-angle glaucoma. Correlation with parameters of visual function. *Arch Ophthalmol,* 102**,** 1011-4.

BENGTSSON, B. 1976. The variation and covariation of cup and disc diameters. *Acta Ophthalmol (Copenh),* 54**,** 804-18.

BENGTSSON, B. 2000. Reliability of computerized perimetric threshold tests as assessed by reliability indices and threshold reproducibility in patients with

suspect and manifest glaucoma. *Acta Ophthalmologica Scandinavica, 78***,** 519-522.

BENGTSSON, B. & HEIJL, A. 2000. False-negative responses in glaucoma perimetry: indicators of patient performance or test reliability? *Invest Ophthalmol Vis Sci,* 41**,** 2201-4.

BENGTSSON, B. & HEIJL, A. 2006. Diagnostic sensitivity of fast blue-yellow and standard automated perimetry in early glaucoma - A comparison between different test programs. *Ophthalmology,* 113**,** 1092-1097.

BENGTSSON, B., OLSSON, J., HEIJL, A. & ROOTZEN, H. 1997. A new generation of algorithms for computerized threshold perimetry, SITA. *Acta Ophthalmol Scand,* 75**,** 368-75.

BERGAMIN, O., ZIMMERMAN, M. B. & KARDON, R. H. 2003. Pupil light reflex in normal and diseased eyes: diagnosis of visual dysfunction using waveform partitioning. *Ophthalmology,* 110**,** 106-14.

BERTUZZI, F., HOFFMAN, D. C., DE FONSEKA, A. M., SOUZA, C. & CAPRIOLI, J. 2009. Concordance of retinal nerve fiber layer defects between fellow eyes of glaucoma patients measured by optical coherence tomography. *Am J Ophthalmol,* 148**,** 148-54.

BJERRE, A., GRIGG, J. R., PARRY, N. R. & HENSON, D. B. 2004. Test-retest variability of multifocal visual evoked potential and SITA standard perimetry in glaucoma. *Invest Ophthalmol Vis Sci,* 45**,** 4035-40.

BODEN, C., SAMPLE, P. A., BOEHM, A. G., VASILE, C., AKINEPALLI, R. & WEINREB, R. N. 2002. The structure-function relationship in eyes with glaucomatous visual field loss that crosses the horizontal meridian. *Archives of Ophthalmology,* 120**,** 907-912.

BOLAND, M. V. & QUIGLEY, H. A. 2007. Risk factors and open-angle glaucoma: classification and application. *J Glaucoma,* 16**,** 406-18.

BONOMI, L., MARCHINI, G., MARRAFFA, M., BERNARDI, P., MORBIO, R. & VAROTTO, A. 2000. Vascular risk factors for primary open angle glaucoma: the Egna-Neumarkt Study. *Ophthalmology,* 107**,** 1287-93.

BOWD, C., ZANGWILL, L. M. & WEINREB, R. N. 2003. Association between scanning laser polarimetry measurements using variable corneal polarization compensation and visual field sensitivity in glaucomatous eyes. *Arch Ophthalmol,* 121**,** 961-6.

BOZKURT, B., IRKEC, M. & ARSLAN, U. 2010. Diagnostic accuracy of Heidelberg Retina Tomograph III classifications in a Turkish primary open-angle glaucoma population. *Acta Ophthalmol,* 88**,** 125-30.

BRENTON, R. S., PHELPS, C. D., ROJAS, P. & WOOLSON, R. F. 1986. Interocular differences of the visual field in normal subjects. *Invest Ophthalmol Vis Sci,* 27**,** 799-805.

BRITTON, R. J., DRANCE, S. M., SCHULZER, M., DOUGLAS, G. R. & MAWSON, D. K. 1987. The area of the neuroretinal rim of the optic nerve in normal eyes. *Am J Ophthalmol,* 103**,** 497-504.

BRUSINI, P. & FILACORDA, S. 2006. Enhanced Glaucoma Staging System (GSS 2) for classifying functional damage in glaucoma. *J Glaucoma,* 15**,** 40-6.

BUDENZ, D. L. 2008. Symmetry between the right and left eyes of the normal retinal nerve fiber layer measured with optical coherence tomography (an AOS thesis). *Trans Am Ophthalmol Soc,* 106**,** 252-75.

BUHRMANN, R. R., QUIGLEY, H. A., BARRON, Y., WEST, S. K., OLIVA, M. S. & MMBAGA, B. B. 2000. Prevalence of glaucoma in a rural East African population. *Invest Ophthalmol Vis Sci,* 41**,** 40-8.

BURGOYNE, C. F., DOWNS, J. C., BELLEZZA, A. J., SUH, J. K. & HART, R. T. 2005. The optic nerve head as a biomechanical structure: a new paradigm for understanding the role of IOP-related stress and strain in the pathophysiology of glaucomatous optic nerve head damage. *Prog Retin Eye Res,* 24**,** 39-73.

CAPRIOLI, J., MILLER, J. M. & SEARS, M. 1987. Quantitative evaluation of the optic nerve head in patients with unilateral visual field loss from primary open-angle glaucoma. *Ophthalmology,* 94**,** 1484-7.

CARTWRIGHT, M. J. & ANDERSON, D. R. 1988. Correlation of asymmetric damage with asymmetric intraocular pressure in normal-tension glaucoma (low-tension glaucoma). *Arch Ophthalmol,* 106**,** 898-900.

CHAUHAN, B. C., DRANCE, S. M. & DOUGLAS, G. R. 1990. The Use of Visual-Field Indexes in Detecting Changes in the Visual-Field in Glaucoma. *Investigative Ophthalmology & Visual Science,* 31**,** 512-520.

CHAUHAN, B. C., HENSON, D. B. & HOBLEY, A. J. 1988. Cluster analysis in visual field quantification. *Doc Ophthalmol,* 69**,** 25-39.

CHAUHAN, B. C., NICOLELA, M. T. & ARTES, P. H. 2009. Incidence and rates of visual field progression after longitudinally measured optic disc change in glaucoma. *Ophthalmology,* 116**,** 2110-8.

CHAUHAN, B. C., O'LEARY, N., ALMOBARAK, F. A., REIS, A. S., YANG, H., SHARPE, G. P., HUTCHISON, D. M., NICOLELA, M. T. & BURGOYNE, C. F. 2013. Enhanced detection of open-angle glaucoma with an anatomically accurate optical coherence tomography-derived neuroretinal rim parameter. *Ophthalmology,* 120**,** 535-43.

CHEN, Y., WYATT, H. J. & SWANSON, W. H. 2005. Pupillary evaluation of retinal asymmetry: development and initial testing of a technique. *Vision Res,* 45**,** 2549-63.

CHEN, Y., WYATT, H. J., SWANSON, W. H. & DUL, M. W. 2008. Rapid pupil-based assessment of glaucomatous damage. *Optom Vis Sci,* 85**,** 471-81.

CHOUDHARI, N. S., GEORGE, R., BASKARAN, M., VE, R. S., RAJU, P. & VIJAYA, L. 2013. Can intraocular pressure asymmetry indicate undiagnosed primary glaucoma? The Chennai Glaucoma Study. *J Glaucoma,* 22**,** 31-5.

COOPS, A., HENSON, D. B., KWARTZ, A. J. & ARTES, P. H. 2006. Automated analysis of heidelberg retina tomograph optic disc images by glaucoma probability score. *Invest Ophthalmol Vis Sci,* 47**,** 5348-55.

CRICHTON, A., DRANCE, S. M., DOUGLAS, G. R. & SCHULZER, M. 1989. Unequal intraocular pressure and its relation to asymmetric visual field defects in low-tension glaucoma. *Ophthalmology,* 96**,** 1312-4.

DANESH-MEYER, H. V., GASKIN, B. J., JAYUSUNDERA, T., DONALDSON, M. & GAMBLE, G. D. 2006. Comparison of disc damage likelihood scale, cup to disc ratio, and Heidelberg retina tomograph in the diagnosis of glaucoma. *Br J Ophthalmol,* 90**,** 437-41.

DANTHUREBANDARA, V. M., SHARPE, G. P., HUTCHISON, D. M., DENNISS, J., NICOLELA, M. T., MCKENDRICK, A. M., TURPIN, A. & CHAUHAN, B. C. 2015. Enhanced structure-function relationship in glaucoma with an anatomically and geometrically accurate neuroretinal rim measurement. *Invest Ophthalmol Vis Sci,* 56**,** 98-105.

DE LEON-ORTEGA, J. E., SAKATA, L. M., MONHEIT, B. E., MCGWIN, G., ARTHUR, S. N. & GIRKIN, C. A. 2007. Comparison of diagnostic accuracy of heidelberg retina tomograph II and heidelberg retina tomograph 3 to discriminate glaucomatous and nonglaucomatous eyes. *American Journal of Ophthalmology,* 144**,** 525-532.

DE MORAES, C. G. V., PRATA, T. S., TELLO, C., RITCH, R. & LIEBMANN, J. M. 2009. Glaucoma With Early Visual Field Loss Affecting Both Hemifields and the Risk of Disease Progression. *Archives of Ophthalmology,* 127**,** 1129-1134.

DE VOOGD, S., IKRAM, M. K., WOLFS, R. C. W., JANSONIUS, N. M., HOFMAN, A. & DE JONG, P. T. V. M. 2005. Incidence of open-angle glaucoma in a general elderly population: The Rotterdam Study. *Ophthalmology,* 112**,** 1487-1493.

DENNISS, J., TURPIN, A., TANABE, F., MATSUMOTO, C. & MCKENDRICK, A. M. 2014. Structure-function mapping: variability and conviction in tracing retinal nerve fiber bundles and comparison to a computational model. *Invest Ophthalmol Vis Sci,* 55**,** 728-36.

DICKMANN, A., PETRONI, S., PERROTTA, V., PARRILLA, R., ALIBERTI, S., SALERNI, A. & SAVASTANO, M. C. 2012. Measurement of retinal nerve fiber layer thickness, macular thickness, and foveal volume in amblyopic eyes using spectral-domain optical coherence tomography. *J AAPOS,* 16**,** 86-8.

DRANCE, S. M. 1969. The early field defects in glaucoma. *Invest Ophthalmol,* 8**,** 84-91.

DREHER, A. W., REITER, K. & WEINREB, R. N. 1992. Spatially resolved birefringence of the retinal nerve fiber layer assessed with a retinal laser ellipsometer. *Appl Opt,* 31**,** 3730-5.

DUGGAN, C., SOMMER, A., AUER, C. & BURKHARD, K. 1985. Automated differential threshold perimetry for detecting glaucomatous visual field loss. *Am J Ophthalmol,* 100**,** 420-3.

ESSOCK, E. A., SINAI, M. J. & FECHTNER, R. D. 1999. Interocular symmetry in nerve fiber layer thickness of normal eyes as determined by polarimetry. *J Glaucoma,* 8**,** 90-8.

ESSOCK, E. A., ZHENG, Y. & GUNVANT, P. 2005. Analysis of GDx-VCC polarimetry data by Wavelet-Fourier analysis across glaucoma stages. *Invest Ophthalmol Vis Sci,* 46**,** 2838-47.

FANKHAUSER, F., 2ND & FLAMMER, J. 1989. Puptrak 1.0--a new semiautomated system for pupillometry with the Octopus perimeter: a preliminary report. *Doc Ophthalmol,* 73**,** 235-48.

FANSI, A. A., BOISJOLY, H., CHAGNON, M. & HARASYMOWYCZ, P. J. 2011. Comparison of different methods of inter-eye asymmetry of rim area and disc area analysis. *Eye (Lond),* 25**,** 1590-7.

FECHTNER, R. D. & WEINREB, R. N. 1994a. Mechanisms of optic nerve damage in primary open angle glaucoma. *Surv Ophthalmol,* 39**,** 23-42.

FECHTNER, R. D. & WEINREB, R. N. 1994b. Mechanisms of optic nerve damage in primary open angle glaucoma. *Survey of Ophthalmology,* 39**,** 23-42.

FEUER, W. J. & ANDERSON, D. R. 1989. Static threshold asymmetry in early glaucomatous visual field loss. *Ophthalmology,* 96**,** 1285-97.

FIELD, M. G., ALASIL, T., BANIASADI, N., QUE, C., SIMAVLI, H., SOBEIH, D., SOLA-DEL VALLE, D., BEST, M. J. & CHEN, T. C. 2014. Facilitating Glaucoma Diagnosis With Intereye Retinal Nerve Fiber Layer Asymmetry Using Spectral-Domain Optical Coherence Tomography. *J Glaucoma*.

FISHMAN, R. S. 1970. Optic disc asymmetry. A sign of ocular hypertension. *Arch Ophthalmol,* 84**,** 590-4.

FLAMMER, J. 1986. The concept of visual field indices. *Graefes Arch Clin Exp Ophthalmol,* 224**,** 389-92.

FORTUNE, B., BURGOYNE, C. F., CULL, G., REYNAUD, J. & WANG, L. 2013. Onset and progression of peripapillary retinal nerve fiber layer (RNFL) retardance changes occur earlier than RNFL thickness changes in experimental glaucoma. *Invest Ophthalmol Vis Sci,* 54**,** 5653-61.

FOSTER, P. J., BUHRMANN, R., QUIGLEY, H. A. & JOHNSON, G. J. 2002. The definition and classification of glaucoma in prevalence surveys. *Br J Ophthalmol,* 86**,** 238-42.

FRIEDMAN, D. S., NORDSTROM, B., MOZAFFARI, E. & QUIGLEY, H. A. 2005. Variations in treatment among adult-onset open-angle glaucoma patients. *Ophthalmology,* 112**,** 1494-9.

GAASTERLAND, D., TANISHIMA, T. & KUWABARA, T. 1978. Axoplasmic flow during chronic experimental glaucoma. 1. Light and electron microscopic studies of the monkey optic nervehead during development of glaucomatous cupping. *Invest Ophthalmol Vis Sci,* 17**,** 838-46.

GARWAY-HEATH, D. F., CAPRIOLI, J., FITZKE, F. W. & HITCHINGS, R. A. 2000. Scaling the hill of vision: The physiological relationship between light sensitivity and ganglion cell numbers. *Investigative Ophthalmology & Visual Science,* 41**,** 1774-1782.

GARWAY-HEATH, D. F., LASCARATOS, G., BUNCE, C., CRABB, D. P., RUSSELL, R. A., SHAH, A. & UNITED KINGDOM GLAUCOMA TREATMENT STUDY, I. 2013. The United Kingdom Glaucoma Treatment Study: a multicenter, randomized, placebo-controlled clinical trial: design and methodology. *Ophthalmology,* 120**,** 68-76.

GHAZALI, N., ASLAM, T. & HENSON, D. B. 2015. New superior-inferior visual field asymmetry indices for detecting POAG and their agreement with the glaucoma hemifield test. *Eye (Lond),* 29**,** 1375-82.

GHERGHEL, D., ORGUL, S., PRUNTE, C., GUGLETA, K., LUBECK, P., GEKKIEVA, M. & FLAMMER, J. 2000. Interocular differences in optic disc topographic parameters in normal subjects. *Curr Eye Res,* 20**,** 276-82.

GORDON, M. O., BEISER, J. A., BRANDT, J. D., HEUER, D. K., HIGGINBOTHAM, E. J., JOHNSON, C. A., KELTNER, J. L., MILLER, J. P., PARRISH, R. K., 2ND, WILSON, M. R. & KASS, M. A. 2002. The Ocular Hypertension Treatment Study: baseline factors that predict the onset of primary open-angle glaucoma. *Arch Ophthalmol,* 120**,** 714-20; discussion 829-30.

GRAHAM, S. L., KLISTORNER, A. I., GRIGG, J. R. & BILLSON, F. A. 2000. Objective VEP perimetry in glaucoma: asymmetry analysis to identify early deficits. *J Glaucoma,* 9**,** 10-9.

GRAMER, E. & TAUSCH, M. 1998. Measurement of the retinal nerve fiber layer thickness in clinical routine. *Curr Opin Ophthalmol,* 9**,** 77-87.

GREENFIELD, D. S., BAGGA, H. & KNIGHTON, R. W. 2003a. Macular thickness changes in glaucomatous optic neuropathy detected using optical coherence tomography. *Arch Ophthalmol,* 121**,** 41-6.

GREENFIELD, D. S., BAGGA, H. & KNIGHTON, R. W. 2003b. Macular thickness changes in glaucomatous optic neuropathy detected using optical coherence tomography. *Archives of Ophthalmology,* 121**,** 41-46.

GREENFIELD, D. S., LIEBMANN, J. M., RITCH, R. & KRUPIN, T. 2007. Visual field and intraocular pressure asymmetry in the low-pressure glaucoma treatment study. *Ophthalmology,* 114**,** 460-5.

GUGLETA, K., ORGUL, S. & FLAMMER, J. 1999. Asymmetry in intraocular pressure and retinal nerve fiber layer thickness in normal-tension glaucoma. *Ophthalmologica,* 213**,** 219-23.

GUPTA, V., GUPTA, S., DHAWAN, M., SHARMA, A., KAPOOR, K. S. & SIHOTA, R. 2011. Extent of asymmetry and unilaterality among juvenile onset primary open angle glaucoma patients. *Clin Experiment Ophthalmol,* 39**,** 633-8.

GURSES-OZDEN, R., TENG, C., VESSANI, R., ZAFAR, S., LIEBMANN, J. M. & RITCH, R. 2004. Macular and retinal nerve fiber layer thickness measurement

reproducibility using optical coherence tomography (OCT-3). *J Glaucoma,* 13**,** 238-44.

HAEFLIGER, I. O. & HITCHINGS, R. A. 1990a. Relationship between asymmetry of visual field defects and intraocular pressure difference in an untreated normal (low) tension glaucoma population. *Acta Ophthalmologica,* 68**,** 564-567.

HAEFLIGER, I. O. & HITCHINGS, R. A. 1990b. Relationship between asymmetry of visual field defects and intraocular pressure difference in an untreated normal (low) tension glaucoma population. *Acta Ophthalmol (Copenh),* 68**,** 564-7.

HANLEY, J. A. & MCNEIL, B. J. 1983. A Method of Comparing the Areas under Receiver Operating Characteristic Curves Derived from the Same Cases. *Radiology,* 148**,** 839-843.

HARASYMOWYCZ, P., DAVIS, B., XU, G., MYERS, J., BAYER, A. & SPAETH, G. L. 2004. The use of RADAAR (ratio of rim area to disc area asymmetry) in detecting glaucoma and its severity. *Can J Ophthalmol,* 39**,** 240-4.

HARASYMOWYCZ, P. J., PAPAMATHEAKIS, D. G., FANSI, A. K., GRESSET, J. & LESK, M. R. 2005. Validity of screening for glaucomatous optic nerve damage using confocal scanning laser ophthalmoscopy (Heidelberg Retina Tomograph II) in high-risk populations - A pilot study. *Ophthalmology,* 112**,** 2164-2171.

HARIZMAN, N., ZELEFSKY, J. R., ILITCHEV, E., TELLO, C., RITCH, R. & LIEBMANN, J. M. 2006. Detection of glaucoma using operator-dependent versus operator-independent classification in the Heidelberg retinal tomograph-II. *British Journal of Ophthalmology,* 90**,** 1390-1392.

HART, W. M., JR. & BECKER, B. 1982. The onset and evolution of glaucomatous visual field defects. *Ophthalmology,* 89**,** 268-79.

HARWERTH, R. S., CARTER-DAWSON, L., SHEN, F., SMITH, E. L., 3RD & CRAWFORD, M. L. 1999. Ganglion cell losses underlying visual field defects from experimental glaucoma. *Invest Ophthalmol Vis Sci,* 40**,** 2242-50.

HARWERTH, R. S., CARTER-DAWSON, L., SMITH, E. L., 3RD, BARNES, G., HOLT, W. F. & CRAWFORD, M. L. 2004. Neural losses correlated with visual losses in clinical perimetry. *Invest Ophthalmol Vis Sci,* 45**,** 3152-60.

HARWERTH, R. S., SMITH, E. L., 3RD & DESANTIS, L. 1997. Experimental glaucoma: perimetric field defects and intraocular pressure. *J Glaucoma,* 6**,** 390-401.

HAWKER, M. J., VERNON, S. A., AINSWORTH, G., HILLMAN, J. G., MACNAB, H. K. & DUA, H. S. 2005. Asymmetry in optic disc morphometry as measured by heidelberg retina tomography in a normal elderly population: the Bridlington Eye Assessment Project. *Invest Ophthalmol Vis Sci,* 46**,** 4153-8.

HAWKER, M. J., VERNON, S. A., TATTERSALL, C. L. & DUA, H. S. 2006. Detecting glaucoma with RADAAR: the Bridlington Eye Assessment Project. *Br J Ophthalmol,* 90**,** 744-8.

HAYASHI, K., TOMIDOKORO, A., LEE, K. Y., KONNO, S., SAITO, H., MAYAMA, C., AIHARA, M., IWASE, A. & ARAIE, M. 2012. Spectral-domain optical coherence tomography of beta-zone peripapillary atrophy: influence of myopia and glaucoma. *Invest Ophthalmol Vis Sci,* 53**,** 1499-505.

HAYREH, S. S. 1995. The 1994 Von Sallman Lecture. The optic nerve head circulation in health and disease. *Exp Eye Res,* 61**,** 259-72.

HAYREH, S. S. 2001. The blood supply of the optic nerve head and the evaluation of it - myth and reality. *Prog Retin Eye Res,* 20**,** 563-93.

HAYREH, S. S. 2009. Ischemic optic neuropathy. *Prog Retin Eye Res,* 28**,** 34-62.

HEALEY, P. R. & MITCHELL, P. 2000. The relationship between optic disc area and open-angle glaucoma. *J Glaucoma,* 9**,** 203-4.

HEIJL, A., LINDGREN, G. & OLSSON, J. 1987a. A package for the statistical analysis of visual fields. *In:* GREVE, E. L. & HEIJL, A. (eds.) *Seventh International Visual Field Symposium, Amsterdam, September 1986.* Dordrecht: Springer Netherlands.

HEIJL, A., LINDGREN, G. & OLSSON, J. 1987b. A package for the statistical analysis of visual fields. *In:* GREVE, E. L. & HEIJL, A. (eds.) *Seventh International Visual Field Symposium, Amsterdam, September 1986.* Springer Netherlands.

HENSON, D., HOBLEY, A., CHAUHAN, B., SPONSEL, W. & DALLAS, N. 1986. Importance of visual field score and asymmetry in the detection of glaucoma. *Am J Optom Physiol Opt,* 63**,** 714-23.

HENSON, D. B., ARTES, P. H. & CHAUHAN, B. C. 1999. Diffuse loss of sensitivity in early glaucoma. *Invest Ophthalmol Vis Sci,* 40**,** 3147-51.

HENSON, D. B. & DIX, S. M. 1984. Evaluation of the Friedmann Visual Field Analyser Mark II. Part 2. Results from a population with induced visual field defects. *Br J Ophthalmol,* 68**,** 463-7.

HERMANN, M. M., THEOFYLAKTOPOULOS, I., BANGARD, N., JONESCU-CUYPERS, C., COBURGER, S. & DIESTELHORST, M. 2004. Optic nerve head morphometry in healthy adults using confocal laser scanning tomography. *Br J Ophthalmol,* 88**,** 761-5.

HITCHINGS, R. A., BROWN, D. B. & ANDERTON, S. A. 1983. Glaucoma screening by means of an optic disc grid. *Br J Ophthalmol,* 67**,** 352-5.

HOLM, O. C., BECKER, B., ASSEFF, C. F. & PODOS, S. M. 1972. Volume of the optic disk cup. *Am J Ophthalmol,* 73**,** 876-81.

HONG, S., NARKIEWICZ, J. & KARDON, R. H. 2001. Comparison of pupil perimetry and visual perimetry in normal eyes: decibel sensitivity and variability. *Invest Ophthalmol Vis Sci,* 42**,** 957-65.

HOOD, D. C. & GREENSTEIN, V. C. 2003. Multifocal VEP and ganglion cell damage: applications and limitations for the study of glaucoma. *Prog Retin Eye Res,* 22**,** 201-51.

HOOD, D. C. & KARDON, R. H. 2007. A framework for comparing structural and functional measures of glaucomatous damage. *Progress in Retinal and Eye Research,* 26**,** 688-710.

HOOD, D. C., SLOBODNICK, A., RAZA, A. S., DE MORAES, C. G., TENG, C. C. & RITCH, R. 2014. Early glaucoma involves both deep local, and shallow widespread, retinal nerve fiber damage of the macular region. *Invest Ophthalmol Vis Sci,* 55**,** 632-49.

HOPE, D. 2014. Photograph of the retina of the human eye, with overlay diagrams showing the positions and sizes of the macula, fovea, and optic disc. *In:* MACULA.SVG (ed.) *My Right Eye.* wikipedia.

HUANG, J., LIU, X., WU, Z., GUO, X., XU, H., DUSTIN, L. & SADDA, S. 2011. Macular and retinal nerve fiber layer thickness measurements in normal eyes with the Stratus OCT, the Cirrus HD-OCT, and the Topcon 3D OCT-1000. *J Glaucoma,* 20**,** 118-25.

HUANG, P., SHI, Y., WANG, X., LIU, M. & ZHANG, C. 2014. Interocular asymmetry of the visual field defects in newly diagnosed normal-tension glaucoma, primary open-angle glaucoma, and chronic angle-closure glaucoma. *J Glaucoma,* 23**,** 455-60.

HUYNH, S. C., WANG, X. Y., BURLUTSKY, G. & MITCHELL, P. 2007. Symmetry of optical coherence tomography retinal measurements in young children. *Am J Ophthalmol,* 143**,** 518-20.

HWANG, Y. H., AHN, S. I. & KO, S. J. 2015. Diagnostic ability of macular ganglion cell asymmetry for glaucoma. *Clin Experiment Ophthalmol,* 43**,** 720-6.

JACOBSEN, A. G., BENDTSEN, M. D., VORUM, H., BOGSTED, M. & HARGITAI, J. 2015. Normal Value Ranges for Central Retinal Thickness Asymmetry in Healthy Caucasian Adults Measured by SPECTRALIS SD-OCT Posterior Pole Asymmetry Analysis. *Investigative Ophthalmology & Visual Science,* 56**,** 3875-3882.

JAMPEL, H. D., FRIEDMAN, D., QUIGLEY, H., VITALE, S., MILLER, R., KNEZEVICH, F. & DING, Y. L. 2009. Agreement Among Glaucoma Specialists in Assessing Progressive Disc Changes From Photographs in Open-Angle Glaucoma Patients. *American Journal of Ophthalmology,* 147**,** 39-44.

JANSONIUS, N. M., SCHIEFER, J., NEVALAINEN, J., PAETZOLD, J. & SCHIEFER, U. 2012a. A mathematical model for describing the retinal nerve fiber bundle trajectories in the human eye: Average course, variability, and influence of refraction, optic disc size and optic disc position. *Experimental Eye Research,* 105**,** 70-78.

JANSONIUS, N. M., SCHIEFER, J., NEVALAINEN, J., PAETZOLD, J. & SCHIEFER, U. 2012b. A mathematical model for describing the retinal nerve fiber bundle trajectories in the human eye: average course, variability, and influence of refraction, optic disc size and optic disc position. *Exp Eye Res,* 105**,** 70-8.

JOHNSON, C. A., ADAMS, A. J., CASSON, E. J. & BRANDT, J. D. 1993. Progression of Early Glaucomatous Visual-Field Loss as Detected by Blue-on-Yellow and Standard White-on-White Automated Perimetry. *Archives of Ophthalmology,* 111**,** 651-656.

JOHNSON, L. N., HILL, R. A. & BARTHOLOMEW, M. J. 1988. Correlation of afferent pupillary defect with visual field loss on automated perimetry. *Ophthalmology,* 95**,** 1649-55.

JONAS, J. B., GUSEK, G. C. & NAUMANN, G. O. 1988. Optic disc, cup and neuroretinal rim size, configuration and correlations in normal eyes. *Invest Ophthalmol Vis Sci,* 29**,** 1151-8.

JONAS, J. B., MARDIN, C. Y., SCHLOTZER-SCHREHARDT, U. & NAUMANN, G. O. 1991. Morphometry of the human lamina cribrosa surface. *Invest Ophthalmol Vis Sci,* 32**,** 401-5.

JONAS, J. B., WANG, Y. X., ZHANG, Q., FAN, Y. Y., XU, L., WEI, W. B. & JONAS, R. A. 2016. Parapapillary Gamma Zone and Axial Elongation-Associated Optic Disc Rotation: The Beijing Eye Study. *Invest Ophthalmol Vis Sci,* 57**,** 396-402.

JONSAS, C. H. 1972. Stereophotogrammetric techniques for measurements of the eye ground. An analysis of the correlation and variation of parameters measured from the optic cup and disc in 115 subjects. *Acta Ophthalmol Suppl,* 117**,** 3-51.

KARDON, R. H. 1992. Pupil perimetry. *Curr Opin Ophthalmol,* 3**,** 565-70.

KASS, M. A., HEUER, D. K., HIGGINBOTHAM, E. J., JOHNSON, C. A., KELTNER, J. L., MILLER, J. P., PARRISH, R. K., WILSON, M. R., GORDON, M. O. & STUD, O. H. T. 2002. The Ocular Hypertension Treatment Study - A randomized trial determines that topical ocular hypotensive medication delays or prevents the onset of primary open-angle glaucoma. *Archives of Ophthalmology,* 120**,** 701-713.

KATZ, J., QUIGLEY, H. A. & SOMMER, A. 1995. Repeatability of the Glaucoma Hemifield Test in automated perimetry. *Invest Ophthalmol Vis Sci,* 36**,** 1658-64.

KERRIGAN-BAUMRIND, L. A., QUIGLEY, H. A., PEASE, M. E., KERRIGAN, D. F. & MITCHELL, R. S. 2000. Number of ganglion cells in glaucoma eyes compared with threshold visual field tests in the same persons. *Invest Ophthalmol Vis Sci,* 41**,** 741-8.

KIM, M. S., KIM, J. M., PARK, K. H. & CHOI, C. Y. 2009. Asymmetry of diurnal intraocular pressure fluctuation between right and left eyes. *Acta Ophthalmol,* 89**,** 352-7.

KIM, T. W., KAGEMANN, L., GIRARD, M. J., STROUTHIDIS, N. G., SUNG, K. R., LEUNG, C. K., SCHUMAN, J. S. & WOLLSTEIN, G. 2013. Imaging of the lamina cribrosa in glaucoma: perspectives of pathogenesis and clinical applications. *Curr Eye Res,* 38**,** 903-9.

KLEIN, B. E., KLEIN, R., MEUER, S. M. & GOETZ, L. A. 1993. Migraine headache and its association with open-angle glaucoma: the Beaver Dam Eye Study. *Invest Ophthalmol Vis Sci,* 34**,** 3024-7.

KOHAVI, R. 1995. A study of cross-validation and bootstrap for accuracy estimation and model selection. *Proceedings of the 14th international joint conference on Artificial intelligence - Volume 2.* Montreal, Quebec, Canada: Morgan Kaufmann Publishers Inc.

KROESE, M. & BURTON, H. 2003. Primary open angle glaucoma. The need for a consensus case definition. *Journal of Epidemiology and Community Health,* 57**,** 752-754.

KURIMOTO, Y., MATSUNO, K., KANEKO, Y., UMIHIRA, J. & YOSHIMURA, N. 2000. Asymmetries of the retinal nerve fibre layer thickness in normal eyes. *Br J Ophthalmol,* 84**,** 469-72.

LAMPARTER, J., RUSSELL, R. A., ZHU, H., ASAOKA, R., YAMASHITA, T., HO, T. & GARWAY-HEATH, D. F. 2013. The influence of intersubject variability in ocular anatomical variables on the mapping of retinal locations to the retinal nerve fiber layer and optic nerve head. *Invest Ophthalmol Vis Sci,* 54**,** 6074-82.

LANDERS, J. A., GOLDBERG, I. & GRAHAM, S. L. 2003. Detection of early visual field loss in glaucoma using frequency-doubling perimetry and short-wavelength automated perimetry. *Archives of Ophthalmology,* 121**,** 1705-1710.

LEE, A. J., MITCHELL, P., ROCHTCHINA, E. & HEALEY, P. R. 2003a. Female reproductive factors and open angle glaucoma: the Blue Mountains Eye Study. *British Journal of Ophthalmology,* 87**,** 1324-1328.

LEE, A. J., ROCHTCHINA, E. & MITCHELL, P. 2004. Intraocular pressure asymmetry and undiagnosed open-angle glaucoma in an older population. *Am J Ophthalmol,* 137**,** 380-2.

LEE, A. J., WANG, J. J., ROCHTCHINA, E., HEALEY, P., CHIA, E. M. & MITCHELL, P. 2003b. Patterns of glaucomatous visual field defects in an older population: the Blue Mountains Eye Study. *Clin Experiment Ophthalmol,* 31**,** 331-5.

LEE, E. J., KIM, T. W., KIM, M., GIRARD, M. J., MARI, J. M. & WEINREB, R. N. 2014a. Recent structural alteration of the peripheral lamina cribrosa near the location of disc hemorrhage in glaucoma. *Invest Ophthalmol Vis Sci,* 55**,** 2805-15.

LEE, J. M., CIRINEO, N., RAMANATHAN, M., NOURI-MAHDAVI, K., MORALES, E., COLEMAN, A. L. & CAPRIOLI, J. 2014b. Performance of the visual field index

in glaucoma patients with moderately advanced visual field loss. *Am J Ophthalmol,* 157**,** 39-43.

LEE, K. Y., TOMIDOKORO, A., SAKATA, R., KONNO, S., MAYAMA, C., SAITO, H., HAYASHI, K., IWASE, A. & ARAIE, M. 2010. Cross-sectional anatomic configurations of peripapillary atrophy evaluated with spectral domain-optical coherence tomography. *Invest Ophthalmol Vis Sci,* 51**,** 666-71.

LESKE, M. C., CONNELL, A. M., SCHACHAT, A. P. & HYMAN, L. 1994. The Barbados Eye Study. Prevalence of open angle glaucoma. *Arch Ophthalmol,* 112**,** 821-9.

LESKE, M. C., HEIJL, A., HYMAN, L. & BENGTSSON, B. 1999. Early Manifest Glaucoma Trial: design and baseline data. *Ophthalmology,* 106**,** 2144-53.

LESKE, M. C., WU, S. Y., HONKANEN, R., NEMESURE, B., SCHACHAT, A., HYMAN, L. & HENNIS, A. 2007. Nine-Year Incidence of Open-Angle Glaucoma in the Barbados Eye Studies. *Ophthalmology,* 114**,** 1058-1064.

LEUNG, C. K., CHEUNG, C. Y., WEINREB, R. N., QIU, Q., LIU, S., LI, H., XU, G., FAN, N., HUANG, L., PANG, C. P. & LAM, D. S. 2009. Retinal nerve fiber layer imaging with spectral-domain optical coherence tomography: a variability and diagnostic performance study. *Ophthalmology,* 116**,** 1257-63, 1263 e1-2.

LEUNG, C. K., CHIU, V., WEINREB, R. N., LIU, S., YE, C., YU, M., CHEUNG, C. Y., LAI, G. & LAM, D. S. 2011. Evaluation of retinal nerve fiber layer progression in glaucoma: a comparison between spectral-domain and time-domain optical coherence tomography. *Ophthalmology,* 118**,** 1558-62.

LEVINE, R. A., DEMIREL, S., FAN, J., KELTNER, J. L., JOHNSON, C. A., KASS, M. A. & OCULAR HYPERTENSION TREATMENT STUDY, G. 2006. Asymmetries and visual field summaries as predictors of glaucoma in the ocular hypertension treatment study. *Invest Ophthalmol Vis Sci,* 47**,** 3896-903.

LI, H., HEALEY, P. R., TARIQ, Y. M., TEBER, E. & MITCHELL, P. Symmetry of Optic Nerve Head Parameters Measured by the Heidelberg Retina Tomograph 3 in Healthy Eyes: The Blue Mountains Eye Study. *American Journal of Ophthalmology*.

LISBOA, R., LEITE, M. T., ZANGWILL, L. M., TAFRESHI, A., WEINREB, R. N. & MEDEIROS, F. A. 2012. Diagnosing preperimetric glaucoma with spectral domain optical coherence tomography. *Ophthalmology,* 119**,** 2261-9.

LIU, J. H., REALINI, T. & WEINREB, R. N. 2011a. Asymmetry of 24-hour intraocular pressure reduction by topical ocular hypotensive medications in fellow eyes. *Ophthalmology,* 118**,** 1995-2000.

LIU, J. H., ZHANG, X., KRIPKE, D. F. & WEINREB, R. N. 2003. Twenty-four-hour intraocular pressure pattern associated with early glaucomatous changes. *Invest Ophthalmol Vis Sci,* 44**,** 1586-90.

LIU, S., LAM, S., WEINREB, R. N., YE, C., CHEUNG, C. Y., LAI, G., LAM, D. S. C. & LEUNG, C. K. S. 2011b. Comparison of Standard Automated Perimetry, Frequency-Doubling Technology Perimetry, and Short-Wavelength Automated Perimetry for Detection of Glaucoma. *Investigative Ophthalmology & Visual Science,* 52**,** 7325-7331.

LOEWENFELD, I. E. & ROSSKOTHEN, H. D. 1974. Infrared pupil camera. A new method for mass screening and clinical use. *Am J Ophthalmol,* 78**,** 304-13.

MAHMUDI, T., KAFIEH, R AND RABBANI, H. Comparison of macular OCTs in right and left eyes of normal people.  SPIE Proceedings on Applications of Digital Image Processing XXXVI, 2013 San Diego, California United States.

MANJUNATH, V., SHAH, H., FUJIMOTO, J. G. & DUKER, J. S. 2011. Analysis of Peripapillary Atrophy Using Spectral Domain Optical Coherence Tomography. *Ophthalmology,* 118**,** 531-536.

MARCUS, D. M., COSTARIDES, A. P., GOKHALE, P., PAPASTERGIOU, G., MILLER, J. J., JOHNSON, M. H. & CHAUDHARY, B. A. 2001. Sleep disorders: a risk factor for normal-tension glaucoma? *J Glaucoma,* 10**,** 177-83.

MEDEIROS, F. A., LISBOA, R., WEINREB, R. N., GIRKIN, C. A., LIEBMANN, J. M. & ZANGWILL, L. M. 2012a. A combined index of structure and function for staging glaucomatous damage. *Arch Ophthalmol,* 130**,** 1107-16.

MEDEIROS, F. A., LISBOA, R., ZANGWILL, L. M., LIEBMANN, J. M., GIRKIN, C. A., BOWD, C. & WEINREB, R. N. 2014. Evaluation of progressive neuroretinal rim loss as a surrogate end point for development of visual field loss in glaucoma. *Ophthalmology,* 121**,** 100-9.

MEDEIROS, F. A., SAMPLE, P. A., ZANGWILL, L. M., LIEBMANN, J. M., GIRKIN, C. A. & WEINREB, R. N. 2006a. A statistical approach to the evaluation of covariate effects on the receiver operating characteristic curves of diagnostic tests in glaucoma. *Invest Ophthalmol Vis Sci,* 47**,** 2520-7.

MEDEIROS, F. A., ZANGWILL, L. M., BOWD, C., MANSOURI, K. & WEINREB, R. N. 2012b. The structure and function relationship in glaucoma: implications for detection of progression and measurement of rates of change. *Invest Ophthalmol Vis Sci,* 53**,** 6939-46.

MEDEIROS, F. A., ZANGWILL, L. M., BOWD, C., SAMPLE, P. A. & WEINREB, R. N. 2006b. Influence of disease severity and optic disc size on the diagnostic performance of imaging instruments in glaucoma. *Invest Ophthalmol Vis Sci,* 47**,** 1008-15.

MEDEIROS, F. A., ZANGWILL, L. M., BOWD, C. & WEINREB, R. N. 2004. Comparison of the GDx VCC scanning laser polarimeter, HRT II confocal scanning laser ophthalmoscope, and stratus OCT optical coherence tomograph for the detection of glaucoma. *Arch Ophthalmol,* 122**,** 827-37.

MEDEIROS FA, Z. L. M. B. C. W. R. N. 2004. COmparison of the gdx vcc scanning laser polarimeter, hrt ii confocalscanning laser ophthalmoscope, and stratus oct optical coherence tomographfor the detection of glaucoma. *Archives of Ophthalmology,* 122**,** 827-837.

MIGLIOR, S., GUARESCHI, M., ALBE, E., GOMARASCA, S., VAVASSORI, M. & ORZALESI, N. 2003. Detection of glaucomatous visual field changes using the Moorfields regression analysis of the Heidelberg Retina Tomograph. *American Journal of Ophthalmology,* 136**,** 26-33.

MIGLIOR, S., ZEYEN, T., PFEIFFER, N., CUNHA-VAZ, J., TORRI, V., ADAMSONS, I. & EUROPEAN GLAUCOMA PREVENTION STUDY, G. 2005. Results of the European Glaucoma Prevention Study. *Ophthalmology,* 112**,** 366-75.

MIKELBERG, F. S. & DRANCE, S. M. 1984. The mode of progression of visual field defects in glaucoma. *Am J Ophthalmol,* 98**,** 443-5.

MOJON, D. S., HESS, C. W., GOLDBLUM, D., BOHNKE, M., KORNER, F. & MATHIS, J. Primary open-angle glaucoma is associated with sleep apnea syndrome. *Ophthalmologica. 2000;214(2):115-8.*

MORENO-MONTANES, J., OLMO, N., ALVAREZ, A., GARCIA, N. & ZARRANZ-VENTURA, J. 2010. Cirrus high-definition optical coherence tomography compared with Stratus optical coherence tomography in glaucoma diagnosis. *Invest Ophthalmol Vis Sci,* 51**,** 335-43.

MUKESH, B. N., MCCARTY, C. A., RAIT, J. L. & TAYLOR, H. R. 2002. Five-year incidence of open-angle glaucoma: the visual impairment project. *Ophthalmology,* 109**,** 1047-51.

MUSCH, D. C., GILLESPIE, B. W., PALMBERG, P. F., SPAETH, G., NIZIOL, L. M. & LICHTER, P. R. 2014. Visual field improvement in the collaborative initial glaucoma treatment study. *Am J Ophthalmol,* 158**,** 96-104 e2.

MUSCH, D. C., LICHTER, P. R., GUIRE, K. E. & STANDARDI, C. L. 1999. The Collaborative Initial Glaucoma Treatment Study: study design, methods, and baseline characteristics of enrolled patients. *Ophthalmology,* 106**,** 653-62.

MWANZA, J. C., DURBIN, M. K., BUDENZ, D. L. & CIRRUS, O. C. T. N. D. S. G. 2011. Interocular symmetry in peripapillary retinal nerve fiber layer thickness measured with the Cirrus HD-OCT in healthy eyes. *Am J Ophthalmol,* 151**,** 514-21 e1.

MWANZA, J. C., DURBIN, M. K., BUDENZ, D. L., SAYYAD, F. E., CHANG, R. T., NEELAKANTAN, A., GODFREY, D. G., CARTER, R. & CRANDALL, A. S. 2012. Glaucoma diagnostic accuracy of ganglion cell-inner plexiform layer thickness: comparison with nerve fiber layer and optic nerve head. *Ophthalmology,* 119**,** 1151-8.

NAGHIZADEH, F. & HOLLO, G. 2014. Detection of early glaucomatous progression with octopus cluster trend analysis. *J Glaucoma,* 23**,** 269-75.

NAKATANI, Y., HIGASHIDE, T., OHKUBO, S., TAKEDA, H. & SUGIYAMA, K. 2010. Evaluation of macular thickness and peripapillary retinal nerve fiber layer thickness for detection of early glaucoma using spectral domain optical coherence tomography. *J Glaucoma,* 20**,** 252-9.

NEMESURE, B., HE, Q., MENDELL, N., WU, S. Y., HEJTMANCIK, J. F., HENNIS, A. & LESKE, M. C. 2001. Inheritance of open-angle glaucoma in the Barbados family study. *Am J Med Genet,* 103**,** 36-43.

OHTS 2008. The accuracy and clinical application of predictive models for primary open-angle glaucoma in ocular hypertensive individuals. *Ophthalmology,* 115**,** 2030-6.

ONEN, S. H., MOURIAUX, F., BERRAMDANE, L., DASCOTTE, J. C., KULIK, J. F. & ROULAND, J. F. 2000. High prevalence of sleep-disordered breathing in patients with primary open-angle glaucoma. *Acta Ophthalmol Scand,* 78**,** 638-41.

ONG, L. S., MITCHELL, P., HEALEY, P. R. & CUMMING, R. G. 1999. Asymmetry in optic disc parameters: the Blue Mountains Eye Study. *Investigative Ophthalmology & Visual Science,* 40**,** 849-57.

PANARELLI, J. F., BANITT, M. R., SIDOTI, P. A., BUDENZ, D. L. & SINGH, K. 2015. Clinical impact of 8 prospective, randomized, multicenter glaucoma trials. *J Glaucoma,* 24**,** 64-8.

PARK, S. B., SUNG, K. R., KANG, S. Y., KIM, K. R. & KOOK, M. S. 2009. Comparison of glaucoma diagnostic Capabilities of Cirrus HD and Stratus optical coherence tomography. *Arch Ophthalmol,* 127**,** 1603-9.

PARK, S. C., DE MORAES, C. G., TENG, C. C., TELLO, C., LIEBMANN, J. M. & RITCH, R. 2012. Enhanced depth imaging optical coherence tomography of deep optic nerve complex structures in glaucoma. *Ophthalmology,* 119**,** 3-9.

PARRISH, R. K., 2ND, SCHIFFMAN, J. C., FEUER, W. J., ANDERSON, D. R., BUDENZ, D. L., WELLS-ALBORNOZ, M. C., VANDENBROUCKE, R., KASS, M. A. & GORDON, M. O. 2005. Test-retest reproducibility of optic disk deterioration detected from stereophotographs by masked graders. *Am J Ophthalmol,* 140**,** 762-4.

PHELPS, C. D. & CORBETT, J. J. 1985. Migraine and low-tension glaucoma. A case-control study. *Invest Ophthalmol Vis Sci,* 26**,** 1105-8.

POINOOSAWMY, D., FONTANA, L., WU, J. X., BUNCE, C. V. & HITCHINGS, R. A. 1998. Frequency of asymmetric visual field defects in normal-tension and high-tension glaucoma. *Ophthalmology,* 105**,** 988-91.

PORTNEY, G. L. 1975. Photogrammetric analysis of volume asymmetry of the optic nerve head cup in normal, hypertensive, and glaucomatous eyes. *Am J Ophthalmol,* 80**,** 51-5.

QUIGLEY, H. A. & ADDICKS, E. M. 1981. Regional differences in the structure of the lamina cribrosa and their relation to glaucomatous optic nerve damage. *Archives of Ophthalmology,* 99**,** 137-143.

QUIGLEY, H. A. & ADDICKS, E. M. 1982. Quantitative studies of retinal nerve fiber layer defects. *Arch Ophthalmol,* 100**,** 807-14.

QUIGLEY, H. A., ADDICKS, E. M. & GREEN, W. R. 1982. Optic nerve damage in human glaucoma. III. Quantitative correlation of nerve fiber loss and visual field defect in glaucoma, ischemic neuropathy, papilledema, and toxic neuropathy. *Arch Ophthalmol,* 100**,** 135-46.

QUIGLEY, H. A. & BROMAN, A. T. 2006. The number of people with glaucoma worldwide in 2010 and 2020. *Br J Ophthalmol,* 90**,** 262-7.

QUIGLEY, H. A., DUNKELBERGER, G. R. & GREEN, W. R. 1989. Retinal ganglion cell atrophy correlated with automated perimetry in human eyes with glaucoma. *Am J Ophthalmol,* 107**,** 453-64.

QUIGLEY, H. A., KATZ, J., DERICK, R. J., GILBERT, D. & SOMMER, A. 1992. An evaluation of optic disc and nerve fiber layer examinations in monitoring progression of early glaucoma damage. *Ophthalmology,* 99**,** 19-28.

QUIGLEY, H. A., VARMA, R., TIELSCH, J. M., KATZ, J., SOMMER, A. & GILBERT, D. L. 1999. The relationship between optic disc area and open-angle glaucoma: the Baltimore Eye Survey. *J Glaucoma,* 8**,** 347-52.

RACETTE, L., MEDEIROS, F. A., ZANGWILL, L. M., NG, D., WEINREB, R. N. & SAMPLE, P. A. 2008. Diagnostic accuracy of the Matrix 24-2 and original N-30 frequency-doubling technology tests compared with standard automated perimetry. *Invest Ophthalmol Vis Sci,* 49**,** 954-60.

RACETTE, L., WILSON, M. R., ZANGWILL, L. M., WEINREB, R. N. & SAMPLE, P. A. 2003. Primary open-angle glaucoma in blacks: a review. *Surv Ophthalmol,* 48**,** 295-313.

RADIUS, R. L. & GONZALES, M. 1981. Anatomy of the lamina cribrosa in human eyes. *Archives of Ophthalmology,* 99**,** 2159-2162.

RAMAKRISHNAN, R., NIRMALAN, P. K., KRISHNADAS, R., THULASIRAJ, R. D., TIELSCH, J. M., KATZ, J., FRIEDMAN, D. S. & ROBIN, A. L. 2003. Glaucoma in a rural population of southern India: the Aravind comprehensive eye survey. *Ophthalmology,* 110**,** 1484-90.

RAO, H. L., SENTHIL, S., CHOUDHARI, N. S., MANDAL, A. K. & GARUDADRI, C. S. 2013. Behavior of visual field index in advanced glaucoma. *Invest Ophthalmol Vis Sci,* 54**,** 307-12.

REIS, A. S., SHARPE, G. P., YANG, H., NICOLELA, M. T., BURGOYNE, C. F. & CHAUHAN, B. C. 2012. Optic disc margin anatomy in patients with glaucoma and normal controls with spectral domain optical coherence tomography. *Ophthalmology,* 119**,** 738-47.

REUS, N. J., LEMIJ, H. G., GARWAY-HEATH, D. F., AIRAKSINEN, P. J., ANTON, A., BRON, A. M., FASCHINGER, C., HOLLO, G., IESTER, M., JONAS, J. B., MISTLBERGER, A., TOPOUZIS, F. & ZEYEN, T. G. 2010. Clinical Assessment of Stereoscopic Optic Disc Photographs for Glaucoma: The European Optic Disc Assessment Trial. *Ophthalmology,* 117**,** 717-723.

RUDNICKA, A. R., MT-ISA, S., OWEN, C. G., COOK, D. G. & ASHBY, D. 2006. Variations in primary open-angle glaucoma prevalence by age, gender, and race: a Bayesian meta-analysis. *Invest Ophthalmol Vis Sci,* 47**,** 4254-61.

RUDNICKA, A. R., OWEN, C. G., DAVID, F. E., BSC, MCOPTOM & ALICJA R RUDNICKA, M. P. M. 2007. Chapter 1 - Epidemiology of primary open angle glaucoma. *Glaucoma Identification & Co-management.* Edinburgh: Butterworth-Heinemann.

SAMPLE, P. A., MEDEIROS, F. A., RACETTE, L., PASCUAL, J. P., BODEN, C., ZANGWILL, L. M., BOWD, C. & WEINREB, R. N. 2006. Identifying glaucomatous vision loss with visual-function-specific perimetry in the diagnostic innovations in glaucoma study. *Invest Ophthalmol Vis Sci,* 47**,** 3381-9.

SAMPLE, P. A. & WEINREB, R. N. 1990. Color Perimetry for Assessment of Primary Open-Angle Glaucoma. *Investigative Ophthalmology & Visual Science,* 31**,** 1869-1875.

SEHI, M., GUAQUETA, D. C., FEUER, W. J. & GREENFIELD, D. S. 2007. Scanning laser polarimetry with variable and enhanced corneal compensation in normal and glaucomatous eyes. *Am J Ophthalmol,* 143**,** 272-9.

SEO, J. H., KIM, T. W. & WEINREB, R. N. 2014. Lamina cribrosa depth in healthy eyes. *Invest Ophthalmol Vis Sci,* 55**,** 1241-51.

SHETH, S. S., RUSH, R. B. & NATARAJAN, S. 2012. Inner and outer retinal volumetric and morphologic analysis of the macula with spectral domain optical coherence tomography in retinitis pigmentosa. *Middle East Afr J Ophthalmol,* 19**,** 227-30.

SIGAL, I. A., WANG, B., STROUTHIDIS, N. G., AKAGI, T. & GIRARD, M. J. 2014. Recent advances in OCT imaging of the lamina cribrosa. *Br J Ophthalmol,* 98 Suppl 2**,** ii34-9.

SMITH, S. D., KATZ, J. & QUIGLEY, H. A. 1996. Analysis of progressive change in automated visual fields in glaucoma. *Invest Ophthalmol Vis Sci,* 37**,** 1419-28.

SOMMER, A., DUGGAN, C., AUER, C. & ABBEY, H. 1985. Analytic approaches to the interpretation of automated threshold perimetric data for the diagnosis of early glaucoma. *Trans Am Ophthalmol Soc,* 83**,** 250-67.

SOMMER, A., ENGER, C. & WITT, K. 1987. Screening for glaucomatous visual field loss with automated threshold perimetry. *Am J Ophthalmol,* 103**,** 681-4.

SPAETH, G. L., HENDERER, J., LIU, C., KESEN, M., ALTANGEREL, U., BAYER, A., KATZ, L. J., MYERS, J., RHEE, D. & STEINMANN, W. 2002. The disc damage likelihood scale: reproducibility of a new method of estimating the amount of optic nerve damage caused by glaucoma. *Trans Am Ophthalmol Soc,* 100**,** 181-5; discussion 185-6.

SUGIYAMA, K., UCHIDA, H., TOMITA, G., SATO, Y., IWASE, A. & KITAZAWA, Y. 1999. Localized wedge-shaped defects of retinal nerve fiber layer and disc hemorrhage in glaucoma. *Ophthalmology,* 106**,** 1762-7.

SULLIVAN-MEE, M., RUEGG, C. C., PENSYL, D., HALVERSON, K. & QUALLS, C. 2013. Diagnostic precision of retinal nerve fiber layer and macular thickness asymmetry parameters for identifying early primary open-angle glaucoma. *Am J Ophthalmol,* 156**,** 567-77 e1.

SUNG, M. S., YOON, J. H. & PARK, S. W. 2014. Diagnostic validity of macular ganglion cell-inner plexiform layer thickness deviation map algorithm using cirrus HD-OCT in preperimetric and early glaucoma. *J Glaucoma,* 23**,** e144-51.

SUSANNA, R., JR., NICOLELA, M. T., SORIANO, D. S. & CARVALHO, C. 1994. Automated perimetry: a study of the glaucoma hemifield test for the detection of early glaucomatous visual field loss. *J Glaucoma,* 3**,** 12-6.

SWANSON, W. H., FELIUS, J. & PAN, F. 2004. Perimetric defects and ganglion cell damage: Interpreting linear relations using a two-stage neural model. *Investigative Ophthalmology & Visual Science,* 45**,** 466-472.

SWANSON, W. H., SUN, H., LEE, B. B. & CAO, D. 2011. Responses of primate retinal ganglion cells to perimetric stimuli. *Invest Ophthalmol Vis Sci,* 52**,** 764-71.

TAFRESHI, A., SAMPLE, P. A., LIEBMANN, J. M., GIRKIN, C. A., ZANGWILL, L. M., WEINREB, R. N., LALEZARY, M. & RACETTE, L. 2009. Visual Function-Specific Perimetry to Identify Glaucomatous Visual Loss Using Three Different Definitions of Visual Field Abnormality. *Investigative Ophthalmology & Visual Science,* 50**,** 1234-1240.

TATHAM, A. J., MIKI, A., WEINREB, R. N., ZANGWILL, L. M. & MEDEIROS, F. A. 2014. Defects of the lamina cribrosa in eyes with localized retinal nerve fiber layer loss. *Ophthalmology,* 121**,** 110-8.

TIELSCH, J. M., KATZ, J., QUIGLEY, H. A., JAVITT, J. C. & SOMMER, A. 1995a. Diabetes, intraocular pressure, and primary open-angle glaucoma in the Baltimore Eye Survey. *Ophthalmology,* 102**,** 48-53.

TIELSCH, J. M., KATZ, J., SOMMER, A., QUIGLEY, H. A. & JAVITT, J. C. 1995b. Hypertension, perfusion pressure, and primary open-angle glaucoma. A population-based assessment. *Arch Ophthalmol,* 113**,** 216-21.

TIELSCH JM, S. A., KATZ J, ET AL. 1991. Racial variations in the prevalence of primary open-angle glaucoma. *JAMA (Chicago, Ill.),* 266**,** 369.

TURPIN, A., MCKENDRICK, A. M., JOHNSON, C. A. & VINGRYS, A. J. 2003. Properties of perimetric threshold estimates from full threshold, ZEST, and SITA-like strategies, as determined by computer simulation. *Invest Ophthalmol Vis Sci,* 44**,** 4787-95.

TURTSCHI, S., BERGAMIN, O., DUBLER, B., SCHOTZAU, A. & ZULAUF, M. 1994. [Pupil perimetry with the Octopus 1-2-3. Initial experiences]. *Klin Monbl Augenheilkd,* 204**,** 398-9.

UM, T. W., SUNG, K. R., WOLLSTEIN, G., YUN, S. C., NA, J. H. & SCHUMAN, J. S. 2012. Asymmetry in hemifield macular thickness as an early indicator of glaucomatous change. *Invest Ophthalmol Vis Sci,* 53**,** 1139-44.

VESTI, E., JOHNSON, C. A. & CHAUHAN, B. C. 2003. Comparison of different methods for detecting glaucomatous visual field progression. *Invest Ophthalmol Vis Sci,* 44**,** 3873-9.

VIZZERI, G., WEINREB, R. N., GONZALEZ-GARCIA, A. O., BOWD, C., MEDEIROS, F. A., SAMPLE, P. A. & ZANGWILL, L. M. 2009. Agreement between spectral-domain and time-domain OCT for measuring RNFL thickness. *Br J Ophthalmol,* 93**,** 775-81.

WANG, J. C., GAZZARD, G., FOSTER, P. J., DEVEREUX, J. G., OEN, F. T., CHEW, P. T., KHAW, P. T. & SEAH, S. K. 2004. Interocular asymmetry of visual field defects in primary open angle glaucoma and primary angle-closure glaucoma. *Eye (Lond),* 18**,** 365-8.

WANG, J. J., MITCHELL, P. & SMITH, W. 1997. Is there an association between migraine headache and open-angle glaucoma? Findings from the Blue Mountains Eye Study. *Ophthalmology,* 104**,** 1714-9.

WEIH, L. M., NANJAN, M., MCCARTY, C. A. & TAYLOR, H. R. 2001. Prevalence and predictors of open-angle glaucoma: Results from the visual impairment project. *Ophthalmology,* 108**,** 1966-1972.

WEINREB, R. N., DREHER, A. W. & BILLE, J. F. 1989. Quantitative assessment of the optic nerve head with the laser tomographic scanner. *Int Ophthalmol,* 13**,** 25-9.

WEINREB, R. N., DREHER, A. W., COLEMAN, A., QUIGLEY, H., SHAW, B. & REITER, K. 1990. Histopathologic validation of Fourier-ellipsometry measurements of retinal nerve fiber layer thickness. *Arch Ophthalmol,* 108**,** 557-60.

WILLIAMS, A. L., GATLA, S., LEIBY, B. E., FAHMY, I., BISWAS, A., DE BARROS, D. M., RAMAKRISHNAN, R., BHARDWAJ, S., WRIGHT, C., DUBEY, S., LYNCH, J. F., BAYER, A., KHANDELWAL, R., ICHHPUJANI, P., GHEITH, M., SIAM, G., FELDMAN, R. M., HENDERER, J. D. & SPAETH, G. L. 2011. The Value of Intraocular Pressure Asymmetry in Diagnosing Glaucoma. *J Glaucoma*.

WOLFS, R. C., KLAVER, C. C., RAMRATTAN, R. S., VAN DUIJN, C. M., HOFMAN, A. & DE JONG, P. T. 1998. Genetic risk of primary open-angle glaucoma. Population-based familial aggregation study. *Arch Ophthalmol,* 116**,** 1640-5.

WOLLSTEIN, G., GARWAY-HEATH, D. F., FONTANA, L. & HITCHINGS, R. A. 2000. Identifying early glaucomatous changes - Comparison between expert clinical assessment of optic disc photographs and confocal scanning ophthalmoscopy. *Ophthalmology,* 107**,** 2272-2277.

WOLLSTEIN, G., GARWAY-HEATH, D. F. & HITCHINGS, R. A. 1998. Identification of early glaucoma cases with the scanning laser ophthalmoscope. *Ophthalmology,* 105**,** 1557-1563.

YAMADA, H., HANGAI, M., NAKANO, N., TAKAYAMA, K., KIMURA, Y., MIYAKE, M., AKAGI, T., IKEDA, H. O., NOMA, H. & YOSHIMURA, N. 2014. Asymmetry analysis of macular inner retinal layers for glaucoma diagnosis. *Am J Ophthalmol,* 158**,** 1318-1329 e3.

ZANGWILL, L. M., BOWD, C., BERRY, C. C., WILLIAMS, J., BLUMENTHAL, E. Z., SANCHEZ-GALEANA, C. A., VASILE, C. & WEINREB, R. N. 2001. Discriminating between normal and glaucomatous eyes using the Heidelberg Retina Tomograph, GDx Nerve Fiber Analyzer, and Optical Coherence Tomograph. *Archives of Ophthalmology,* 119**,** 985-993.

ZEYEN, T., MIGLIOR, S., PFEIFFER, N., CUNHA-VAZ, J. & ADAMSONS, I. 2003. Reproducibility of evaluation of optic disc change for glaucoma with stereo optic disc photographs. *Ophthalmology,* 110**,** 340-4.